https://doi.org/10.61092/iaea.jqbt-zmjb
INDC(NDS)-0790
Distr. G,NM,PH

IAEA
International Atomic Energy Agency

INDC International Nuclear Data Committee

Strength Functions derived from the Discrete and Average Resonance Capture

Jiri Kopecky
JUKO Research
Alkmaar, The Netherlands

and

S. Goriely
Universite Libre de Bruxelles
Belgium

July 2019

IAEA Nuclear Data Section
Vienna International Centre, P.O. Box 100, 1400 Vienna, Austria

Selected INDC documents may be downloaded in electronic form from

http://nds.iaea.org/publications

or sent as an e-mail attachment.

Requests for hardcopy or e-mail transmittal should be directed to
NDS.Contact-Point@iaea.org

or to:

Nuclear Data Section
International Atomic Energy Agency
Vienna International Centre
PO Box 100
1400 Vienna
Austria

Printed by the IAEA in Austria

July 2019

INDC(NDS)-0790
Distr. G,NM,PH

Strength Functions derived from the Discrete and Average Resonance Capture

Jiri Kopecky
JUKO Research
Alkmaar, The Netherlands

and

S. Goriely
Universite Libre de Bruxelles
Belgium

July 2019

Contents

1. Introduction

Properties of neutron resonances are one of the most exciting and widely studied fields of low-energy neutron nuclear physics. Starting from 1960, the resonance behavior of neutron interactions with matter was studied in many laboratories using the white TOF spectra at accelerators or reactors. General interest in resonance properties lasted for about 30 years and was later replaced by studies of materials important for applications only. During that 30 years period, the traditional transmission experiments were often extended by neutron capture measurements on discrete resonances – *Discrete Resonance Capture* (DRC) – used primarily for spectroscopic studies of initial and final states of the compound or product nuclide [1.1]. In some cases, however, the gamma-decay properties and the gamma-strength behavior of different multipole radiations were analyzed as it was realized that these observables give interesting insight into the rules governing the de-excitation of the excited nucleus at energies below the particle-emission threshold which form the tail of the Giant Dipole Resonance (GDR).

Another similar experiment is the *Average Resonance Capture* (ARC). In this case, the neutron beams are produced by transmission through filter materials (^{10}B, ^{45}Sc or ^{56}Fe), which yield neutron beams with bell-shaped energy distributions and different full-width at half maximum (FWHM) at neutron energies of about 150 eV, 2 keV and 24 keV, respectively. The boron-filtered beam primarily removes the thermal component, while for Sc and Fe filters the thermal neutron-capture cross-section interference dips yield quasi mono-energetic beams a few keV wide. Facilities for measuring ARC data were built in four laboratories in the US: Argonne National Laboratory ANL [1.2], the National Bureau of Standards [1.3], the Idaho Nuclear Engineering Laboratory INEL [1.4] and Brookhaven National Laboratory BNL [1.5], during the period between 1970 and 1980. Outside the US, only three laboratories have ever published ARC data, two in the USSR (IAEP/PPEI Obninsk [1.6] and Kiev [1.7]) and one in Germany (KfK Karlsruhe [1.8]). The BNL facility turned out to be the most efficient one in all aspects, primarily due to the high neutron fluence and superior processing tools, and therefore the majority of all the adopted data originate from BNL.

The first compilation of photon strength functions (PSFs) $f_{XL}(E_\gamma)$ based on experimental DRC data from resonance or thermal capture reactions was published in 1981 [1.9,1.10]. This database was reviewed and extended by including measurements performed between 1981 and 1994, in the framework of a BNL-ECN (the Energy Centrum Netherlands) collaboration. The atomic mass A dependence of the average strength functions $f_{E1}(E_\gamma)$ and $f_{M1}(E_\gamma)$ was derived and finalized in the ECN report [1.11] in 1994, using the latest values of the s-wave spacing D_0. This compilation was included in the RIPL database and documentation and remained unchanged throughout all the RIPL releases up to 2009. Recently, a new interest in photonuclear data and gamma-ray strength functions that emerged at the IAEA Consultant's Meeting [1.12] led to a new IAEA CRP on "*Updating the Photonuclear Data Library and Generating a Reference Database for Photon Strength Functions"* (2016 – 2019) [1.13-1.15].

This report includes the description and results of a new evaluation of PSFs based on resonance neutron capture experiments which was performed in the frame of the above CRP. All available data from 1960 were revisited and re-analyzed. The report is organized as follows. In Section 1 a new analysis of the DRC data is presented. In Section 2 the ARC data from available measurements are presented. The conversion of the data into a strength function with a detailed description of the

uncertainties is described in Section 2.1. In Section 2.2 the re-evaluated final PSF are internally validated against the DRC data. Finally, in Section 2.3 the ARC E1 and M1 data are compared with recent calculations using an axially-symmetric-deformed HFB+QRPA model. Conclusions are given in Section 2.4. In Section 3 the Total Atlas combining both DRC and ARC data is presented as the final recommended database of PSF derived from neutron resonance capture measurements.

References to Section 1:

[1.1] G A. Bartholomew et al., Adv.Nucl.Phys. 7 (1973) 229

[1.2] L.M. Bollinger and G.E. Thomas, Phys.Rev. C2 (1970) 1951; L.M. Bollinger, "Photonuclear Reactions and Applications" Pacific Grove, California (1973) 783

[1.3] R.B. Schwartz et al., Proc, Int. Symposium on Neutron Capture Gamma-rays Spectroscopy and related Topics, Petten (NH) (1974) 346

[1.4] R. Greenwood and C. Reich, Nucl.Phys. A 223, (1974) 66

[1.5] R. Greenwood and R. Chrien, Nucl.Instr.Meth. 138 (1976) 125

[1.6] A.F. Gamalii et al., Sov. J. Nucl. Phys 15, 1 (1972)

[1.7] Proc. 40th Ann. Conf. Nucl. Structure At. Nuclei, (Leningrad 1990)

[1.8] H. Ottmar et al., Proc, Int. Symposium on Neutron Capture Gamma-rays Spectroscopy and related Topics, Petten (NH) (1974) 658

[1.9] C.M. McCullagh, PhD thesis, Stony Brook, (1979)

[1.10] C.M. McCullagh, M. Stelts and R.E. Chrien, Phys. Rev. C23, 1394 (1981)

[1.11] J. Kopecky and M. Uhl, "Present status of experimental gamma-ray strength functions" ECN-RX-94-103, ECN (1994)

[1.12] P. Dimitriou et al., "Compilation and Evaluation of Reaction Gamma-Ray data" INDC(NDS)-0649 (2013). Available at: https://www-nds.iaea.org/publications/indc/indc-nds-0649/

[1.13] S. Goriely and P. Dimitriou, "Updating the IAEA Photonuclear Data Library and Generating a Reference Database for Photon Strength Functions", Summary Report of the 1st RCM, 4─8 April 2016, INDC(NDS)-0712 (2016). Available at: https://www-nds.iaea.org/publications/indc/indc-nds-0712/

[1.14] S. Goriely, M. Wiedeking and P. Dimitriou, "Updating the IAEA Photonuclear Data Library and Generating a Reference Database for Photon Strength Functions", Summary Report of the 2nd RCM, 16─20 October 2017, INDC(NDS)-0745 (2018). Available at: https://www-nds.iaea.org/publications/indc/indc-nds-0745/

[1.15] M. Wiedeking, D. Filipescu and P. Dimitriou, "Updating the IAEA Photonuclear Data Library and Generating a Reference Database for Photon Strength Functions", Summary Report of the 3rd RCM, 17─21 December 2018, INDC(NDS)-0745 (2019). Available at: https://www-nds.iaea.org/publications/indc/indc-nds-0745/

2. Direct Resonance Capture

2.1. Gamma-ray strength function – definition

The compound nucleus reaction mechanism is the dominant process for neutron capture reactions up to several MeV of incident neutron energy. Therefore, the statistical model is generally used to describe and calculate the capture cross sections and spectra at these energies. Exceptions to this general rule are thermal or resonance capture reactions in certain mass regions, where non-statistical processes become important.

The γ-ray transmission coefficient T_{XL} (used in statistical model calculations) is related to the γ-ray strength function f_{XL} (for a mode X and multipolarity L) by

$$T_{XL} = 2\pi E_\gamma^{2L+1} f_{XL}(E_\gamma) , \tag{2.1}$$

where E_γ is the γ-ray energy and L is the multipolarity of the radiation. Therefore, the knowledge of both theoretical and experimental f_{XL} is very important for the calculation of photon emission cross sections in all the reaction channels.

The $f_{XL}(E_\gamma)$ data are derived from the experimental partial radiative widths $\Gamma_{\gamma i}$ which are determined from the measured absolute gamma-ray intensities. The two types of experiments described in the previous section are usually used, *i.e.* capture on isolated resonances using TOF spectrometry and the average resonance capture (ARC) using filtered beams. Common to both experiments is the necessity to average over Porter-Thomas fluctuations which govern the distribution of the partial radiative width.

The differential strength function, determined for a number of primary transitions with known multipolarity, is defined as

$$f_{XL}(E_{\gamma i}) = \langle \Gamma_{\gamma i} / E_{\gamma i}^{2L+1} \rangle \cdot 1/D_\ell , \tag{2.2}$$

where $\Gamma_{\gamma i}$ is the partial radiative width and D_ℓ is the ℓ-wave resonance spacing. The partial radiative width is derived from

$$\Gamma_{\gamma i} = I_\gamma \cdot \Gamma_\gamma , \tag{2.3}$$

where I_γ is the absolute intensity of the gamma transition and Γ_γ is either the radiation width of the considered resonance or if this is not known, then the average radiative width $\langle\Gamma_\gamma\rangle$ is used.

In order to increase the statistical accuracy of the extracted strength function, the averaged quasi-mono energetic strength function was introduced. The average is taken over a selected number of primary transitions in a narrow energy region, neglecting the additional energy dependence above the phase factor. For an energy range equivalent to a FWHM of about 1 MeV, this is an acceptable assumption. The mean energy of the considered data is usually in the range of 6 – 7 MeV. This additional averaging is expressed by the double average symbols << >>:

$$\langle f_{XL}(E_{\gamma i})\rangle = \langle\langle \Gamma_{\gamma i} / E_{\gamma i}^{2L+1} \rangle\rangle \cdot 1/D_\ell , \tag{2.4}$$

where $\langle \Gamma_{\gamma i} / E_{\gamma i}^{2L+1} \rangle$ is a weighted mean over the used primary transitions.

2.2. Survey of early DRC measurements

Laboratories involved in DRC measurements were ORNL, LNL and BNL in the US, Chalk River in Canada and at the UKAEA Harwell, JINR Dubna and IRM Geel in Europe. The most recent measurements have been carried out in Dubna and Geel during the second half of the 1990s. The pioneering group which performed the largest number of measurements was the Neutron Physics Group at BNL headed by R.E. Chrien. It was not a surprise that this group published the first comprehensive collection of DRC data to compare the experimental gamma-ray decay properties with the predictions of the Single Particle or Giant Resonance models in 1981 [2.1]. The main output of this work was a database of binned model-dependent k(E1,M1) or S(E1) strength functionvalues, averaged not only over measured resonances but also over a number of gamma transitions in order to increase the statistical accuracy of the averaging procedure, which was often limited due to the small number of resonances. This database was later taken over by ECN in the frame of the BNL/ECN collaboration.

The first task of the present project was to review the neutron spacing values originating from the BNL book [2.2]. In this revision, the earlier resonance spacings D were updated using the 2006 BNL Atlas of Neutron Resonances [2.3]. The revised D values were published as an INDC report in Ref. [2.4]. The final listing of entries in Ref. [2.4] has been used as a starter file of chosen parameters to be used in further analyses.

The recent survey of DRC measurements resulted in a total number of 58 nuclides, ranging from ^{20}F up to ^{240}Pu, and the full listing with references is shown in Table 2.1. The measured data include mainly s-resonances with an exception in the low mass region ($A < 100$) where there are many p-resonances from the 3p neutron strength function giant resonance. The time spread of publications ranges from 1967 up to 2003, however, the majority of experiments were carried out in the 1970 – 1985 period. Only s- and p-wave resonances were considered, whereas a small number of d-wave resonances at very low A targets was used for ^{25}Mg and ^{29} Si nuclides only.

The format of the measured transition rate is also shown in Table 2.1, because this quantity forms the starting experimental input for processing and converting these data into the PSF format. The absolute calibration of the transition rate is taken from the original references and is considered as fixed. No attempt has been made to perform again this procedure.

Table 2.1 List of DRC measurements

#res - number of resonances, E1 and M1 transitions
ℓ_n - neutron orbital momentum of resonances
Ref. DRC - references listed in Appendix A
Tran. rate - absolute intensity/neutron capture ($I_{\gamma i}$) or partial radiative width ($\Gamma_{\gamma i}$) in eV
$\Gamma_{\gamma i^*}$ - stands for transition strength expressed in the GRM model formalism see Ref. [2.1]

Product nuclide	**#res**	**ℓ_n**	**Ref.**	**Tran. rate**	**Product nuclide**	**#res**	**ℓ_n**	**Ref.**	**Tran. rate**
F-20	2	*p*	[1]	$I_{\gamma\iota}$	Nd-144	10	*s*	[3]	$\Gamma_{\gamma\iota}$
Mg-25	1	*p*	[2]	$I_{\gamma\iota}$	Nd-146	10	*s*	[23]	na
Al-28	2	*s*	[3]	$I_{\gamma\iota}$	Sm-148	12	*s*	[24]	$I_{\gamma\iota}$
Si-29	2	*P*	[4]	$I_{\gamma\iota}$	Sm-150	3	*s*	[25] [26]	$I_{\gamma\iota}$
Si-30	1	*P*	[4]	$I_{\gamma\iota}$	Gd-153		*s*	[26]	$\Gamma_{\gamma\iota}$*
S-33	1	*P*	[1]	$I_{\gamma\iota}$	Gd-155	15	*s*	[27]	$\Gamma_{\gamma\iota}$*
Cl-36	1	*p*	[3] [5]	$I_{\gamma\iota}$	Gd-157	na	*s*	[26]	$\Gamma_{\gamma\iota}$*
Sc-46	2	*s*	[6]	$\Gamma_{\gamma\iota}$*	Gd-159	12	*s*	[26] [28]	$I_{\gamma\iota}$
Cr-53	1	*p*	[7]	$I_{\gamma\iota}$	Er-168	45	*s*	[30]	$\Gamma_{\gamma\iota}$
Cr-54	23	*s*+*p*	[8]	$\Gamma_{\gamma\iota}$*	Er-169	7	*s*	[31]	$\Gamma_{\gamma\iota}$
Fe-57	1	*p*	[9]	$\Gamma_{\gamma\iota}$	Tm-170	9	*s*	[32]	$I_{\gamma\iota}$
Fe-59	2	*p*	[10]	$I_{\gamma\iota}$	Lu-176	11	*s*	[33]	$I_{\gamma\iota}$
Co-60	1	*s*	[11]	$\Gamma_{\gamma\iota}$	Lu-177	6	*s*	[26] [34]	$I_{\gamma\iota}$
Cu-64	3	*s*	[12]	$I_{\gamma\iota}$	Yb-174	22	*s*	[15] [34]	$\Gamma_{\gamma\iota}$*
Ge-74	5	*s*	[13]	$I_{\gamma\iota}$	Hf-178	37	*s*	[35]	$I_{\gamma\iota}$
Nb-94	7	*s*+*p*	[14]	$\Gamma_{\gamma\iota}$	Ta-182	19	*s*	[3] [36]	$\Gamma_{\gamma\iota}$*
Mo-93	9	*s*+*p*	[15]	$\Gamma_{\gamma\iota}$	W-183	7	*s*	[3]	$I_{\gamma\iota}$
Mo-99	17	*s*+*p*	[16]	$I_{\gamma\iota}$	W-184	6	*s*	[3]	$I_{\gamma\iota}$

Product nuclide	**#res**	**ℓ_n**	**Ref.**	**Tran. rate**	**Product nuclide**	**#res**	**ℓ_n**	**Ref.**	**Tran. rate**
Ru-100	4	*s*	[17][18]	$\Gamma_{\gamma\iota}$	Pt-196	22	*s*	[37]	$\Gamma_{\gamma\iota}$*
Ru-102	6	*s*	[17][18]	$\Gamma_{\gamma\iota}$	Au-198	4	*s*	[38]	$I_{\gamma\iota}$
Rh-104	6	*s*	[19]	$I_{\gamma\iota}$	Hg-199	2	*s*	[39]	$I_{\gamma\iota}$
Pd-106	8	*s*	[3] [20]	$\Gamma_{\gamma\iota}$	Hg-200	3	*s*	[39]	$I_{\gamma\iota}$
Ag-108		*s*			Hg-202	3	*s*	[39]	$I_{\gamma\iota}$
In-116	31	*s*	[21]	$I_{\gamma\iota}$	Th-233	5	*s*	[40]	$I_{\gamma\iota}$
Sb-122	12	*s*	[22]	$I_{\gamma\iota}$	U-235	4	*s*	[40]	$\Gamma_{\gamma\iota}$
Sb-124	4	*s*	[22]	$I_{\gamma\iota}$	U-236	19	*s*	[41]	$I_{\gamma\iota}$
Te-126	6	*s*	[3]	$\Gamma_{\gamma\iota}$	U-237	7	*s*	[3] [42]	$\Gamma_{\gamma\iota}$
I-128	8	*s*	[3]	$I_{\gamma\iota}$	U-239	23	*s*	[43]	$\Gamma_{\gamma\iota}$
Ba-136	6	*s*	[3]	$\Gamma_{\gamma\iota}$	Pu-240	7	***s***	[44]	$\Gamma_{\gamma\iota}$

The following parameters, relevant for data processing, have been reviewed and updated where necessary:

1. The resonance angular momentum ℓ_n, initial spin J_i^{π}, the average capture width $\langle\Gamma_\gamma\rangle_{s,p}$ and the partial width $\Gamma_{\gamma i}$ values.
2. The absolute values of D_0 or D_1 used in the original compilations [2.5,2.6], have been updated several times and have therefore been the primary focus for the present re-evaluation. Two latest *D* compilations were reviewed in Ref. [2.4] and the conclusions were carefully re-examined in this work against the latest release of *Atlas of Neutron Resonances* in 2018 [2.7]. Lacking any comprehensive experimental knowledge of the spin dependence of level spacing $D(J)$, in cases where needed, the estimate based on the $(2J+1)$ dependence of the level density was applied.
3. The parameters of the final states of the product nucleus, such as their spin J_f and parity π, have been verified against the ENDSF database [2.8]. These parameters play an important role in the classification of measured primary transitions in E1, M1 or E2 modes.

The results of this parameter analysis are summarized in the table in Appendix B.

2.3. Processing DRC data in the PSF format

The next step in processing the DRC data is the conversion of the measured transition rates, using Eq. (2.3), into the PSF format. The following steps have been followed:

1. The list of measured transitions has been checked to confirm the assignment of primary transitions against the listing of final states and their spin and parity values from the ENSDF database.
2. Only transitions with $I_\gamma > dI_\gamma$ have been considered, transitions to final states not included in the ENSDF database have not been used for any conclusive PSF treatment.
3. The measured transition rates are usually given in absolute intensities I_γ per 100 or 1000 captured neutrons or in partial radiative widths $\Gamma_{\gamma i}$ in eV.
4. For the conversion of I_γ intensities to $\Gamma_{\gamma i}$ values the product of I_γ and Γ_γ was used, using either the average *s*- or *p*-wave Γ_γ width of all resonances or the partial width of discrete resonances in the DRC experiment. Values from Ref. [2.7] have been adopted for both cases. It seems that both approaches, in the view of all the other sources of uncertainties, differ negligibly and either can be safely used.
5. If the $\Gamma_{\gamma i}$ values were given in the data source, these values were adopted without any change. The reason for that is that the original I_γ could not be retrieved for recalculation and the applied Γ_γ are usually not quoted.
6. The average partial width $<\Gamma_{\gamma i}>$ over measured resonances for a given transition is determined by an unweighted average over all resonances of the same spin and parity as in Ref. [2.9]. However, a partial width equal to zero may occur due to experimental sensitivity limits and Porter-Thomas fluctuations. This effect was accounted for in Ref. [2.9] by the application of a missed intensity correction from the Porter-Thomas distribution using the intensity ratio of the smallest observed transition to the observed partial average width of this transition as an input parameter. This correction was neglected in the present analysis, for two reasons. In many data entries, the extraction of the above-mentioned ratio is not possible and further the effect is small in cases with many transitions measured. However, for nuclides ($A > 50$) with a limited number of transitions, the average $<\Gamma_{\gamma i}>$ may be slightly increased due to this omission.
7. Special care was devoted to ℓ_n assignments of measured resonances, especially, for light nuclides.
8. The dependence of the spacing on initial resonance spin has been taken into account for measurements with only one single resonance and/or for cases with more resonances but with only one spin value. See further discussion in the next section.
9. After implementation of the above steps, average partial radiative widths $<\Gamma_{\gamma i}>$ can be used in Eq. (2.4) to calculate the PSF. For dipole transitions, the average value of $<\Gamma_{\gamma i}>$ over measured resonances, reduced by the phase factor E_γ^3, and with a $D_{0,1}$ value adopted from Ref. [2.7], then gives the average partial strength function $<f(L)_i>$ using Eq. (2.4) (see an example in Table 2.3) given in 10^{-8} MeV^{-3} units.
10. The quoted uncertainties are standard errors based on the mean of statistical uncertainties from the gamma-ray spectra analysis taken from the original sources if the transition strength was given in $\Gamma_{\gamma i}$. For some nuclides (with strength in I_γ) the statistical and normalization ($\Gamma_{\gamma i}$) uncertainty was assumed to be 25%, as a conservative guess.

11. A special approach was applied for nuclides with contributions from both *s*- and *p*-wave resonances. The corresponding datasets have been treated separately and are then combined in one dataset including E1 and M1 transitions, *e.g.* E1 transitions in the *s*-wave capture becomes pure M1 transitions in the *p*-wave capture. A typical example of such a situation is shown for ^{93}Mo in Fig. 2.1.

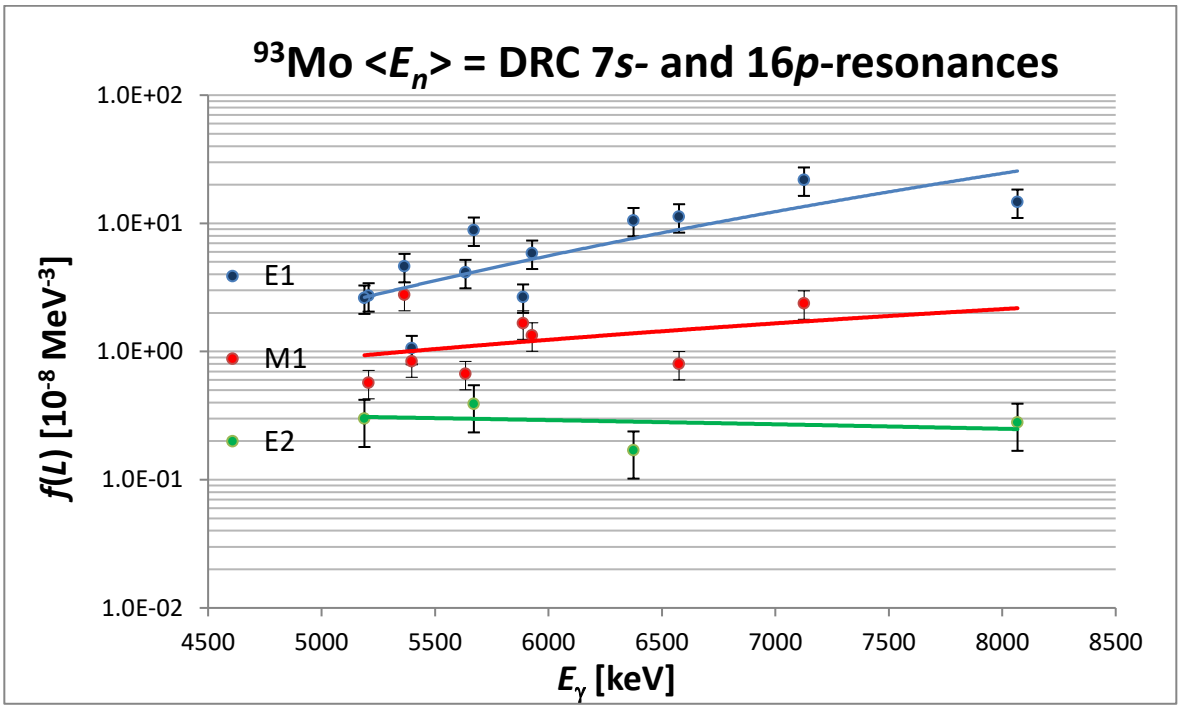

FIG. 2.1 *Two measurements combined in one data set with E1 and M1 transitions of the same energy originating from s- and p–wave capture. E1 and M1, E2 data originate from p- and s-wave capture, respectively. Note the rather good averaging (relatively small data dispersion) due to averaging over 23 resonances.*

The final data are given in Excel spreadsheets, as for the ARC data [2.10] and are stored in a database called "ATLAS DRC *f*(*L*)" for 57 nuclides. The data format is organized as follows: The basic information on the data source, transition strength units, measured resonances with used Γ_γ and resonance spacing is included in the heading. In cases where the original data source gives the transition strength in partial $\Gamma_{\gamma i}$ values, these results are directly adopted. Further, the Porter-Thomas dispersion estimate $1+ dPT = 1 + \sqrt{(2/\upsilon)}$, with υ = number of resonances, which can serve as a crude classification of the averaging power.

2.4. Comment on the data dispersion

Some features of averaging of DRC data are discussed, which may influence the dispersion of measured partial $f(L)_i$ values. A clarifying remark is needed to show the difference in averaging between two PSF experiments. In the filtered beam ARC experiments, the averaging over all resonances present in the neutron window is done in the experiment itself as what is measured is the combined transition strength from all the resonances. In the TOF DRC measurements, the transition strength of the primary transitions is measured in discrete resonances and stored as such. The averaging over all measured resonances is then calculated as a mean value for N entries, where N is the number of measured resonances.

1. The first two reasons which cause the data dispersion are the statistical uncertainty of measured gamma ray intensities and the Porter-Thomas fluctuations of the transition strength, which is the major source of fluctuations. They both belong to the physics of the experiment. The statistical uncertainty depends on the quality of the experimental set-up (neutron flux, detection quality, …) and is typically 5 – 20 % for strong transitions but can be up to 50% for the very weak ones. The size of Porter-Thomas dispersion is decreased by measuring more resonances and possibly also by averaging over several gamma transitions. The Porter-Thomas fluctuations usually significantly dominate the statistical fluctuations. Additional contributions to errors and uncertainties of derived $\langle f(L)\rangle_i$ are the uncertainties in the values of the total radiative width Γ_γ and of the resonance level spacing D. They are typically of the order 10 – 20%. They are not included in the quoted errors in Table 2.3 but considered for the final data systematics.

2. Another source of data dispersion originates from the multiple spins J_i of the initial states. If the initial resonance spin can have two values, e.g. $J_t \pm 1/2$ for *s*-wave resonance, the dipole transitions to outer spins ($J_t \pm 3/2$) can come from only one resonance spin (see Fig. 2.2 taken from Ref. [2.11]) and this is considered in the averaging procedure. For *p*-wave capture the situation is even more complicated.

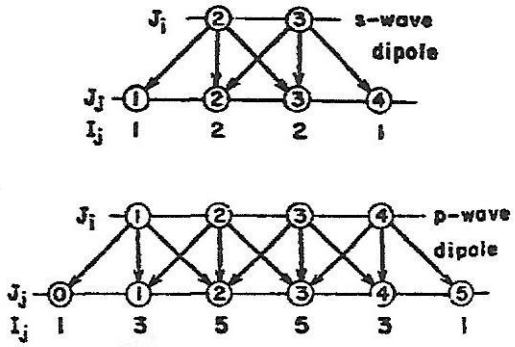

FIG.2.2 *Schematic picture of multiple populations from $J_i \pm ½$ and $J_i \pm ½ \pm 3/2$ final spins in s- or p-wave captures. The multiple population correction factors are shown as I_j estimates.*

This effect has been accounted for in the filtered beam experiments (ARC data) and has been corrected in the processing [2.11]. Due to the large number of resonances there is usually an equal number of initial spins present and the simplified correction factors, shown in Fig. 2.2 as I_j, can be applied. This approach was confirmed by Monte Carlo

simulations [2.12]. However, an important condition is needed, namely an unambiguous knowledge of the final spins J_j is required. This is usually only true for several of the largest primary transitions. Therefore, a few transitions remain uncorrected but due to the very good averaging of ARC experiments this does not severely influence the trend of the transition strength as a function of E_γ.

3. Another situation is present in DRC experiments, where transitions from discrete resonances are measured and a multiple population of final states is not present. The data can be processed (averaged) separately in groups with the same initial spin and later averaged over these groups. In several recent publications this approach is applied, and the final data are presented in separate J_i spins groups (Refs. [2.13-2.15]). However, this approach needs a reasonably large number of resonances, in order to make the second averaging (over spin groups) correct. If this condition is not fulfilled (e.g. for light mass nuclei or a measurement with small number of transitions) then the double averaging may be misleading due the weight of strongly deviating entries. In such cases a careful application of the I_j correction factors (as for ARC experiments) may be used.
4. Another complication in the interpretation of DRC results can come from the non-statistical mechanism in the reaction channel, which may influence the transition strength. This happens typically in low-mass A nuclides and may dominate over the statistical nature of the capture process. This effect has been reported in several experiments, such as ^{36}Cl, ^{53}Cr or ^{57}Fe p-wave capture [2.16-2.18]. In these measurements there is a strong positive correlation between thermal and resonance capture intensities and/or spectroscopic factors and an explanation by the one step particle transfer or two step valence capture via doorway states in s- and p-wave levels was proposed. In these measurements, the M1 strength is often larger than the E1 strength. The use of such data to derive the systematic dependence of $f(L)$ on the mass A can be misleading, because it may incorrectly influence the general trend of compound nucleus modeling.

The data file *"ATLAS DRC f(L)"* includes all available DRC measurements for 57 nuclides stored in the standard E_γ, $f(L)$, $df(L)$, E_x and J^π format. This is the first time that DRC data were processed as differential data into a database in a similar manner as for the ARC measurements. Some of the DRC data have, due the presence of a small number of resonances, an inferior accuracy, as demonstrated in Fig. 2.3, but in general many of them can form a rich complementary extension to the *"ATLAS ARC f(L)"* [2.10].

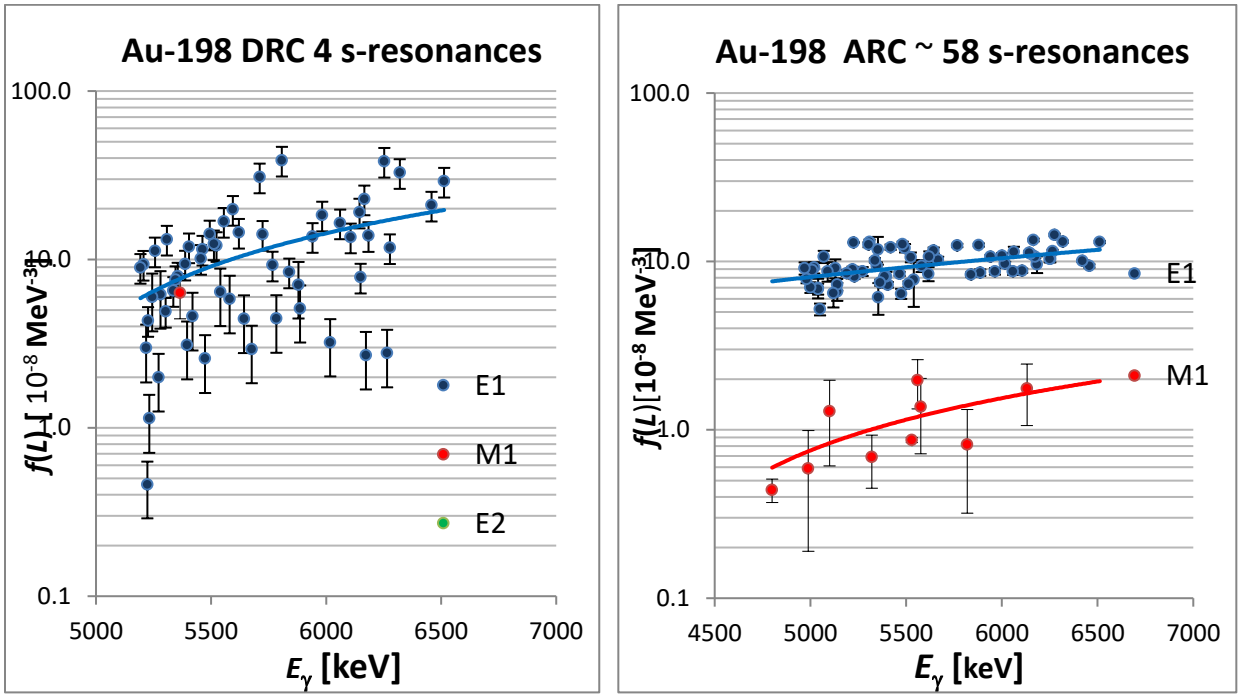

FIG.2.3 *PSF partial data averaged over 4 s-wave resonances. Note the dispersion of E1 data over more than one decade, slightly more than the Porter-Thomas estimate. For a comparison with the filtered ARC beam experiment the plot of the same nuclide is shown for the Sc filter. Note the improvement in the dispersion and the detection of M1 transitions due to the higher flux of the filtered beam.*

2.5. Processing the quasi-mono energetic strength functions

In order to increase the statistical accuracy of DRC data, the averaged quasi-mono energetic strength function was introduced in Eq. (2.4). The advantage of this approach is that the data can be used either for a direct calibration of averaged ARC measurements or for derivation of the $\langle f(L) \rangle$ systematic as a function of the mass A.

Data for each nuclide from Table 2.1 have been inspected and E1 and M1 transitions selected for the averaging of binned gamma transitions with the mean energy $\langle E_{\gamma i} \rangle$. Following Eq. (2.4) the phase factor reduction $\langle E_\gamma^3 \rangle$ is applied and no additional energy dependency is assumed, which is appropriate if the energy region is sufficiently narrow. An inspection of these data shows that for the majority of f(E1) and f(M1) values the $\langle E_\gamma \rangle$ value does not deviate too much from the 6 – 7 MeV energy range (see Fig. 2.4).

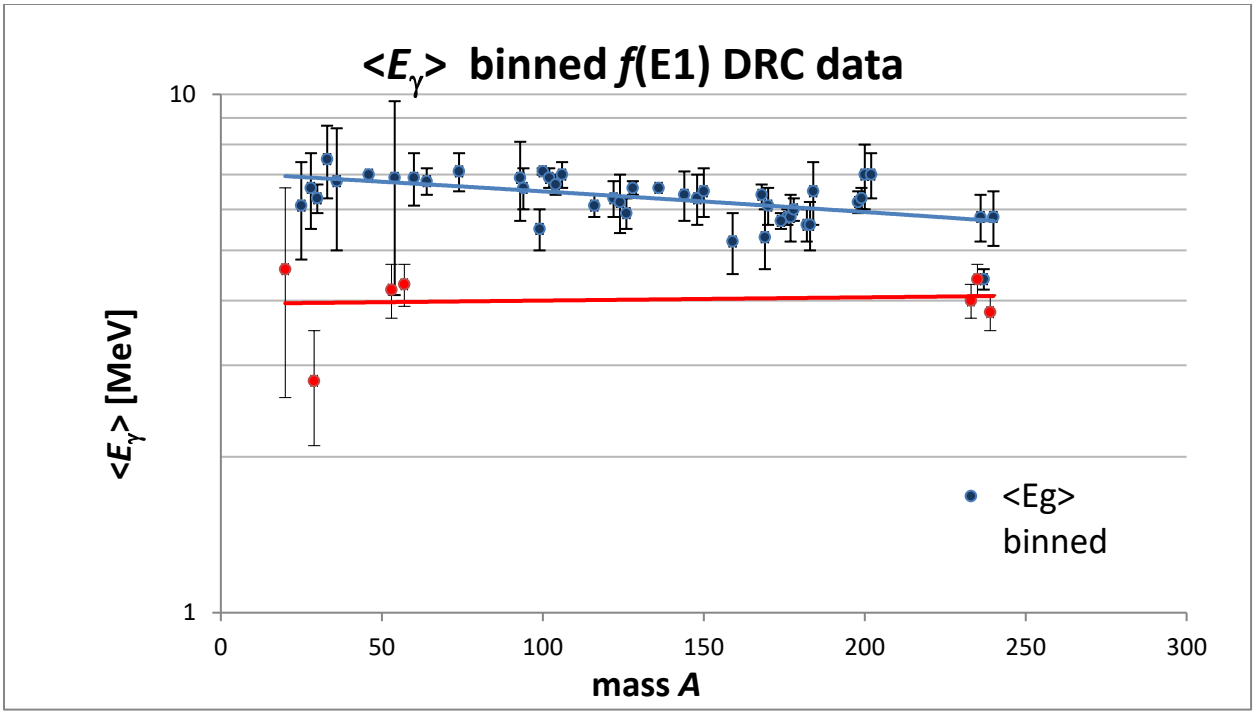

FIG. 2.4 *The mean energy <E_γ> used in the derivation of <<f(E1)>> values; the window width is plotted as an error bar. The red data points show nuclides which significantly differ from the main trend 6 – 7 MeV and may be influenced by the difference in the <E_γ^3> phase factor.*

Data significantly outside this region, such as ^{20}F and/or the actinides, may deviate from the general trend dependence, and the energy correction due to the additional energy dependence $(E_\gamma/< E_\gamma>)^2$ may be considered.

Results of the analysis are shown in Table 2.4. The relevant parameters used are shown, each nuclide has two lines, the upper one includes results from Ref. [2.4], printed (in small italic font), and the present results are in the lower one. The number of resonances and gamma-rays used in the evaluation indicates the degree of averaging. The mean value of <E_γ> for the adopted data is <E_γ> = 6.0 MeV for both E1 and M1 multipolarities.

Table 2.4 Evaluation of the quasi-mono energetic strength function f(L)

#res - number of included resonances with their ℓ_n assignment
E1, M1 - number of selected E1 and M1 transitions for the averaging
Spacing - spacing used for the evaluation in Eq. (2.2)
$D0^J$ $D1^J$ - estimated spin dependent value of the spacing D_0 and D_1 for the spin J
<f(L)/d(L)> - the average PSF value with the uncertainty
$< E_\gamma >/\Delta$ - mean energy $E_\gamma \pm \Delta$ of the 2Δ window

Nuclide	**# res**	**E1**	**M1**	**Spacing**	**<*f*(E1)> (*d*<*f*(E1)>)**	**$<E_\gamma>/\Delta$**	**<*f*(M1)> (*d*<*f*(M1)>)**	**$<E_\gamma>/\Delta$**
				eV	**10^{-8} MeV^{-3}**	**MeV**	**10^{-8} MeV^{-3}**	**MeV**
F-20	*2(p)*	*5*	*3*	*D1=33200*	*1.8(11)*	*4.4*	*4.26(310)*	*4.4*
	2(p)	7	3	D_1=60000	0.63(20)	4.6/2.0	2.41(23)	5.0/0.3
Mg-25	*1(p)*	*4*		*D1=158000*	*4.68(344)*	*6*		
	1(p)	4		$D1^{3/2}$=237000	2.21(30)	6.1/1.3		
	1(d)		4	$D2^{3/2}$=220000			0.16(3)	6.1/1.3
Al-28	*2(s)*	*5*	*2*	*D0=53700*	*0.55(34)*	*6.6*	*0.77(51)*	*6.9*
	1(s) 1(p)	4	 2	$D0^3$=90630 $D1^3$=97412	0.11(3)	6.6/1.1	 0.38(9)	 7.2/0.5
Si-29	*2(p,d)*	*5*	*2*	*D0=332200*	*0.03(2)*	*6*	*0.02(1)*	*5.4*
	1(p)							
	1(d)	2	4	$D2^{5/2}$=136800	0.35(10)	2.8/0.7	0.30(3)	7.4/1.3
Si-30	*1(p)*	*2*		*D1=52400*	*1.09(75)*	*6.9*		
	1(p)	2		$D1^2$=94320	2.59(56)	6.3/0.4		

S-33	*1(p)*	*4*	*3*	*D0=179000*	*0.17(12)*	*7.5*	*7.5(8)*	*????*
	1(p)	3	3	$D1^{3/2}$=138900	0.33(3)	7.5/1.2	0.71(13)	4.2/1.2
Cl-36	*1(p)*	*9*	*5*	*D0=22300*	*0.14(7)*	*7.2*	*0.33(20*	*5.4*
	1(p)	9	5	$D1^{2}$=192000	0.45(7)	6.8/1.8	0.83(6)	5.6/1.0
Sc-46	*2(s)*	*13*	*9*	*D0=1030*	*2.03(74)*	*7*	*1.48(75)*	*7.2*
	2(s)	12	5	D0=1030	0.46(10)	7	0.63(20)	7.2
Cr-53	*na*							
	1(p)	2	8	$D1^{3/2}$=15750	5.44 (167)	4.2/0.5	1.53(13)	6.3/1.6
Cr-54	*23(sp)*	*33*	*31*	*D0=5960?*	*2.07(24)*	*6.7*	*0.70(7)*	*6.7*
	8(s)	15	31	D0=7100	9.80(150)	6.9/2.8	0.59(7)	6.7/2.3
	15(p)	5		D1=2200	6.90(170)	5.9/0.8		
	s+p	20			8.35(160)	6.9/2.8		
Fe-57	*na*							
	1(p)	3	17	$D1^{1/2}$=23100	0.17(9)	4.3/0.4	0.48(10)	5.5/2.2
Fe-59	*na*							
	2(p)		8	D1=5030			0.33(13)	5.4/1.2
Co-60	*1(s)*	*8*		*D0=1390*	*2.06(111)*	*7*		
	1(s)	8		$D0^{4}$=3128	2.45(60)	6.9/0.8		
Cu-64	*3(s)*	*9*		*D0=722*	*1.33(34)*	*7.5*		
	4(s)	10	2?	D0=700	2.72(68)	6.8/0.4	4.08(102)	6.3/0.1

Ge-74	*5(s)*	*7*	*7*	*D0=64???*	*2.64(90)*	*7.1*	*2.05(70)*	*7.9*
	6(s)	5	6	D0=99	5.65(140)	7.1/0.6	2.17(55)	7.6/1.1
Nb-94	*7(sp)*	*15*	*16*	*D0=84.8*	*2.24(55)*	*6.5*	*0.53(13)*	*6.5*
	3(s)		14	D0=84.8			0.15(3)	6.6/0.6
	4(p)	16		D1=50	4.96(124)	6.6/0.6		
Mo-93	*8(s)??*	*10*		*D0=970??*	*1.91(36)*	*5.5*	*0.26(4)*	*5.5*
	7(s)		8	D0=2700			1.38(35)	6.4/0.7
	16(p)	10		D1=780	7.36 (220)	6.9/1.2		
Mo-99	*17(sp)*	*7*	*8*	*D0=970*	*1.91(36)*	*5.5*	*0.26(5)*	*5.5*
	6(s)		8	D0=970			0.44(11)	5.5/0.5
	11(p)	9		D1=286	6.28(159)	5.5/0.5		
Ru-100	*4(s)*	*5*	*10*	*D0=21.7*	*4.3(6)*	*6.9*	*3.07(171)*	*7.4*
	4(s)	4	8	D0=21.3	8.48(212)	7.1/0.1	2.42(0.73)	7.2/0.4
Ru-102	*6(s)*		*5*	*D0=18.5*			*5.32(213)*	*7.8*
	6(s)	4	7	D0=18	21.7(54)	6.9/0.3	10.5(26)	7.1/0.5
Rh-104	*6(s)*	*4*	*2*	*D0=24.2*	*3.96(32)*	*6.9*	*0.52(31)*	*6.9*
	7(s)	10	9	D0=32	4.72(118)	6.7/0.3	1.31(39)	6.8/0.2

Pd-106	*8(s)*	*10*	*12*	*D0=10.9*	*4.14(95)*	*7.9*	*1.3(3)*	*7.9*
	9(s)	10	10	D0=10.9	3.87 (39)	7.0/0.4	0.91(28)	8.1/0.9
Ag-108	*9(s)*			*D1=36.8*	*2.19(35)*	*7.3/0.6*	*0.32(15)*	*7.3/0.6*
	na							
In-116	*31(s)*	*12*	*12*	*D0=9*	*5.87(168)*	*5.9*	*1.19(32)*	*6.1*
	23(s)	8	9	D0=9	11.9(30)	6.1/0.3	0.91(23)	6.1/0.2
Sb-122	*12(s)*	*9*	*9*	*D0=10*	*4.12(82)*	*6.1*	*0.82(16)*	*5.9*
	12(s)	10	7	D0=10	12.3(31)	6.3/0.5	1.64(46)	6.3/0.5
Sb-124	*4(s)*	*11*	*13*	*D0=24*	*3.0(2)*	*5.6*	*0.71(18)*	*5.8*
	4(s)	8	6	D0=24	4.79(126)	6.2/0.2	0.8(2)	6.3/0.2
Te-126	*6(s)*		*10*	*D0=42.7*			*1.4(3)*	*7.7*
	6(s)	8	16	D0=42.7	6.83(167)	5.9/0.4	1.32(46)	5.9/0.5
I-128	*8(s)*	*7*	*12*	*D0=9.7*	*1.9(5)*	*6.5*	*0.31(5)*	*6.5*
	8(s)	6	10	D0=9.7	8.54(256)	6.6/0.2	1.08(38)	6.6/0.3
Ba-136	*6(s)*	*1*	*4*	*D0=40*	*5.0(3)*	*6.6*	*1.67(84)*	*7.9*
	10(s)	1	7	D0=40	6.17(123)	6.6	1.10(38)	7.0/0.3
Nd-144	*10(s)*	*3*	*1*	*D0=37.6*	*5.40(22)*	*6.6*	*0.36(27)*	*6.3*
	10(s)	6	1	D0=37.6	6.17(117)	6.4/0.7	0.27(10)	6.3

Nd-146	*10(s)*	*2*		*D0=17.8*	*4.50(18)*	*6.7*		
	na							
Sm-148	*12(s)*	*16*		*D0=5.7*	*4.5(9)*	*6.6*		
	23(s)	18	11	D0=5.7	4.39(117)	6.3/0.7	1.39(35)	5.3/0.3
Sm-150	*3(s)*	*13*		*D0=2.2*	*7.83(157)*	*6.5*		
	3(s)	14		D0=2.2	5.42 (136)	6.5/0.7		
Gd-153	*na*	*na*		*na*	*11.0(3)*	*na*		
	na							
Gd-155	*15(s)*	*8*		*D0=13.8*	*8.70(18)*	*5.9*		
	na							
Gd-157	*na*	*5*		*D0=30.5*	*12.4(223)*	*6*		
	na							
Gd-159	*12(s)*	*8*	*9*	*D0=87*	*8.8(29)*	*5.3*	*1.5(3)*	*5.1*
	12(s)	9	8	D0=87	9.21(230)	5.2/0.7	1.22(32)	5.1/0.3
Er-168	*45(s)*	*6*	*4*	*D0=4*	*15.9(148)*	*6.4*	*4.7(5)*	*6.4*
	81(s)	10	4	D0=4	16.6(325)	6.4/0.3	4.23(102)	6.4/0.3

Er-169	*7(s)*	*6*	*9*	*D0=94*	*6.4(15)*	*4.9*	*1.6(9)*	*5.2*
	4(s)	9	1	D0=94	7.31(119)	5.3/0.7	1.56(47)	5.4
Tm-170	*9(s)*	*16*		*D0=7.28*	*4.72(101)*	*5.9*		
	10(s)	16	2	D0=7.28	6.31(126)	6.1/0.5	1.42(43)	6.0/0.2
Lu-176	*11(s)*	*8*	*2*	*D0=3.45*	*7.4(25)*	*5.8*	*3.2(14)*	*5.8*
	12(s)	8		D0=3.45	4.57(62)	5.8/0.2		
Lu-177	*6(s)*	*15*		*D0=-1.61*	*8.9(41)*	*5.9*		
	6(s)	13		$D0^{15/2}$=3.03	3.23(59)	5.8/0.6		
Y-174	*22(s)*	*5*		*D0=8.06*	*19.4(32)*	*6.3*		
	24(s)	12		D0=8.06	37.8(67)	5.7/0.2		
Hf-178	*37(s)*	*18*	*3*	*D0=2.4*	*18.5(35)*	*6.5*	*3.8(15)*	*6.2*
	20(s)	21	5	D0=2.32	31.7(676)	6.0/0.3	4.62(88)	6.0/0.3
Ta-182	*19(s)*	*66*	*1*	*D0=4.17*	*11.3(16)*	*5.2*	*7.17(384)*	*4.3*
	19(s)	24	5	D0=4.4	9.2(19)	5.6/0.4	1.3(3)	5.6/0.4
W-183	*7(s)*	*15*	*5*	*D0=66*	*10.7(33)*	*5.2*	*4.4(19)*	*4.7*
	7(s)	6	1	D0=63.4	10.6(26)	5.6/0.6	0.2(1)	4.9
W-184	*6(s)*	*13*		*D0=12*	*28.1(97)*	*6.3*		
	6(s)	10		D0=12	36.9(99)	6.5/0.9		
Pt-196	*22(s)*	*9*		*D0=16.3*	*17.2(22)*	*7*		
					No data			

Au-198	*4(s)*	*5*		*D0=15.7*	*11.4(53)*	*6.4*		
	4(s)	17	1	D0=15.7	20.0(41)	6.2/0.3	6.34(19)	5.4
Hg-199	*2(s)*	*4*		*D0105*	*55.3(253)*	*6.5*		
	2(s)	8	3	D0=105	27.8(30)	6.3/0.3	1.3(6)	5.6/0.3
Hg-200	*3(s)*	*9*		*D0=100*	*9.62(356)*	*7.2*		
	3(s)	11		D0=85	14.3(209)	7.0/1.0		
Hg-202	*3(s)*	*3*		*D0=100.5*	*8.47(693)*	*7.2*		
	3(s)	7		D0=90	33.7(80)	7.0/0.7		
Th-233	*5(s)*	*3*	*1*	*D0=18.2*	*21.1(88)*	*4.2*	*10.2(6)*	*4.5*
	5(s)	12	21	D0=18.2	33.4(836)	4.0/0.3	9.67(242)	4.2/0.3
U-235	*4(s)*	*53*	*19*	*D0=12.3*	*13.7(44)*	*3.9*	*2.4(9)*	*4.4*
	3(s)	11	8	D0=12.3	9.8(19)	4.4/0.3	2.46(11)	4.4/0.3
U-236	*na*							
	19(s)	6		D0=0.49	7.14(131)	5.8/0.6		
U-237	*7(s)*	*2*	*3*	*D0=14.7*	*8.55(369)*	*4.6*	*0.39(17)*	*4.8*
	7(s)	7	6	D0=14.7	4.45(112)	4.4/0.2	0.23(6)	4.6/0.5

U-239	*23(s)*	*9*	*5*	*D0=16.4*	*10.29(254)*	*3.8*	*2.6(8)*	*4.4*
	23(s)	10	5	D0=16.4	7.70(173)	3.8/0.3	2.10(57)	4.2/0.6
Pu-240	*na*							
	7(s)	5	2	$D0^1$ = 2.73	18.0(48)	5.8/0.7	2.68(67)	6.1/0.4

The given uncertainties for binned transitions include the average statistical errors of $\langle I_{\gamma i} \rangle$ or $\langle \Gamma_{\gamma i} \rangle$ taken from the original references. The Porter Thomas fluctuation has not been included in the quoted errors. It depends on the number of isolated resonances "υ" and may be estimated from the expression $\sqrt{(2/\upsilon)}$. Another quantity which may influence the calculation of $\langle\langle f(L) \rangle\rangle$ is the uncertainty in the resonance spacing. In several critical reviews some significant disagreements were spotted, and these may introduce an additional uncertainty to the evaluated strength functions (see [2.19]).

All surveyed data with their newly analyzed $\langle\langle f(L) \rangle\rangle$ values are displayed in Figs. 2.5 and 2.6 as a function of the mass number *A*. The dotted lines represent one standard deviation (SD) uncertainty (68% confidence limit) to give an impression of the size of fluctuations.

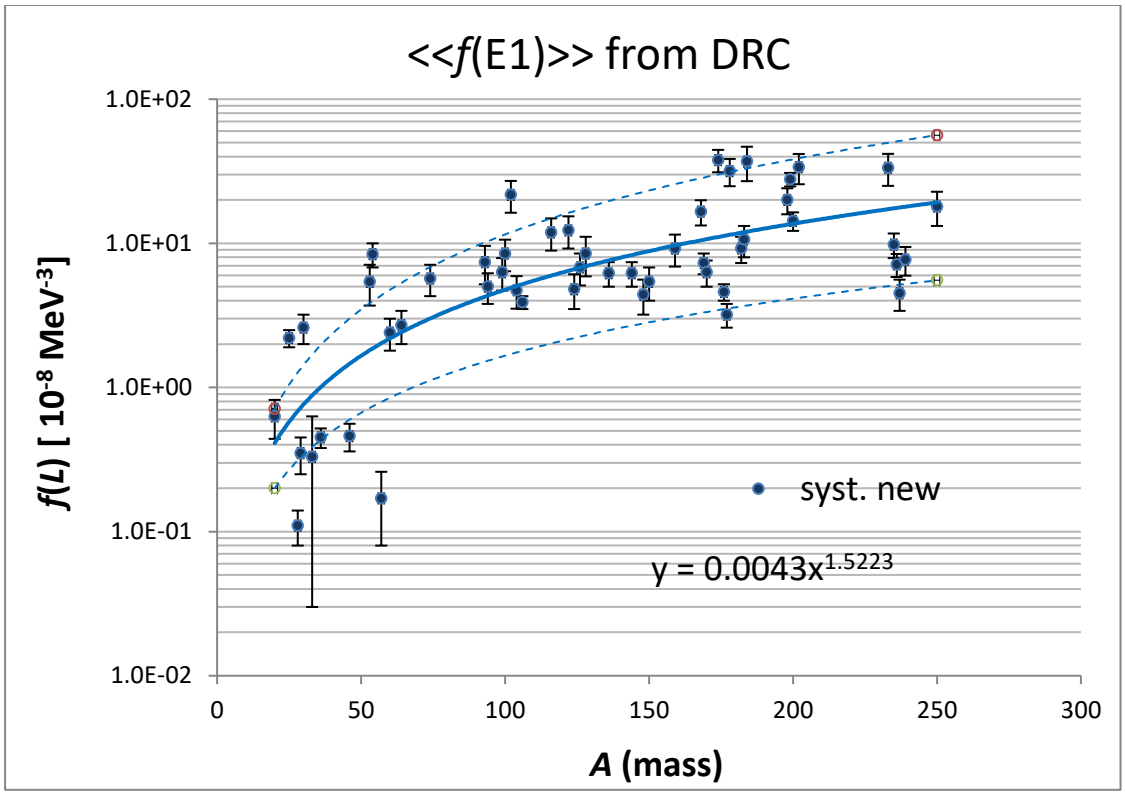

FIG. 2.5 *Quasi-mono energetic doubly average strength functions <<f(E1)>> from the present analysis with trend curve systematic as a function of the mass A. The dotted line is one SD dispersion from the LSQ procedure.*

The least square (LSQ) fit of the data using a power function with respect to the mass number A results in the following expression for the E1 and M1 strength function systematics:

$$<<f(\mathrm{E1})>> = 0.004\, A^{1.52\pm0.21} \text{ and } <<f(\mathrm{M1})>> = 0.12\, A^{0.49\pm0.10}, \qquad (2.5)$$

where $R^2 = 0.6$ and $R^2 = 0.13$ for E1 and M1, respectively. R^2 is a measure of the goodness of the fit to the data. The quoted uncertainties are one SD errors from the LSQ fit increased further by Γ_γ and D uncertainty estimates of 10%.

The E1 data reasonably follow the expected smooth trend (see Fig. 2.5) with two exceptions, the mass regions with $A < 50$ and $170 < A < 190$. The major outliers for light nuclides are now discussed in detail. The basic feature for these nuclides is that only one or two resonances are used (often *p*-wave capture); see ^{25}Mg, ^{28}Al, ^{29}Si, ^{30}Si, ^{36}Cl, ^{53}Cr, ^{57}Fe and ^{60}Co nuclides and the applied spacing has to reflect the spin dependence. The spin dependence of the spacing $D(J)$ was determined from the $(2J+1)$ dependence of the level density. Further, the non-statistical character of some primary transitions may be impacting the results. As discussed in Section 2.3, in the valence capture via doorway states in *s*- and *p*-wave levels, the M1 strength is larger than the E1 strength. This may be the explanation for these data points falling below the trend.

The scatter in the $170 < A < 190$ region is more complex and is greatly influenced by an enhancement by 3 major outliers, ^{174}Yb, ^{184}W and ^{202}Hg. One explanation may be that they are deformed nuclides, see also other entries in the $160 < A < 190$ region, with an increased gamma

strength, as discussed in Ref. [2.20], and for which an empirical enhancement factor had to be introduced in the EGLO model. It is, however, difficult to postulate any additional excitation mode in this region from the present data, because of the data dispersion. Finally, a strong overestimation of the trend line was found for the ^{102}Ru nuclide, both for E1 and M1 radiations. There is no explanation available for this nuclide.

The situation for M1 radiation is complicated for several reasons. The systematic trend of the M1 strength function (see Fig. 2.6) shows a similar mass dependence as the E1 case. However, the data fluctuation is broader, which may point to larger inaccuracies of M1 compared to E1 data. Possible reasons may be less statistical accuracy, inadequate averaging, etc. To deal with this situation, the two SD criterion has been used to identify the outliers. The most probable theoretical model for M1 transition strength above 5 MeV is a standard Lorentzian based on the spin-flip resonance and the Brink hypothesis. In such a case the presented data are close to the resonance maximum or its tail at lower energies.

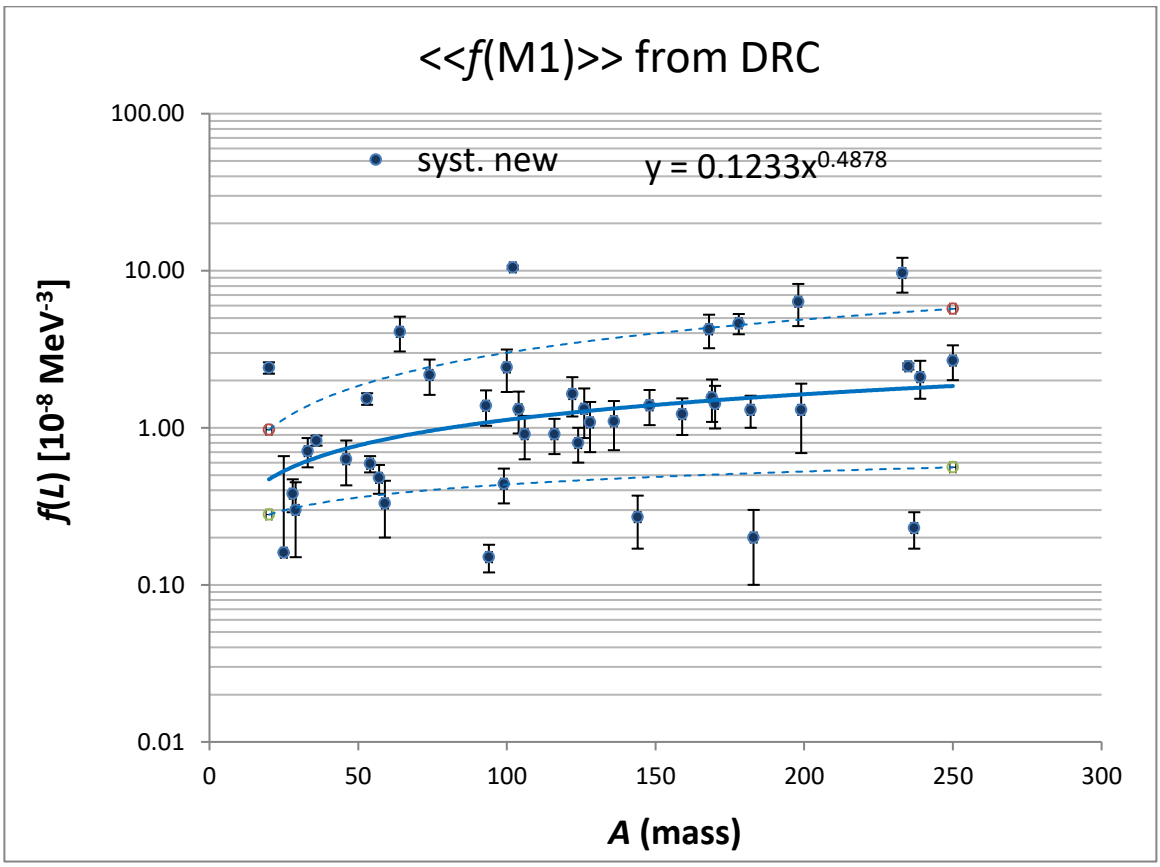

FIG. 2.6 *Quasi-mono energetic doubly average strength functions <<f(M1)>> from the present analysis with trend curve systematic as a function of the mass A. The dotted line is two SD dispersion from the LSQ procedure.*

The strongly enhanced point of ^{102}Ru nuclide is discussed above in the E1 section. Three strongly underestimated data points above A = 150 belong to ^{144}Nd, ^{183}W and ^{237}U, with only one M1 transition and therefore the uncertainty is very large. Some of the data in the mass range A = 150

– 200 seem to cluster again in an enhanced structure. A more detailed discussion of the major outliers is given for both E1 and M1 data in Ref. [2.20].

The dispersion of the doubly average <<*f*(E1)>> strength function data in Fig. 2.4 comes primarily from the Porter-Thomas fluctuations (insufficient averaging), the statistical uncertainty of the gamma-ray analysis, the mass dependence of the *f*(E1) model above the E_γ^2 factor from the tail of the GDR but also from the uncertainty in the absolute detector efficiency standards converting the relative gamma-ray intensity in absolute scale per captured neutron or partial radiative width. Besides the considered uncertainties (statistical errors of the gamma-ray spectra analysis and of quantities Γ_γ and the spacing *D*) and the Porter Thomas dispersion, another uncertainty may play a role. This uncertainty arises from the TOF absolute calibration of the measured intensities I_γ which is usually performed in a separate measurement using the Au 4.9 eV standard or some other known resonances present in the target sample. This procedure is, however, dependent on the parameters used which may have changed considerably in the period since 1960. This fact has never been accounted for in the DRC processing yet and may in some cases be the reason for some of the outliers. To renormalize the data in the literature with the most recent standards is an action beyond the scope of the present project. Furthermore, to extract the original experimental data from some older references is not possible. These arguments support the conclusion that the trend <<*f*(E1)>> systematic is most probably the best absolute E1 strength information.

2.6. Comparison with previous DRC analysis

Both latest evaluations, the present one and that of Ref. [2.4], in general, agree (see Figs. 2.7 and 2.8) with comparable data dispersion. In both plots the data points together with the systematics curve are shown and in the lower part (green data points) the ratio of "old/new" data is given using the scaling 10^{-3} for E1 and 10^{-2} ratio for M1. The reason for showing this comparison is that these two independently processed data may point out to and possibly verify some shortcomings in applied assignments or incorrect use of parameters.

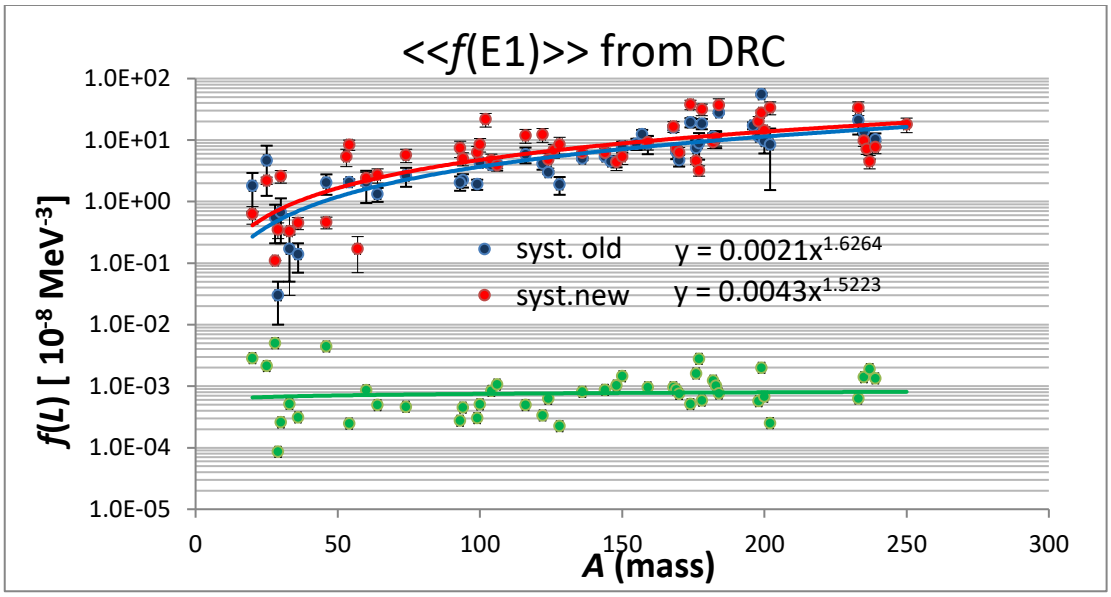

FIG. 2.7 *Quasi-mono energetic doubly average strength functions <<f(E1)>>from the present (new) and previous (old) analysis with trend curve systematic as a function of the mass A. Green data show the ratio of old/new systematic data point using a 10^{-3} scale.*

Both evaluations show a rather similar trend and agree rather well. For the E1 radiation the recent systematic for nuclides with $A < 100$ is slightly higher and this may be due to several low mass data points in the earlier data set, which show some differences in both treatments. Another reason may come from several newly introduced assignments of E1 instead of M1 transitions based on the recent J^{π} values of final states. For M1 radiation both systematic equations give almost the same trend.

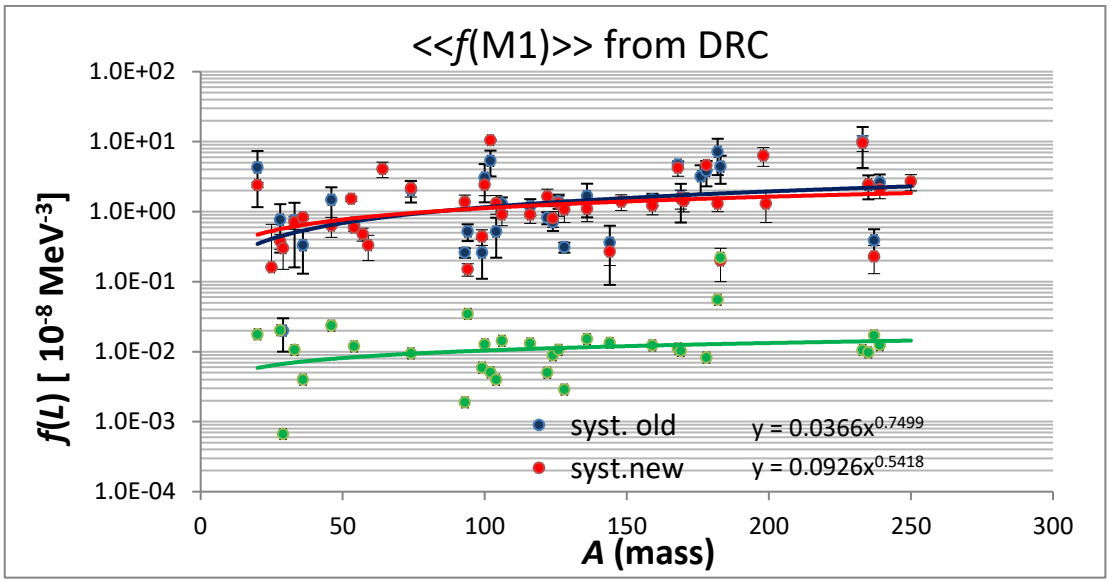

FIG. 2.8 *Quasi-mono energetic doubly average strength functions <<f(M1)>> from the present (new) and previous (old) analysis with trend curve systematic as a function of the mass A. Green data show the ratio of old/new systematic data point using a 10^{-2} scale.*

2.7. The absolute calibration of the E1 strength

The importance of DRC data and the recent analysis is not only to provide new PSF data but also to make available a tool for absolute normalization of the ARC data. The comparison of the quasi-mono energetic strength function data of the present and previous analyses from Ref. [2.4] show a very good agreement of the systematics equations $<<f(\mathrm{E1})>> = 0.004A^{1.52}$ and $<<f(\mathrm{E1})>> = 0.002A^{1.63}$, respectively. This result demonstrates that even though some data in these two data sets differ, the final data dispersion is almost equal. Even the older data from 1994 [2.6] are in satisfactory agreement (see Fig. 2.9).

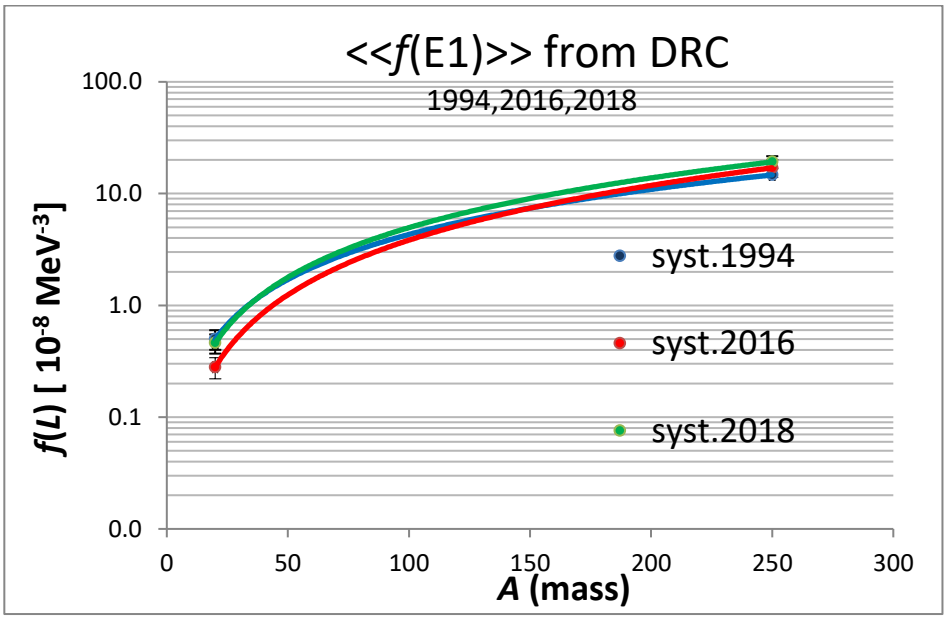

FIG. 2.9 *Comparison of << f(E1)>> trend systematic from Refs. [2.11,2.15] and the present data from Eq. (2.6).*

Majority of data lie between 6-7 MeV, except for the low mass and actinide nuclides. Therefore, we may conclude that the average E1 strength at the excitation of 6 – 7 MeV can be described by the equation

$$<<f(\mathrm{E1})>> = 0.004\mathrm{A}^{1.52}, \qquad (2.6)$$

and can be used as an absolute normalization of experimental results or theoretical predictions. Because the M1 strength is always present in such studies, the calibration of the M1 strength may be related to the absolute E1 strength.

The E1 systematic trend has been successfully applied for absolute normalization of the *ATLAS f (L)_ARC_ 2017* database [2.20] for nuclides without corresponding DRC measurements. The agreement between the systematics from 2016 and 2018 was satisfactory but for a new normalization of the next *ATLAS f (L)_ ARC+DRC,* the present results are recommended.

2.8. Conclusions

The earlier DRC measurements have been revisited and newly processed into average strength functions, both as differential (for the first time) and binned (transitions in a gamma energy window) data for 57 nuclides from ^{20}F up to ^{240} Pu [2.21]. Several DRC nuclides include enough resonances and may be used to extract PSFs that can be included in the new comprehensive database of PSFs using combined data from both DRC and ARC measurements (as described in Sections 2 and 3).

Finally, another assessment concerns the use of quasi-mono energetic strength function data for the normalization of the corresponding ARC data (see Sect. 3.1.4). The performance of the trend systematic therefore raises a question whether the use of Eq. (2.6) should not be applied generally for all nuclides. Some more testing of this procedure is recommended in the future.

References to Section 2:

[2.1] G A. Bartholomew et al., Adv.Nucl.Phys. 7 (1973) 229

[2.2] S.F. Mughabghab "Atlas of Neutron Resonances" (Academic Press 1981, 1984)

[2.3] S.F. Mughabghab "Atlas of Neutron Resonances" (Elsevier 2006)

[2.4] J. Kopecky, "Present status of experimental gamma-ray strength functions derived from neutron capture" INDC(NED)-013 (2016)

[2.5] C.M. McCullagh, M. Stelts and R.E. Chrien, Phys. Rev. C23, 1394 (1981)

[2.6] J. Kopecky and M. Uhl, "Present status of experimental gamma-ray strength functions" ECN-RX-94-103, ECN (1994)

[2.7] S.F. Mughabghab "Atlas of Neutron Resonances" (Elsevier 2018)

[2.8] Evaluated Nuclear Structure Data File (ENSDF), http://www.nndc.bnl.gov/ensdf/

[2.9] C.M. McCullagh, PhD thesis, Stony Brook, (1979)

[2.10] J. Kopecky, "Atlas of average resonance capture data (Starter file)" INDC(NDS)-0738 (2017)

[2.11] R.E. Chrien, "Neutron resonance averaging with filtered beams" BNL- 36646 report (1985)

[2.12] R.E. Chrien, "Fourth Int. Symposium on Neutron Induced Reactions", Smolenice (1985) 200

[2.13] F. Becvar et al., J. of Nucl.Phys. (Russian) 46 (1987) 3

[2.14] F. Becvar et al., Proc. Of the Int. Conference on Neutron Physics, Kiev (1988) p.8

[2.15] F. Becvar et al., Yad.Fiz. 46 (1987) 392

[2.16] R.E. Chrien and J. Kopecky, Phys.Rev.Lett. 39 (1977) 911

[2.17] J. Kopecky et al., Nucl.Phys. A334 (1980) 35

[2.18] R .E. Chrien and J. Kopecky, Phys.Rev. C1 (1970) 973

[2.19] J. Kopecky, "Atlas of average resonance capture data (Starter file)" INDC(NED)- 0772 (2017)

[2.20] J. Kopecky, M. Uhl and R.E. Chrien, Phys.Rev. C47 (1993) 312

[2.21] J. Kopecky, "Revisions and Updates of Experimental Gamma-ray Strength Functions derived from the Discrete Neutron Resonance Capture" INDC(NDS)-0738 (2018)

3. Average Resonance Capture

3.1. Survey of early ARC measurements

The ARC technique was developed to overcome the Porter-Thomas fluctuations of the primary intensities from thermal or isolated resonance capture. It was realized that by simultaneous averaging over many resonances the Porter-Thomas fluctuations can be reduced and the primary transitions to the final states of given J^{π} have approximately the same intensity and can represent the distribution of partial radiative width.

Three types of experiments are usually used in the average resonance capture (ARC) technique with filtered beams. The instrumental part and the basis of the average resonance capture method have been well documented in previous surveys [3.1-3.6]. The principle of the statistical analysis has been covered in the following references [3.7-3.11]. The materials, ^{10}B, ^{45}Sc or ^{56}Fe, have been used for ARC experiments where the neutron beams are produced by transmission through filter materials yielding neutron beams with bell-shaped energy distribution having different FWHM at neutron energies of about 150 eV, 2 keV and 24 keV, respectively. The boron-filtered beam primarily removes the thermal component, while for Sc and Fe the neutron-capture cross section interference dips yield quasi mono-energetic beams of a few keV wide. For specific information about filtered beam facilities see the Introduction and Ref. [3.12].

3.2. Data extraction

We have re-analyzed all available ARC data from different beam facilities. The list of data sources used in this re-evaluation is given in Appendices C and D. It includes all measurements, which have been recovered from the period after 1970 with their references. Some of the data, originating from the former collaboration between BNL (R.E. Chrien) and ECN (J. Kopecky), are referred to here as BNL/ECN database and include some published and unpublished data. The motivation behind this effort was to form a complete starter file of ARC measurements to be used for extracting PSF data; however, the job was not completed at that time.

The ENDSF and EXFOR databases were searched for ARC data sources. This action resulted in the selection of about 60 references. They include all the measurements whose data could be recovered. Corresponding references are quoted; some of the unpublished data are included in a private database denoted as BNL/ECN database. The majority of publications focused on the spectroscopy of final states in the product nucleus and only a few publications provided the measured data as PSF results [3.13-3.16]. The recommended set of data for the final $fL(E_{\gamma})$ database is shown in the 5th column of the table in Appendix C.

The average differential strength function $\langle fL \rangle$, determined for a number of primary transitions with $L = 1$, is defined as

$$\langle fL(E_{\gamma i}) \rangle = \langle \Gamma_{\gamma i} \rangle / E_{\gamma i}^{3} / D_0 \ , \qquad (3.1)$$

where $\Gamma_{\gamma i}$ is the partial radiative width, $E_{\gamma i}$ is the transition energy and D_0 is the *s*-wave resonance spacing. Note that for the DRC measurements the parameters of the initial state are well defined by a single resonance (with orbital momentum ℓ_n and J^{π}) and the averaging over more resonances is performed in the data processing. In contrast, in the ARC experiment the averaging is performed effectively during the measurement itself, due to the large number of resonances present in the

filtered beam neutron window. However, the information on $< \Gamma_{\gamma i}>$ is not available and a normalization of the measured average gamma-ray intensity $<I_\gamma>$ to a standard value taken from DRC data is applied.

The ARC results are usually given in reduced intensities either as $<I_\gamma/E_\gamma^3>$ (assuming a common phase factor for both dipoles and quadrupole transitions) or as $<I_\gamma/E_\gamma^5>$ values (the assumed energy dependence of the Brink-Axel model) in arbitrary units. All the retrieved measurements have been re-analyzed and the resulting $<I_\gamma/E_\gamma^3>$ values form the starter database of ARC data (AtlasIgE3). The AtlasIgE3 file includes all the retrieved data, even if the same reaction was studied by several authors. The major effort was to convert all the results (often presented also as I_γ only) in the common $<I_\gamma/E_\gamma^3>$ format and furthermore to reconfirm the multipolarity assignments of E1, M1 and E2 groups. For this purpose, for every target input the corresponding final states, with their J^π assignments taken from the recent ENDSF file, are included and compared with the previous assignments. For some transitions the corresponding final state was not quoted or was in conflict with the assignment, and for these cases the 24 keV data were used for further information. In particular, the kinematic shift between 2 and 24 keV data was employed and furthermore the standard 2/24 keV intensity ratio was used for parity assignment.

All errors quoted in the retrieved publications have been adopted as experimental statistical errors in the AtlasIgE3 data base. They include the uncertainty of the gamma-ray spectrum analysis, namely the statistical accuracy and absolute intensity calibration, derived from the spectrum fitting and calibration treatment, respectively. These errors, for moderately large and strong transitions, are of the order of 10 - 20%. However, lower γ-ray energies where one observes a high density of γ-lines or transitions with peak intensity close to the experimental sensitivity limit, these errors may be much larger.

3.3. ARC - input data processing

3.3.1. Data dispersion (final state population dependence)

The first reason for data dispersion is due to the dependence of averaged intensities on the spin of the final state. This is due to the different population of J_f spin groups ($J_t + 1/2$ and $J_t + 3/2$) from the initial s-wave capture state with $J_i = J_t + 1/2$ (see Fig. 1) and J_t the target spin. For data adopted in the BNL/ECN source, the dependence of averaged reduced intensities on the spin of the final state has been removed using the SPARC or RACA codes [3.7, 3.8]. Where such analysis is missing, an approximate factor based on the equation for the statistical factor

$$Q(J_i J_f) = (J_i + ½) / 2(J_t + ½) \tag{3.2}$$

has been used. As shown in Ref. [3.8], such approximation does not significantly influence results compared to the Monte-Carlo approach and the difference remains within the statistical accuracy of the I_γ/E_γ^3 values.

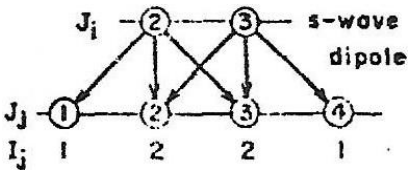

FIG. 3.1 *Schematic picture of double population of J_i^{+}1/2 final spin.*

The $Q(J_iJ_f)$ correction factors used for $fL(E_\gamma)$ data files are shown in Table 3.1 for different spin configurations involved. The RACA calculated values are combined with a simplified approach, using the statistical factors for the generation of the capture states with spins J_i.

Table 3.1 The correction factors for the ($J_i = J_t \pm 1/2$, $J_i \rightarrow J_f$) population dependence on the final spin J_f.

Nucleus	J_t^π	$Q(J_iJ_f)$ Stat. factor	$Q(J_iJ_f)$ RACA code	Nucleus	J_t^π	$Q(J_iJ_f)$ Stat. factor	$Q(J_iJ_f)$ RACA code
As-76	3/2-	2		Yb-172	1/2-		1.51
Zr-92	5/2+	2		Yb-174	5/2-	2	
Mo-96	5/2+		2.02/1.8	Lu-176	7/2+		2.02/1.9
Mo-98	5/2+	2		Hf-178	7/2-	2	
Ru-102	5/2+		2.04/1.8	W-184	1/2-	1.33	
Pd-106	5/2+	2		W-185	0+	1	1
Cd-114	1/2+		1.62	W-187	0+	1	1
Te-124	1/2+	1.33		Os-188	1/2-	1.33	
I-128	5/2+	2		Os-189	0+	1	1
Ba-135	0+	1	1	Os-191	0+	1	1
Ba-136	3/2+	2		Os-193	0+	1	1
Nd-146	7/2-	2		Ir-192	3/2+	2	
Sm-155	0+	1	1	Ir-194	3/2+	2	
Gd-155	0+	1	1	Pt-195	0+	1	1
Gd-156	3/2-	2		Pt-196	1/2-	1.33	
Gd-157	0+	1	1	Pt-197	0+	1	1
Gd-158	3/2-	2		Pt-199	0+	1	1
Gd-159	0+	1	1	Au-198	3/2+	2	
Dy-162	5/2+		2.02/1.9	Th-233	0+	1	1
Dy-163	0+	1	1	U-236	7/2-	2	
Dy-164	5/2-		2.03/1.9	U-239	0+	1	1
Dy-165	0+	1	1	U-239	0+	1	1
Ho-166	7/2-	2		Pu-240	1/2+	1.33	
Er-168	7/2+		2.32/1.7				

3.3.2. Data dispersion from Porter-Thomas fluctuations

A major source of data dispersion is due to the Porter Thomas (PT) fluctuations. In the analysis of the BNL measurements the Porter-Thomas uncertainty is estimated from the Monte-Carlo simulation code RACA [3.8]. This estimate can be applied as an uncertainty band over data points for the same multipolarity and is not added to individual transitions as an additional error. Since the code RACA is not available anymore, we have looked for an approximation, which was employed before the code RACA was implemented in ARC processing procedure.

A simple approach can be adopted, as a useful approximation. The relative variance is given by the factor 2/υ factor, where υ is number of degrees of freedom. In the present situation υ is equal to the number of resonances present in the 2 keV window and can be estimated from the full width at half maximum (FWHM) spread of the Sc filter. In the adopted data, the E1, M1 and sometimes E2 groups are clearly separated from each other by the satisfactory experimental averaging and their multipolarity assignments are well known. The FWHM of the BNL Sc filtered beam facility has been determined to be 900 eV [3.6] and the number of resonances can be estimated using $\upsilon = 900/D_0(\text{eV})$ leading to the dispersion $d\text{PT} = \sqrt{2/\upsilon}$. For a boron filter, the FWHM is estimated about 1000 eV broad [3.11].

The beam profile has the maximal neutron flux at its center which then decreases at the beam boundaries, reducing the effective number of degrees of freedom, and the number of resonances. This can be compensated by using a smaller effective FWHM value of 600 eV. Furthermore, the presence of *p*-wave resonances may influence the dispersion. Despite all these effects, this approximation gives sufficient information to judge the dispersion of the data due to the PT fluctuations within the E1, M1 and E2 experimental data groups. The derived PT dispersion factors for all studied nuclides are shown in Table 3.2.

Table 3.2 The estimated PT dispersion for all nuclides, using the D_0 values from RIPL-3 [3.18] and BNL compilation [3.19].

Nucleus	D_0	$1+d\mathrm{PT}=\sqrt{2}/\upsilon$		Nucleus	D_0	$1+d\mathrm{PT}=\sqrt{2}/\upsilon$	
	[eV]	FWHM n-beam			[eV]	FWHM n-beam	
		900keV	600keV			900keV	600keV
As-76	93	1.44	1.56	Tm-170	7.28	1.13	1.21
Zr-92	536	2.10	2.34	Yb-172	6.08	1.12	1.14
Mo-96	81.4	1.43	1.52	Yb-174	8.06	1.13	1.16
Mo-98	46.5	1.32	1.39	Lu-176	3.45	1.09	1.11
Ru-102	18.5	1.20	1.25	Hf-178	2.4	1.07	1.09
Pd-106	10.9	1.16	1.19	Ta-182	4.17	1.10	1.17
Cd-114	24.8	1.23	1.29	W-184	12	1.16	1.20
Te-124	25.1	1.24	1.29	W-185	81	1.42	1.52
I-128	9.7	1.15	1.18	W-187	93	1.46	1.56
Ba-135	360	1.89	2.09	Os-188	4.56	1.10	1.12
Ba-136	40	1.29	1.36	Os-189	40	1.29	1.36
Nd-146	17.8	1.13	1.19	Os-191	70	1.39	1.48
Sm-155	114	1.50	1.62	Os-193	115	1.51	1.62
Eu-154	1.14	1.05	1.12	Ir-192	1.68	1.06	1.07
Gd-155	13.8	1.17	1.21	Ir-194	3.98	1.09	1.11
Gd-156	1.8	1.06	1.08	Pt-195	82.6	1.43	1.53
Gd-157	30.5	1.26	1.32	Pt-196	19.2	1.21	1.25
Gd-158	87	1.44	1.54	Pt-197	214	1.69	1.84
Gd-159	82	1.43	1.52	Pt-199	340	1.87	2.07
Dy-162	2.14	1.07	1.09	Au-198	15.7	1.19	1.23
Dy-163	62.9	1.37	1.46	Th-233	15.8	1.19	1.23
Dy-164	7.28	1.13	1.16	U-236	0.49	1.03	1.05
Dy-165	144	1.57	1.69	U-239	16.4	1.19	1.23
Ho-166	4.20	1.07	1.09	Pu-240	2.07	1.07	1.08
Er-168	4	1.10	1.12				

For illustration, the PT dispersion band for E1 and M1 transitions in the ^{197}Au(n,γ) reaction are shown in Fig. 3.2. The calculated trend lines were applied to guide the eye and are broadened by the estimated factor (1+*d*PT) =1.19. It seems that the number of outliers, considering the statistical errors, is reasonably small.

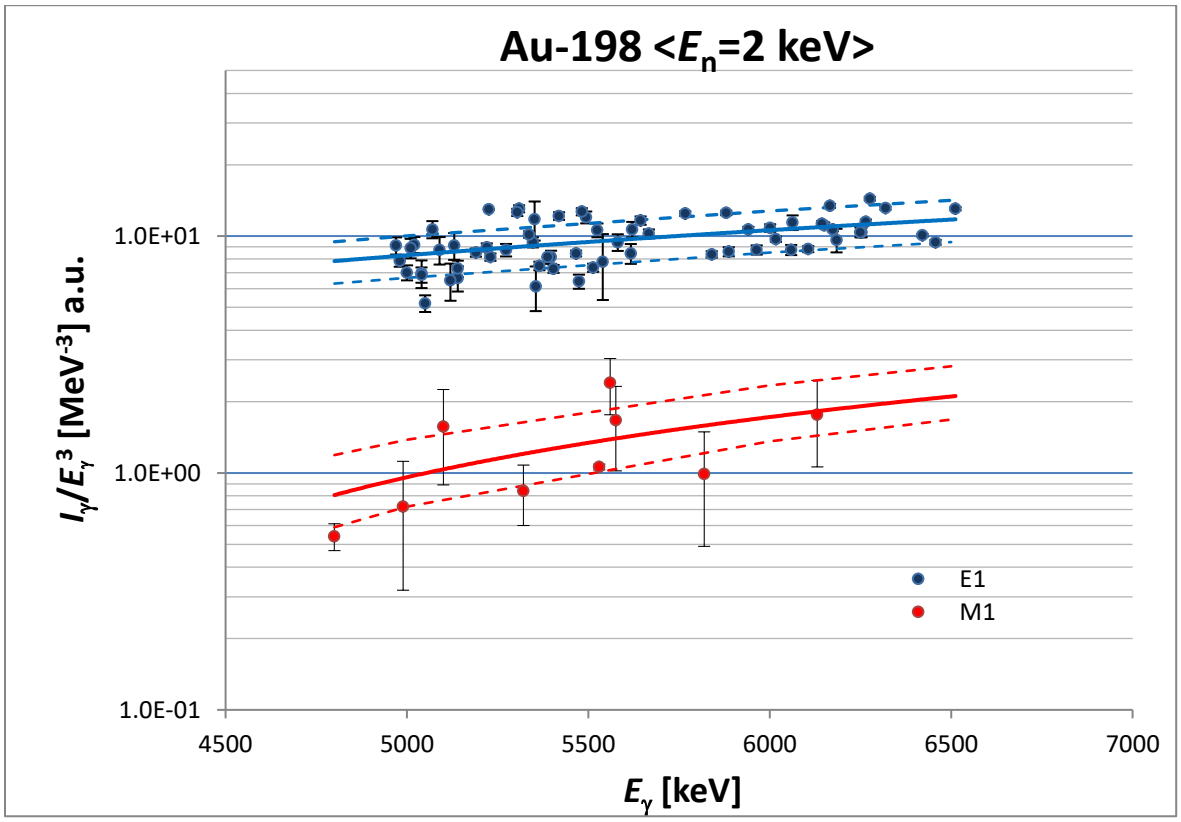

FIG. 3.2 *The PT dispersion estimated from the √ 2/υ approximation for ^{198}Au. The 2 keV input data in I_γ/E_γ^3 arbitrary scale are plotted. The dashed trend fit curves describe the PT dispersion boundary around the arbitrary mean trend value.*

The resonances from the tails of the bell shape neutron spectrum are weak and contribute less to the averaging. To illustrate this effect the dPT is also shown for a smaller window in order to accommodate this effect by smaller effective FWHM. However, the comparison of the √2/υ approximation with the Monte Carlo calculation [3.9,3.19] indicates that the statistical uncertainties can mask the dPT effect.

3.4. PSF - data processing

The absolute calibration of the processed ARC input file has been executed in two separate actions. Firstly, the DRC experimental and systematic results 2016 version (See Ref. [3.12]) has been applied which resulted in the ARC data file ATLAS_ARC_2017 (further ARC 2017) and was described in detail in Ref. [3.20] with the main conclusions in this report. After completion of the new independent DRC analysis in 2018, these results have been used in the renormalization of the starter ARC 2017 data in the final library ATLAS_ARC_2019 (further ARC 2019).

3.4.1. Conversion to the absolute PSF scale (ATLAS_ARC_2017)

After the dispersion is corrected for double population (see Fig. 3.1), the data are ready for converting from the adopted $\langle I_\gamma/E_\gamma^3 \rangle$ values to the γ-ray strength function scale of 10^{-8}MeV^{-3} (see comment about common phase factor for L = 1 and L = 2 transitions in Sect. 3.2). Because the initial state in the filtered beam experiments is a mixture of many initial states (resonances) and cannot be uniquely defined, some external information has to be used. This information is taken from the DRC data. As matter of fact, normalizing the reduced ARC intensities to corresponding DRC results, is the only way to generate absolute PSF from ARC filtered beam experiments, because these former experiments involve resonances with known J^π. The DRC is the same physical process as the ARC, at a similar neutron energy, but involving resonances with well-defined orbital angular momentum and parity parameters.

The calibration of reduced intensities to the DRC data is performed as follows:

$$\langle f(I_\gamma/E_\gamma^3)_{ARC} \rangle / \langle f(\mathrm{E1})_{DRC} \rangle = \mathrm{C} \tag{3.3}$$

$$f(\mathrm{E1})_{ARC} = \mathrm{C} \times (I_\gamma/E_\gamma^3)_{ARC}. \tag{3.4}$$

The E1 transitions are preferred mainly because of their superior statistical accuracy and their purity (the negligible effect of *p*-wave contribution). The calibration against DRC f(M1) values has not been used for two reasons: firstly, the statistical accuracy is inferior to E1 data and secondly the M1 radiation from the capture of 2 keV neutron beam is slightly polluted by E1 radiation from the *p*-wave capture (see below).

The normalization constant C may be derived in two ways. When DRC measurements are available, the information can be taken using the mean value of $f(\mathrm{E1})_{DRC}$, averaged over the transitions in the energy range used (usually of about 1 MeV broad), as documented in Ref. [3.12]. The advantage of this procedure is that the same transitions measured in both DRC and ARC experiments are used. The DRC then gives the absolute transition strength.

If the DRC measurement is not available, the f(E1) systematic equation is used:

$$\langle f(\mathrm{E1}) \rangle = 0.0021\, A^{1.69\pm0.17}\ [10^{-8}\ \mathrm{MeV}^{-3}]. \tag{3.5}$$

The systematics f(E1) is based on a fit to measured DRC data as a function of the atomic mass A at E_γ energies around 6.3 ± 0.5 MeV and is shown in Fig. 2 of Ref. [3.12].

The value of the gamma-ray energy assumed in the systematics may form an additional uncertainty for targets for which the dominant E1 transitions are not in the vicinity of 6.5 MeV. In such a case, the systematic value must be adjusted assuming an additional E2 dependence from the Brink-Axel model (see further). The calibration procedure is summarized in Table 3.3 including all normalization factors applied.

Table 3.3 List of nuclides with the ARC calibration in to the absolute PSF data

$<E_\gamma>$ - the mean energy of the energy interval of transitions used for the calibration in MeV
$<f(\mathrm{E1})>$- PSF values derived from DRC or systematic, bold font values adopted, in $10^{-8}\mathrm{MeV}^{-3}$
M1) - No E1 transitions present, M1 systematic used instead

Nucleus	**n**	$<E_\gamma>$	$<f(\mathrm{E1})>$ **EXP**	$<f(\mathrm{E1})>$ **SYS**	**Nucleus**	**n**	$<E_\gamma>$	$<f(\mathrm{E1})>$ **EXP**	$<f(\mathrm{E1})>$ **SYS**
As-76	Sc	6.7		2.35	Tm-170	Sc	6.1	4.72	8.66
Zr-92	Sc	6.2	--	3.20 M1)	Yb-172	Sc	6.8		8.83
Mo-96	Sc	6.1		3.43	Yb-174	B	6.6	19.4	8.99
Mo-98	Sc	6.6		3.55	Lu-176	Sc	5.9	7.4	9.16
Ru-102	Sc	6.8		3.78	Hf-178	Sc	6.8	18.5	9.33
Pd-106	B	7.2	4.14	4.03	W-184	B	6.8	28.1	9.85
Cd-114	Sc	6.2		4.53	W-185	Sc	5.4		9.93
Te-124	Sc	7.1	--	1.44 M1)	W-187	Sc	4.6		10.11
I-128	Sc	6.6	1.90	5.47	Ta-182	Sc	5.8	11.3	9.67
Ba-135	Sc	5.1		5.96	Os-188	Sc	6.3		10.20
Ba-136	Sc	6.6	5.0	6.03	Os-189	Sc	4.5		10.28
Nd-146	B	6.4	4.5	6.77	Os-191	Sc	5.4		10.46
Sm-155	Sc	5.4		7.46	Os-193	Sc	5.5		10.60
Eu-154	Sc	7.9		7.38	Ir-192	Sc	6.1		10.55
Gd-155	Sc	5.9	9.2	7.46	Ir-194	Sc	5.9		10.73
Gd-156	B	7.4		7.53	Pt-195	Sc	4.9		10.82
Gd-157	Sc	5.9	12.4	7.61	Pt-196	Sc	6.3	17.4	10.91
Gd-158	B	6.4		7.69	Pt-197	Sc	4.7		11.00
Gd-159	Sc	5.4	8.81	7.77	Pt-199	Sc	4.6		11.18
Dy-162	Sc	6.8		8.01	Au-198	Sc	6.0	11.4	11.09
Dy-163	Sc	5.7	7.26		Th-233	Sc	4.1	20.3	14.44
Dy-164	Sc	7.2	8.17	8.09	U-236	Sc	6.0		15.6
Dy-165	Sc	5.4		8.24	U-239	B	4.0	10.29	15.04
Ho-166	B	6.0		8.33	Pu-240	Sc	5.6	19.9	15.1
Er-168	B	6.4	15.9	8.50					

3.4.2. The $<E_\gamma>$ dependence of the normalization

The mean energy of the energy regions (on average about 0.5-1 MeV wide), used for normalization of the I_γ/E_γ^3 input data, is shown in the first column of Table 3.4. The values of the mean energy range between 3.6 and 7.2 MeV. In cases where the measured DRC data are used for normalization and the identical transitions are also chosen, no energy difference between DRC and ARC data occurs. However, the situation is different if the ARC data are based on the DRC systematics. The average reference energy of the $<f(\mathrm{E1})>$ systematic equation is 6.3 ± 0.5 MeV whereas some of the used energy regions are significantly different from this value. In such cases, for the renormalization to this energy a correction factor has to be applied. The additional energy behavior is generally assumed to be E_γ^2 as predicted by the Brink-Axel Giant Resonance model. The resulting $<E_\gamma>$ listing is given in Table 3.4.

Table 3.4 The E_γ dependence correction factor $F = <E_\gamma>_{ARC}/<E_\gamma>_{DRC}$ for data normalized to the $<f(\mathrm{E1})>_{DRC}$ from DRC measurements or DRC systematic at 6.2 MeV. The 3rd column gives the F^2 ratio for DRC measurements, while the 4th column gives the DRC systematic.

Nucleus	$<E_\gamma>_{ARC}$	<DRC> F^2	< SYS> F^2	Nucleus	$<E_\gamma>_{ARC}$	<DRC> F^2	< SYS> F^2
		used	used			used	used
As-76	6.7		0.86	Tm-170	6.1		1.03
Zr-92	6.2		1 M1	Yb-172	6.8		0.82
Mo-96	6.1		1.03	Yb-174	6.6	0.95	
Mo-98	6.6		0.88	Lu-176	5.9	0.98	
Ru-102	6.8		0.83	Hf-178	6.8	0.95	
Pd-106	7.2	0.96		W-184	6.8	0.94	
Cd-114	6.2		1.0	W-185	5.4		**1.32**
Te-124	7.1	1 M1		W-187	4.6		**1.82**
I-128	6.6	1.03		Ta-182	5.8		
Ba-135	5.1		**1.48**	Os-188	6.3		0.97
Ba-136	6.6	1.03		Os-189	4.5		1.90
Nd-146	6.4	1.09		Os-191	5.4		1.32
Sm-155	5.4		**1.32**	Os-193	5.5		1.27
Eu-154	7.9		**0.62**	Ir-192	6.1		1.03
Gd-155	5.9	1.20		Ir-194	5.9		1.10
Gd-156	7.4		**0.7**	Pt-195	4.9		**1.60**
Gd-157	5.9	0.96		Pt-196	6.3		0.97
Gd-158	6.4		0.94	Pt-197	4.7		**1.74**
Gd-159	5.4	0.89		Pt-199	4.6		**1.82**

Nucleus	$<E_\gamma>_{ARC}$	<DRC> F^2	< SYS> F^2	Nucleus	$<E_\gamma>_{ARC}$	<DRC> F^2	< SYS> F^2
		used	used			used	used
Dy-162	6.8		0.83	Au-198	6.0	1.0	
Dy-163	5.7			Th-233	4.1		**2.29**
Dy-164	7.2		**0.74**	U-236	6.0		1.07
Dy-165	5.4		**1.32**	U-239	4.0	**2.40**	
Ho-166	6.0		1.07	Pu-240	5.6	1.26	
Er-168	6.4	1.0					

The following nuclides, normalized with the systematic equation and with $<E_\gamma>$ outside the 5.7 – 6.7 MeV range, have been chosen for the correction using the factor $(<E_\gamma>_{ARC}/6.2)^2$. They are: ^{135}Ba, ^{155}Sm, ^{154}Eu, ^{156}Gd, ^{164,165}Dy, ^{185,187}W, ^{195,197,199}Pt, ^{233}Th and ^{239}U.

3.4.3. The *p*-wave contribution

The ARC experiments use neutron beam energies spreading from about 100 eV (B) through 2 keV (Sc) and up to 24 keV (Fe). The dominance of *s*-wave capture, close to thermal energies, decreases with increasing neutron energy, so that *p*-wave resonances start to contribute to the capture process. This effect has been included in the code RACA as the Monte-Carlo modelling of the partial cross sections and is discussed in Refs. [3.8,3.9]. In the spectroscopic application of the ARC method, the *p*-wave capture is primarily used for the parity determination of the final states by means of the intensity ratio of the 24 keV to the 2 keV data. The boron filtered beam with its low neutron mean energy of about 150 eV has negligible *p*-wave component, except nuclides from the 3*p*-giant resonance of the *p*-wave strength around $A = 100$. This influenced only Pd-106 in the present PSF data.

However, for PSF application, the *p*-wave capture both at 2 and mainly 24 keV complicates the determination of the absolute strength of M1 radiation, increasing the *s*-wave M1 strength by the *p*-wave E1 admixture. In all BNL/ECN data the p-wave admixture at 2 keV was estimated from RACA calculations and the results are shown in Table 3.5. The size of this contribution follows the distribution of *3p* and 4*p* giant resonances. Contrary to that, the E1 *s*-wave capture is negligibly increased by M1 *p*-waves due the weaker M1 strength. In all calculated cases was the M1 *p*-wave contribution to E1 transitions smaller than + 5% (see Table 3.5).

Table 3.5. The results of RACA calculations of the *p*-wave component at 2 keV ARC experiments (from private BNL/ECN collaboration logbook).

Nuclide	$\langle f(\mathrm{M1})\rangle_{p\text{-waves}}$ in $\langle f(\mathrm{E1})\rangle_{s\text{-waves}}$	$\langle f(\mathrm{E1})\rangle_{p\text{-waves}}$ in $\langle f(\mathrm{M1})\rangle_{s\text{-waves}}$
Mo-96	0.09	0.66
Ru-102	0.04	0.33
Cd-114	0.04	0.24
Sm-155	0.04	0.21
Gd-157	0.01	0.15
Dy-162	0.01	0.13
Dy-164	0.02	0.18
Yb-172	0.01	0.09
Lu-176	0.01	0.15
Pt-195	0.02	0.31
Th-233	0.02	0.39
U-239	0.03	0.37

For a number of the ARC data processed in the BNL-ECN database, the E1 component present in the M1 radiation was estimated by the RACA code calculations. For the remaining data, with no correction, this effect is estimated in the following way. The theoretical description of the formula for the ratio of *s*- and *p*-wave capture can be found in Refs. [3.7-3.11] (Eq. 7 in [3.9]) and is a function of several ingredients, such as S_0, S_1, $\Gamma_{\gamma 0}$ and $\Gamma_{\gamma 1}$. If we use the assumptions that, $\Gamma_n << \Gamma_\gamma$ is independent of the orbital momentum and $D_J = D_0/2J+1$, then the approximation of the theoretical equation for average cross section at 2 keV [3.9] can be simplified as

$$\langle \sigma_{Jf} \rangle \sim \Sigma_{s\text{-wave}} \langle \Gamma_{\gamma f}(\mathrm{E1}, \mathrm{M1}) \rangle + S_{1f}/S_0 \ \Sigma_{p\text{-wave}} \langle \Gamma_{\gamma f}(\mathrm{E1}, \mathrm{M1}) \rangle \quad (3.6)$$

The factor $f = (ka)^2/(1+(ka)^2)$ is the penetrability of *p*-wave neutrons relative to *s*-wave neutrons.

The dominant factor in this formalism is the S_1/S_0 ratio. We have plotted the calculated $(f(\mathrm{E1})_{p\text{-wave}}/(f(\mathrm{M1})_{s\text{-wave}})$ ratio against the S_1/S_0 ratio and found it most instructive to estimate the E1 (*p*-wave) component (see Fig. 3.3).

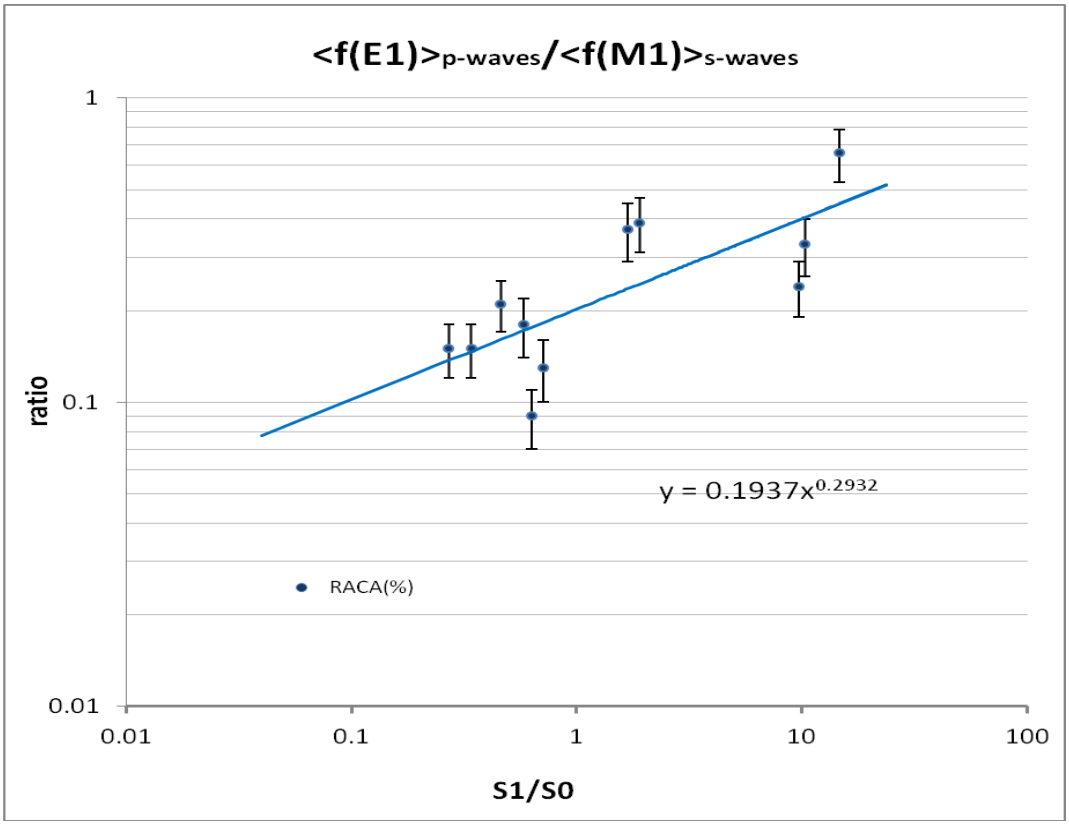

FIG. 3.3 *The calculated <f(E1)>p-waves/<f(M1)>s-waves ratios as a function of S_1/S_0. The fitted trend line is used as a systematic estimate of the p-wave admixture.*

We used the RACA calculated contributions within the BNL/ECN collaboration for 11 nuclides (no S_1/S_0 value for ^{195}Pt). The derived trend function $\langle f(\mathrm{E1})\rangle_{p\text{-waves}}/\langle f(\mathrm{M1})\rangle_{s\text{-waves}} = 0.19\,(S_1/S_0)^{0.29}$ was used to estimate this effect for all remaining nuclei. The applied corrections to the M1 strength are shown in Table 3.6.

Table 3.6 List of nuclides with the p-wave corrections.

S_1/S_0 - S_0 and S_1 values taken from RIPL3

a) S_1 values estimated from Fig. 2.2 or optical model calculations in [3.18]
b) No S_0 value available

p-wave - the calculated p-wave E1 contribution in M1 *s*-wave transitions at $<E_n> = 2$ keV

a) RACA calculations (BNL-ECN database),
b) boron estimate assumed with negligible *p*-wave contribution
c) empirical estimate in this work from $E1_p/M1_s = 0.19(S_1/S_0)^{0.29}$
d) estimated from the DRC data

Nucleus	n-beam	S_1/S_0	*p*-wave E1 in M1 estimate	*p*-wave E1 in M1 applied	Nucleus	n-beam	S_1/S_0	*p*-wave E1 in M1 estimate.	*p*-wave E1 in M1 applied
As-76	Sc	0.96	0.19	0.19 [3)]	Tm-170	Sc	0.60 [a)]	0.17	0.2 [3)]
Zr-92	Sc	18.1	0.45	0.45 [3)]	Yb-172	Sc	0.63	0.17	0.09 [1)]
Mo-96	Sc	14.66	0.43	0.66 [1)]	Yb-174	B	0.54	0.16	0.16 [3)]
Mo-98	Sc	23.79	0.49	0.49 [3)]	Lu-176	Sc	0.27	0.13	0.15 [1)]
Ru-102	Sc	10.34	0.38	0.33 [1)]	Hf-178	Sc	0.38	0.14	0.14 [3)]
Pd-106	B	10.27	0.36	0.33 [4)]	Ta-182	Sc	0.38	0.14	0.14 [3)]
Cd-114	Sc	9.68	0.37	0.24 [1)]	W-184	B	0.38	0.14	0 [2)]
Te-124	Sc	1.90 [a)]	0.23	0.23 [3)]	W-185	Sc	0.23	0.12	0.12 [3)]
I-128	Sc	2.57	0.26	0.26 [3)]	W-187	Sc	0.17	0.11	0.11 [3)]
Ba-135	Sc	1.77	0.23	0.23 [3)]	Ta-182	Sc	0.35	0.14	0.14 [3)]
Ba-136	Sc	1.3	0.21	0.21 [3)]	Os-188	Sc	0.2	0.12	0.12 [3)]
Nd-146	B	1.10 [a)]	0.20	0 [2)]	Os-189	Sc	0.13	0.10	0.10 [3)]
Sm-155	Sc	0.68 [a)]	0.17	0.21 [1)]	Os-191	Sc	[b)]		0.2 [3)]
Eu-154	Sc	2.20	0.24	0.24 [3)]	Os-193	Sc	[b)]		0.2 [3)]
Gd-155	Sc	0.75 [a)]	0.18	0.18 [3)]	Ir-192	Sc	0.26 [a)]	0.13	0.13 [3)]
Gd-156	B	1.68	0.23	0 [2)]	Ir-194	Sc	0.38 [a)]	0.15	0.15 [3)]
Gd-157	Sc	0.34	0.14	0.15 [1)]	Pt-195	Sc	0.25 [a)]	0.13	0.31 [1)]
Gd-158	B	1	0.19	0 [2)]	Pt-196	Sc	0.28 [a)]	0.14	0.14 [3)]
Gd-159	Sc	0.81	0.18	0.18 [3)]	Pt-197	Sc	0.28 [a)]	0.14	0.14 [3)]
Dy-162	Sc	0.71	0.17	0.13 [1)]	Pt-199	Sc	0.36 [a)]	0.15	0.15 [3)]
Dy-163	Sc	0.63	0.17	0.17 [3)]	Au-198	Sc	0.84	0.18	0.18 [3)]
Dy-164	Sc	0.58	0.16	0.18 [1)]	Th-233	Sc	1.79	0.23	0.39 [1)]
Dy-165	Sc	0.7	0.17	0.17 [3)]	U-236	Sc	1.84	0.23	0.23 [3)]
Ho-166	B	0.54	0.25	0 [2)]	U-239	B	1.68	0.22	0 [2)]
Er-168	B	0.52	0.16	0 [2)]	Pu-240	Sc	1.55	0.22	0.22 [3)]

3.4.4. Conversion to the absolute PSF scale (ATLAS_ARC_2019)

The next step in the processing of ARC data is to use the most recent DRC evaluation in the normalization procedure (see Section 2 and Ref. [3.21]). As a starter file, we used the ARC 2017 [3.21] in the pre-processed form, *i.e.* before calibrating to the absolute DRC data. These ARC data include all the other averaging procedures and corrections which are made prior to the absolute calibration. The starter file is now normalized to the new recommended DRC experimental values or to the new systematic equation for *f*(E1) data described in Section 2 and Ref. [3.21] to give the Atlas_ARC_2019 file.

An inspection of the binned data in Table 2.4 and Fig. 2.5 in Section 2, shows that for the majority of *f*(E1) the $<E_\gamma>$ value does not deviate too much from the 6 – 7 MeV range in both DRC evaluations (see Refs. [3.12, 3.21]) and therefore we can apply the same procedure as in [3.12, 3.21]. The difference from the previous calibrations is that the DRC experimental data have been re-evaluated and a new set of recommended data is adopted, while the systematics *f*(E1) have also been updated.

The LSQ fit using a power function of the mass number *A*, applied in both previous DRC evaluations, resulted in the following expressions for the E1 strength function systematics:

$$<<f(\mathrm{E1})>> = 0.0021\, A^{1.69\pm0.17} \rightarrow \mathrm{DRC}_{2016}$$
$$<<f(\mathrm{E1})>> = 0.004\, A^{1.52\pm0.21} \rightarrow \mathrm{DRC}_{2018} \qquad (3.7)$$

The quoted uncertainties are 1 standard deviation (SD) errors from the least squares (LSQ) fit further increased by Γ_γ and *D* uncertainty estimates of 10%.

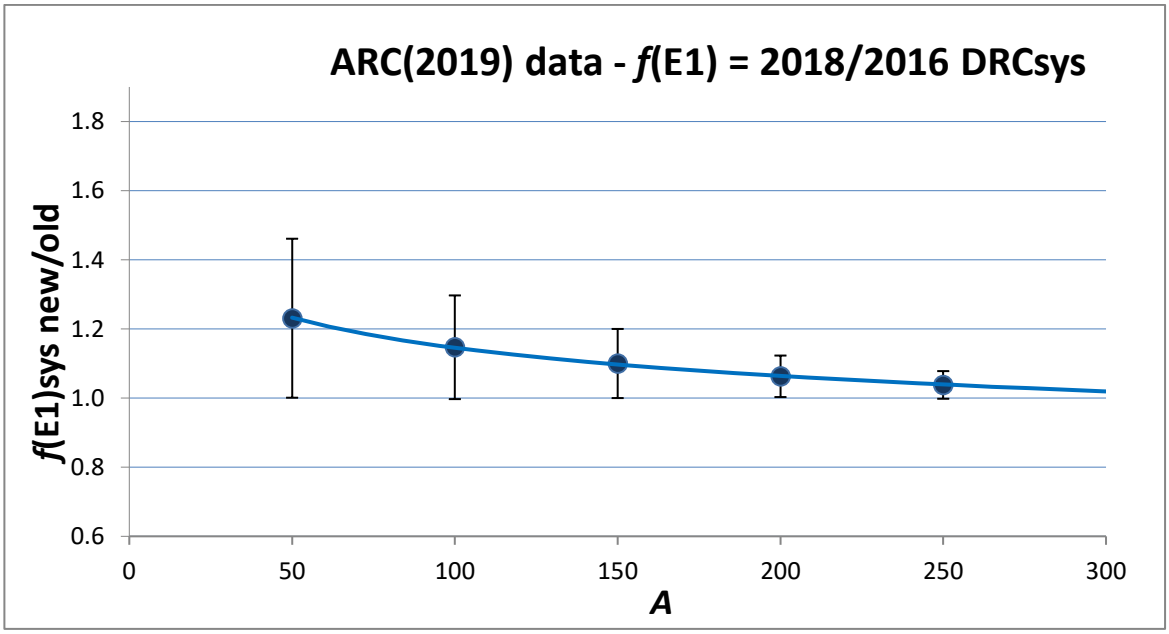

FIG. 3.4 *The ratio F of SYS(2018) over SYS(2016) as a function of the mass A.*

The ratio of these two equations is plotted in Fig. 3.4 and applied to the conversion of the 2017 data into the recent 2019 release. There is a difference of about 20% for light nuclides, while for

data with $A > 100$ the difference becomes 10% and less. The comparison of the calibration factors for both ARC files is given in Table 3.7.

Table 3.7 List of nuclides with calibration of PSF data in the two recent ARC databases: *ARC 2017* and *ARC 2019*

$<E_\gamma>$ - the mean energy of the energy interval of transitions used for the calibration
<<***f*(E1)**>> - PSF values derived from DRC or systematic**, bold values** adopted
<<*f*(E1)>> - PSF values derived from DRC experiments disregarded as doubtful
M1 - No E1 transitions present, M1 systematic used instead
F - *ARC19/ ARC17* ratio
SYS16 - *f*(E1) systematics from INDC(NED)-13, 2016
SYS18 - *f*(E1) systematics from INDC(NDS)-0772, 2018
Bold values - used for calibration
EXP values - in brackets disregarded for calibration

			ARC 17	ARC 17	*F*	ARC19	ARC19
Nucleus	n-beam	$<E_\gamma>$	<<*f*(E1)>> E1 DRC EXP16	<*f*(E1)> E1 DRC SYS16		<<*f*(E1)>> E1 DRC EXP18	<*f*(E1)> E1 DRC SYS18
		MeV	$10^{-8}MeV^{-3}$	$10^{-8}MeV^{-3}$		$10^{-8}MeV^{-3}$	$10^{-8}MeV^{-3}$
As-76	Sc	6.7		**2.44**	1.18		**2.89**
Zr-92	Sc	6.2		**1.14** M1	0.25		**0.28** M1
Mo-96	Sc	6.1		**3.58**	1.15		**4.12**
Mo-98	Sc	6.6		**3.70**	1.15		**4.25**
Ru-102	Sc	6.8		**3.95**	1.15		**4.52**
Pd-106	B	7.2	**4.14**	4.29	0.93	**3.87**	4.79
Pd-109	Sc	5.9		**1.29** M1	0.93		**1.20** M1
Cd-114	Sc	6.2		**4.73**	1.13		**5.35**
Te-124	Sc	7.1		**1.44**M1	0.88		**1.27** M1
I-128	Sc	6.6	1.9	**5.71**	1.12	**8.54**	6.38
Ba-135	Sc	5.1		**6.23**	1.11		**6.92**
Ba-136	Sc	6.6	**5.0**	6.31	1.23	**6.17**	7.00
Nd-146	B	6.4	**4.5**	7.08	1.00	**4.5** *	7.80
Sm-148	B	6.5	**4.5**	7.24	1.10	4.5*	**7.96**
Sm-150	B	6.3	**7.83**	7.40	1.10	**7.83***	8.12
Sm-155	Sc	5.4		**7.81**	1.09		**8.54**
Eu-154	Sc	7.9		**7.72**	1.09		**8.45**
Gd-155	Sc	5.9	**8.7**	7.81	1.01	**8.81**	8.54
Gd-156	B	7.4		**7.89**	1.09		**8.62**

			ARC 17	ARC 17	*F*	ARC19	ARC19
Nucleus	n-beam	$<E_\gamma>$	$<<f(E1)>>$ E1 DRC EXP16	$<f(E1)>$ E1 DRC SYS16		$<<f(E1)>>$ E1 DRC EXP18	$<f(E1)>$ E1 DRC SYS18
		MeV	$10^{-8}MeV^{-3}$	$10^{-8}MeV^{-3}$		$10^{-8}MeV^{-3}$	$10^{-8}MeV^{-3}$
Gd-157	Sc	5.9	**12.4 ****	7.97	0.7		**8.71**
Gd-158	B	6.4		**8.05**	1.09		**8.79**
Gd-159	Sc	5.4	**8.81**	8.14	1.04	**9.21**	8.88
Dy-162	Sc	6.8		**8.39**	1.09		**9.13**
Dy-163	Sc	5.7	**7.26****	8.47	1.27		**9.22**
Dy-164	Sc	7.2	**8.17****	8.56	1.09		**9.30**
Dy-165	Sc	5.4		**8.64**	1.09		**9.39**
Ho-166	B	6.0		**8.73**	1.09		**9.48**
Er-168	B	6.4	**15.9**	8.90	1.04	**16.6**	9.65
Tm-170	Sc	6.1	4.72	**9.08**		6.21	**9.83**
Yb-172	Sc	6.8		**9.25**	1.08		**10.0**
Yb-174	B	6.6	**19.4**	9.43		37.8	**10.18**
Lu-176	Sc	5.9	**7.4**	9.60		4.57	**10.36**
Hf-178	Sc	6.8	**18.5**	9.78		31.7	**10.54**
Hf-180	B	6.0		**10.00**	1.08		**10.72**
W-184	B	6.8	**28.1**	10.32		36.9	**11.08**
W-185	Sc	5.4		**10.42**	1.07		**11.17**
W-187	Sc	4.6		**10.60**	1.07		**11.36**
Ta-182	Sc	5.8	**11.3**	10.14	0.81	**9.2**	10.90
Os-188	Sc	6.3		**10.69**	1.07		**11.45**
Os-189	Sc	4.5		**10.79**	1.07		**11.54**
Os-191	Sc	5.4		**10.97**	1.07		**11.73**
Os-193	Sc	5.5		**11.16**	1.07		**11.92**
Ir-192	Sc	6.1		**11.07**	1.07		**11.82**
Ir-194	Sc	5.9		**11.25**	1.07		**12.01**
Pt-195	Sc	4.9		**11.35**	1.07		**12.10**
Pt-196	Sc	6.3	**17.4**	10.96	1.07	17.4*	**12.20**
Pt-197	Sc	4.7		**11.06**	1.07		**12.29**
Pt-199	Sc	4.6		**11.73**	1.06		**12.48**
Au-198	Sc	6.0	**11.4**	11.64		20	**12.39**
Th-233	Sc	4.1	20.3	**15.17**		33.4	**15.87**
U-236	Sc	6.0		**15.6**	1.04		**16.18**

			ARC 17	ARC 17	*F*	ARC19	ARC19
Nucleus	n-beam	$<E_\gamma>$	$<<f(E1)>>$ E1 DRC EXP16	$<f(E1)>$ E1 DRC SYS16		$<<f(E1)>>$ E1 DRC EXP18	$<f(E1)>$ E1 DRC SYS18
		MeV	$10^{-8}MeV^{-3}$	$10^{-8}MeV^{-3}$		$10^{-8}MeV^{-3}$	$10^{-8}MeV^{-3}$
U-239	B	4.0	**10.29**	15.81		**7.7**	16.49
Np-238	Sc	5.3		**15.71**	1.04		**16.34**
Pu-240	Sc	5.6	**19.9**	15.92	0.92	**18**	16.60

* no un-binned data available EXP17 adopted
** data source not found, the experimental value disregarded in 2018

The performance of the adopted ARC 19 database for E1 and M1 data in binned format at 6.6 MeV is shown in Fig. 3.5.

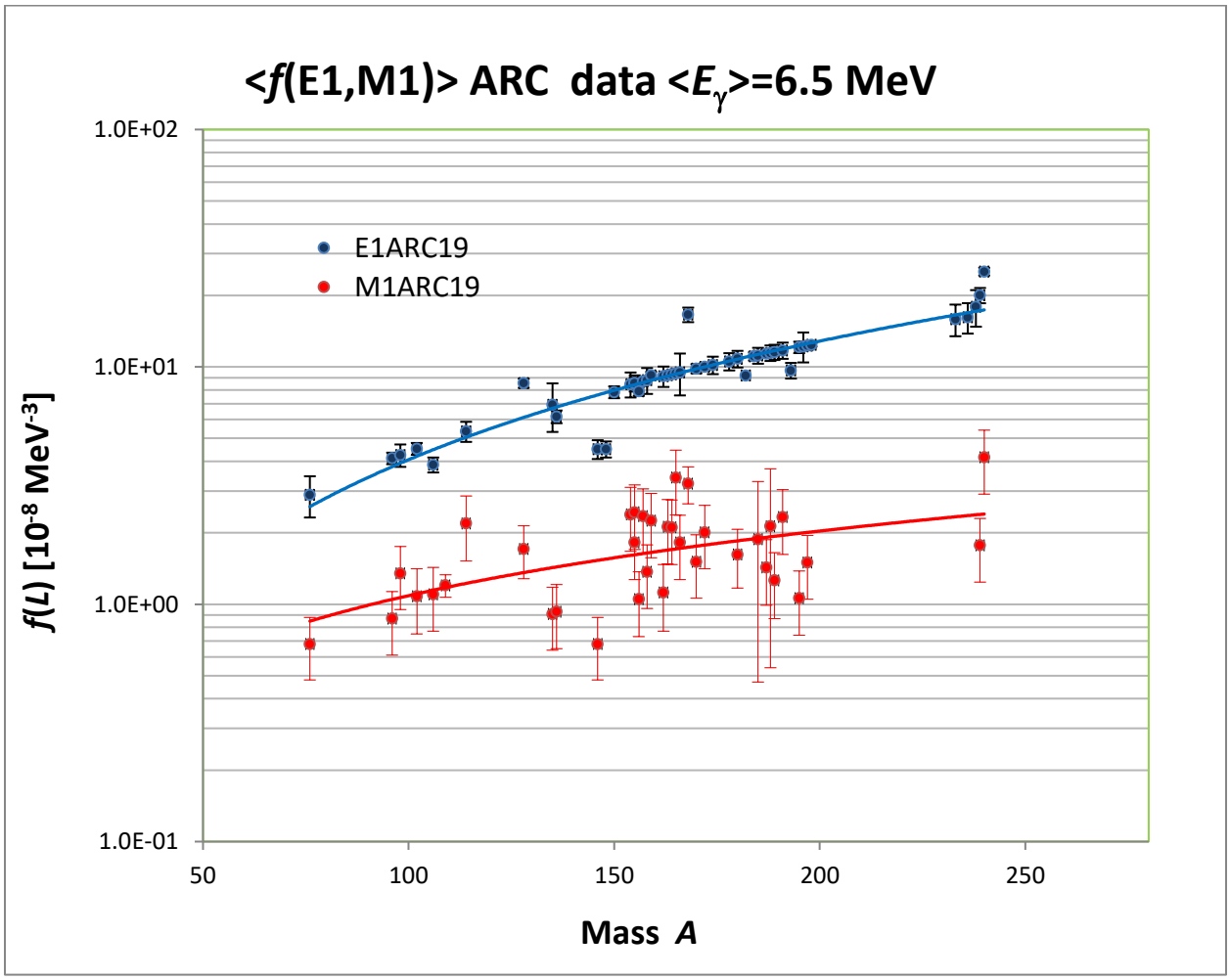

FIG. 3.5 *The adopted <f(E1)> and <f(M1> values at 6.5 MeV of the final ARC 19 database.*

Special attention was given to the experimental <<*f*(E1)>> values that were adopted. In principle, experimental values should always be preferred as the main source of information. However, some of the data looked suspicious and were rejected and replaced by the systematic values as listed in Table 3.8. Detailed discussion on the reasons for rejecting the data can be found in Ref. [3.21] in the section on data outliers.

The *f*(E1) strength function shape, below the separation energy, has a smooth power dependence on the energy E_γ expected from the E1 GRM and its other model variations. This was also shown in the results of the recent D1M + QRPA model (see Refs. [3.20,3.22-3.25]). In view of this, there are two possible explanations for the significant (above the statistical dispersion) outliers from the smooth E1 systematics. Firstly, the absolute calibration of TOF measurements used to derive DRC data may be incorrect and this may result in a wrong DRC <<*f*(E1)>> absolute value. It was beyond the scope of this work to search for detailed information on the TOF calibration procedure (the relevant information is often not mentioned in the databases or publications) and the data were taken as they were given in the references. The other reason may be that another excitation E1 mode (pygmy resonance) is contributing and the final strength function is a superposition of both.

One way to check whether the latter suggestion is true is to look at the E1/M1 ratio, which in the case of an additional E1 excitation mode should increase above the trend value. For DRC measurements, the E1 and M1 strengths are not affected by any conversion uncertainties and their ratio reflects directly the ratio of absolute strength. For ARC data, however, the ratio of the E1 and M1 strengths remains independent of the conversion only if the competing E1 contribution to M1 transitions from *p*-wave capture is properly accounted. The E1/M1 ratio of DRC data is plotted in Fig. 3.6.

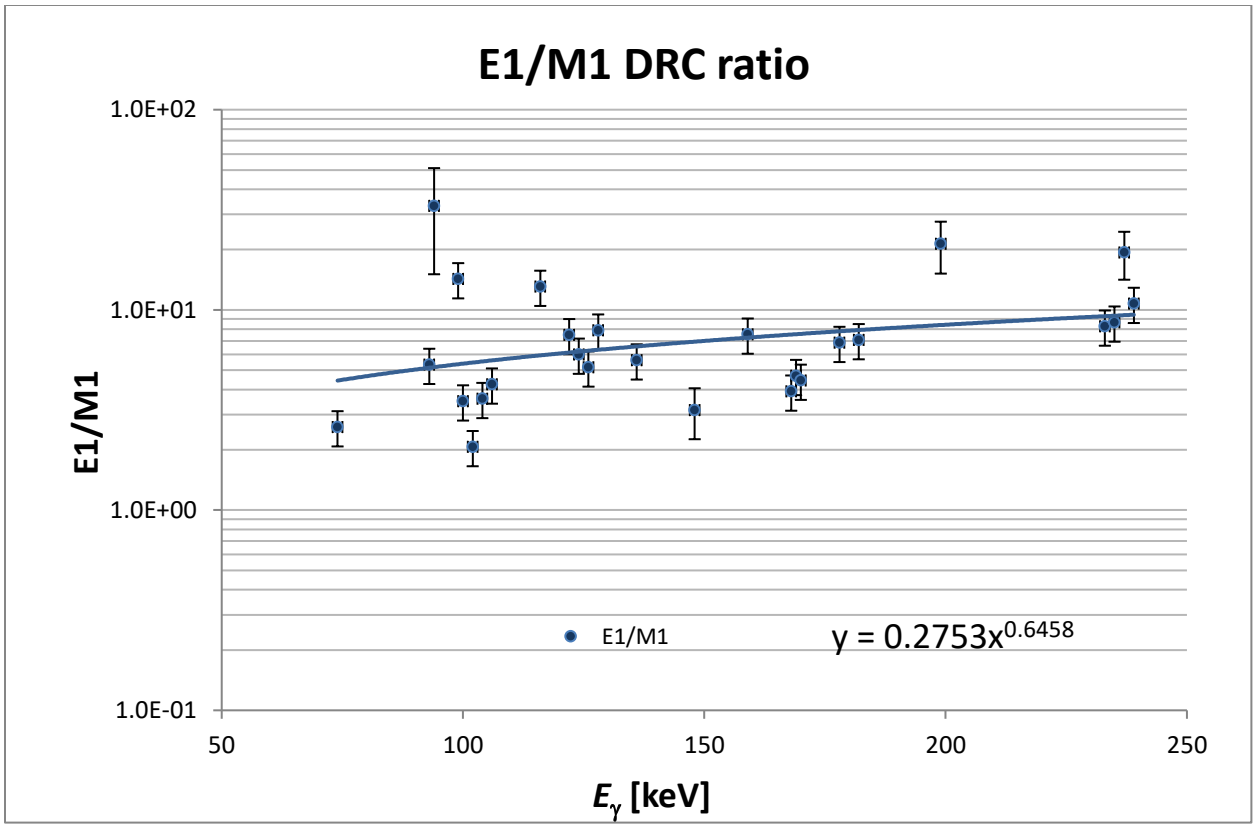

FIG. 3.6 *The E1/M1 ratio from binned DRC data at <6.5> MeV. Data of ^{233}Th and ^{235,237,239}U renormalized by (6.5/<E_γ>)^2 factor. The only strong outlier is ^{94}Nb, with E1 from s-wave and M1 p-wave capture, which may be the source of uncertainty (uncertain spacings).*

The E1/M1 trend systematic looks reasonably smooth, with only one strong outlier ^{94}Nb, discussed in the figure caption. The E1/M1 ratio against the systematic trend is given in the third column of Table 3.8. Comparing results in Table 3.8 (third column) for all suspicious E1 experimental (enhanced) data, there seems to be no evidence that the enhancement is present in E1 excitation mode. Unfortunately, for three nuclides (^{174}Y, ^{176}Lu and ^{184}W) no M1 data are available. In case of enhanced E1 strength, the (E1/M1) ratio against the systematics should be significantly larger than 1 and this was not observed.

Table 3.8 List of nuclides with uncertain DRC experimental <<*f*(E1)>> values and its behavior against the systematic predictions

Nuclide	**<<*f*(E1)>>/<*f*(E1)>$_{sys}$**	**(E1/M1)/ (E1/M1)$_{sys}$**
Sm-148	0.57	0.36
Tm-170	0.63	0.56
Yb-174	3.71	No M1
Lu-176	0.44	No M1
Hf-178	3.01	0.87
W-184	3.33	No M1
Au-198	1.61	1.0
Th-233	2.10	0.85
U-239	0.47	1.1

On the theoretical side, we have compared ARC data normalized to the DRC experimental values with QRPA calculations in Fig. 3.7. The QRPA predictions have been already successfully used to validate the ARC 2017 data [3.20,3.25].

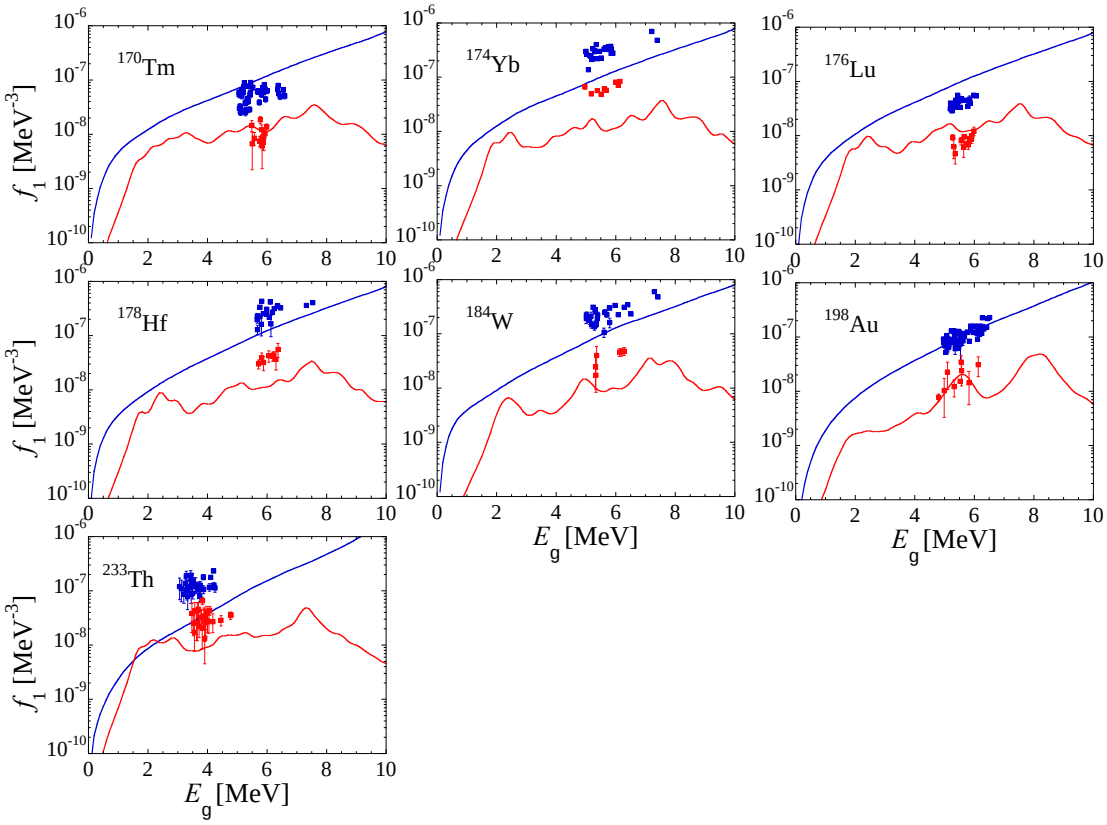

FIG. 3.7 *Comparison of ARC E1 and M1 strength function with the D1M+QRPA calculations*

As can be seen in Fig. 3.7, except for ^{198}Au nuclide, in all the other cases the calculations and data are discrepant, which further supports the suggestion that there may be a hidden uncertainty in the corresponding TOF DRC experiments. Based on these results, the calibration to the DRC systematics is preferred to the DRC experimental data, and therefore, for the final version of ATLAS_ARC_2019, the absolute calibration given in Table 3.7 was used. The detailed theoretical comparison and validation is given in Section 4.

3.5. PSF internal validation

3.5.1. <*f*(M1)> comparison with DRC data

The M1 transitions were not used for *f*(*L*) normalization, except for two nuclides without E1 data. It may be, therefore, of interest for validation of the results to compare two independent sets of M1 data from DRC and ARC experiments. The results of the <*f*(M1)> comparison is shown in Fig. 3.8. The data in absolute units can be compared directly, because in both experiments similar energy regions have been used. Both data sets are in very good agreement, which is also supported by two trend lines, which are close to each other. We may conclude that the adopted normalization procedure using exclusively E1 transitions gives good results for the M1 strength and verifies the applied correction of the E1 admixtures from the *p*-wave capture.

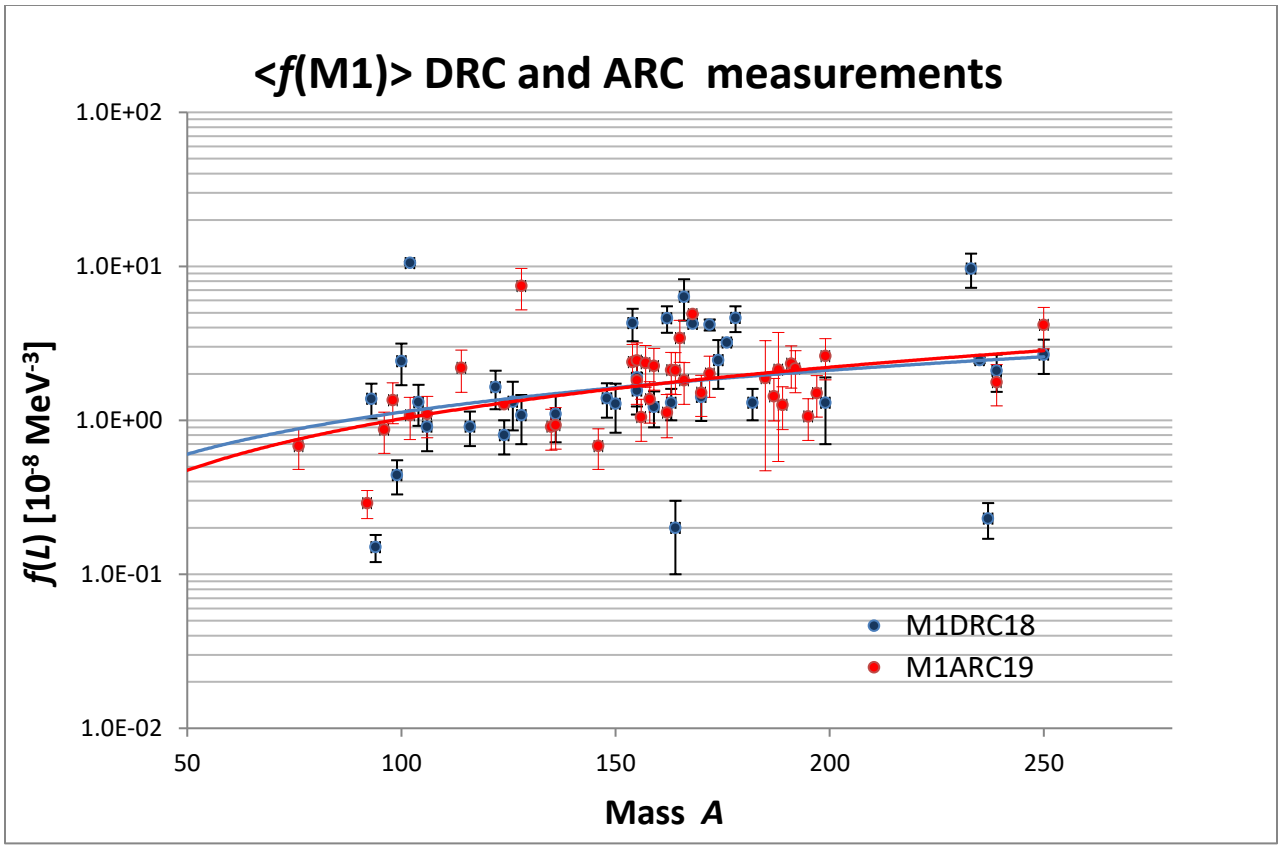

FIG. 3.8 *Comparison of <f(M1)> values from DRC measurements [3.21] and recent ARC data taken from the present ARC 2019 file. DRC data with A < 50 not used.*

3.5.2. The E1/M1 ratio in ARC and DRC (comparison)

The ratio of the E1 to M1 strengths remains independent of the procedure used to convert from the intensities I_γ/E_γ^3 into PSF format. For the ARC data the correction of the competing E1 contribution to M1 transitions from the *p*-wave capture is needed. A comparison of E1/M1 ARC data is another test of the M1 ARC data for this correction, as it is expected that both trend curves should be close to each other.

We show in Fig. 3.8 the E1-to-M1 ratio as a function of the atomic mass *A* from the original ARC data at energies ranging between 3.6 and 7.2 MeV and after renormalizing the data of the actinide targets to the average reference energy of 6.5 ± 0.5 MeV.

The energy regions of E1 and M1 data (on average about 1 MeV wide) were identical in energy to minimize the internal energy dependence between them. As can be seen in Fig. 3.9, both trend curves have the same slope and are in very good agreement. This is additional confirmation that the M1 ARC data are in good agreement with those from DRC experiments and also demonstrates that the *p*-wave corrections have been applied successfully.

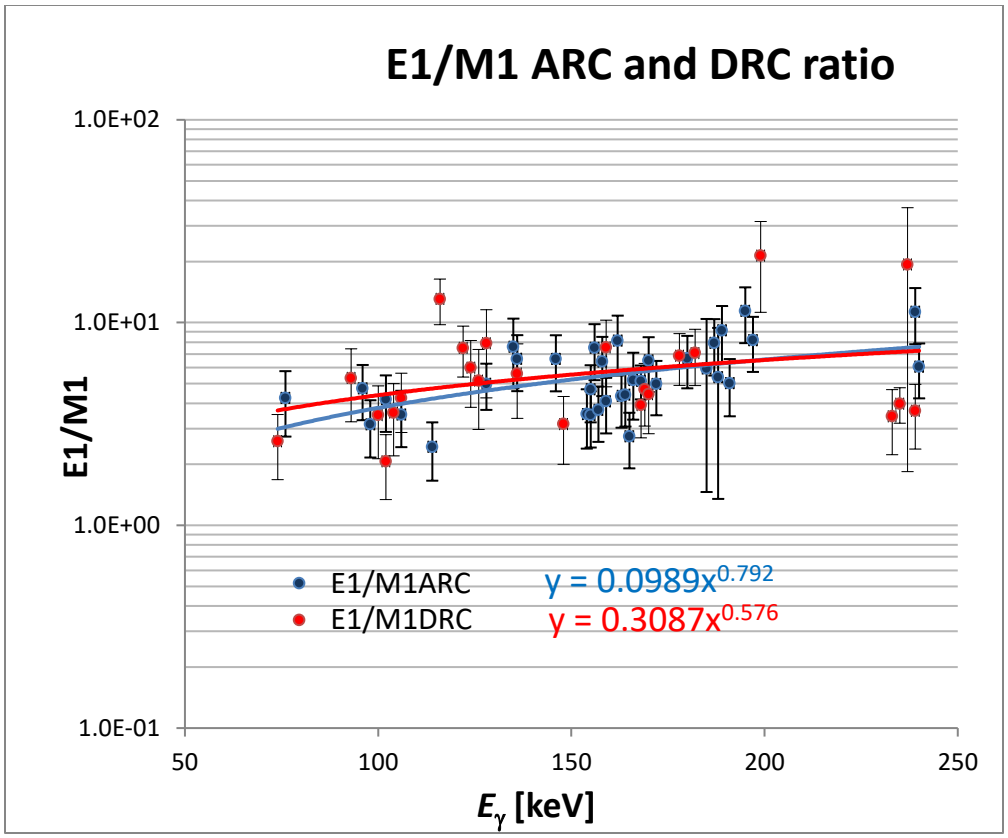

FIG. 3.9 *The E1 to M 1 strengths ratio extracted from DRC and ARC data as a function of the atomic mass A for data with $<E_\gamma>$ = 6.5 ± 0.5 MeV. The solid blue line is the newly proposed systematics f(E1)/f(M1) at 6.5 MeV for the ARC data and the red line belongs to the DRC data (see Fig. 3.5).*

3.6. Conclusions

ARC data measured at different filter beam facilities have been re-analyzed. They include all measurements made at ANL, INEL and BNL between 1970 and 1990, but until now only partially exploited. This is the first time that a comprehensive re-evaluation of all measured data was completed and applied for a systematic comparison with estimated PSF in the mass range 70 < A < 240. Updated spectroscopic information on the states of interest is used to extract the E1 and M1 transition groups in the PSF. This re-evaluation provides new experimental information on the E1 and M1 strength function around the neutron binding energy and provides new constraints for existing γ-ray strength models used in statistical reaction codes. The earlier release of ARC data in 2017, included in the ATLAS_ARC_2017 library, has been used as a starter file for the recent update. In the update, the recent DRC information was applied for the absolute PSF calibration and resulted in the ATLAS_ARC_2019 file.

References to Section 3

[3.1] L.M. Bollinger and G.E. Thomas, Phys. Rev. C2 (1970) 1951 and L.M. Bollinger, "Photonuclear Reactions and Applications" Pacific Grove, California (1973) 783

[3.2] R.B. Schwartz et al., Proc, Int. Symposium on Neutron Capture Gamma-rays Spectroscopy and related Topics, Petten (NH) (1974) 346
[3.3] G.A. Bartholomew et al., Adv. Nucl. Phys. 7 (1973) 229
[3.4] M.A. Lone, "Neutron Gamma Ray Spectroscopy and Related Topics", Plenum New York, 1979, 161
[3.5] R. Greenwood and C. Reich, Nucl. Phys. A 223, (1974) 66
[3.6] R. Greenwood and R. Chrien, Nucl. Instr. Meth. 138 (1976) 125
[3.7] M.L. Stelts, "Nuclear Cross Sections for Technology" (Knoxwille Conf.) Nat.Bur. of Stds.Sp.Publ.594, (1980) 936
[3.8] R.E. Chrien, "Neutron-Capture Gamma-Ray Spectroscopy and related Topics, Physics Conf. Seriers No 62", (The Inst. of Phys., Bristol and London) 1982, 342
[3.9] J. Kopecky, "Neutron Gamma Ray Spectroscopy and Related Topics" Knowville, (Tennessee (1984)
[3.10] R.E. Chrien, "Fourth Int. Symposium on Neutron Induced Reactions", Smolenice (CZ) (1985) 200
[3.11] R.E. Chrien, "5rd Int. School on Neutron Physics", Alushta (USSR) October 1986 and BNL-38900 report
[3.12] J. Kopecky, "Present Status of Experimental Gamma-ray Strength Functions derived from Neutron Capture", INDC(NED)-013 (September 2016)
[3.13] R.E. Chrien, et al., Nucl. Phys. A436 (1985) 205
[3.14] J. Kopecky and R. Chrien, Nucl. Phys. A 468, (1987) 285
[3.15] J. Kopecky and M. Uhl, Phys. Rev. C 41, (1990) 1941
[3.16] J. Kopecky, et al., Phys.Rev. C47 (1993) 312
[3.17] R. Capote et al., Nuclear Data Sheets 110, 3107 (2009)
[3.18] S.F. Mughabghab "Atlas of Neutron Resonances" (Elsevier 2018)
[3.19] U. Mayerhofer et al., Nucl. Phys. A492(1989) 1
[3.20] J. Kopecky, "Atlas of Average Resonance Capture data- Starter File" INDC(NED)-0738 (August 2017)
[3.21] J. Kopecky, "Revision and Update of Experimental Gamma-ray Strength Functions Derived from the Discrete Neutron Resonance Capture", INDC(NDS)-0772 (December 2018)
[3.22] M. Martini et al. Phys. Rev. C94 0143 04(2016)
[3.23] S. Goriely et al., Phys. Rev. C94 044306 (2016)
[3.24] S. Goriely et al., Phys. Rev. C94 044306 (2016)
[3.25] J. Kopecky et al., Phys. Rev. C95 054317 (2017)

4. Comparison with QRPA calculations

Recently, axially-symmetric-deformed QRPA estimates based on Hartree-Fock-Bogoliubov (HFB) calculations using the finite-range D1M Gogny interaction have been shown to provide rather satisfactory predictions of the E1 and M1 strength functions [4.1-4.4]. For this reason, this so-called D1M+QRPA approach has been chosen for comparison with the present DRC+ARC data from the latest TOTAL-2019 database. A comparison with the SYS models can be found in Ref. [4.5].

When considering the deexcitation PSF, as derived from DRC and ARC data, deviations from the QRPA photoabsorption strength are expected, especially for gamma-ray energies approaching the zero limit. As proposed in [4.2,4.4], a constant E1 strength and an M1 upbend, both inspired by shell-model calculations, can be assumed for gamma-ray energies approaching zero. The E1 and M1 PSFs predicted by the D1M+QRPA model and including the low-energy contributions is denoted as D1M+QRPA+0lim. All details can be found in Ref. [4.4] and references therein.

The E1 QRPA prediction typically follows a Lorentzian-type shape centred at the GDR excitation and characterized by an energy-dependent width. In the case of the M1 strength, a significant difference is found for spherical and deformed nuclei. More specifically, for spherical nuclei a rather peaked spin-flip resonance is obtained around 9MeV, while for deformed nuclei, the spin-flip mode is spread to lower energies, but also an additional low-energy M1 component stemming from the scissors mode around 3MeV is predicted [4.2,4.4].

4.1. Comparison of binned DRC-2018 data

The quasi-monoenergetic binned data have been compared with the D1M+QRPA predictions. The theoretical values of $fL(E_\gamma)$ have been derived from the QRPA predictions for the same E_γ energy window as the experimental DRC binned results. This increases the sensitivity of the comparison to the energy dependence of the PSF shapes. The resulting E1 and M1 strengths are shown in Figs. 4.1 and 4.2.

The agreement between theoretical and experimental f(E1) values is rather good and confirms the role of the E1 radiation strength as an absolute calibrator of PSF data at energies between 6 – 7 MeV. The situation for M1 is more complicated. The DRC trend curve is higher than the theoretical curve, especially for light nuclei below A < 100. This may be due to non-statistical contributions from p-wave resonances which are often present in this mass region, for which M1 is stronger than E1 radiation. Another reason may stem from the fact that the PSF obtained from microscopic calculations of different M1 excitation modes has a far more complicated form than the smooth E1 shape. Some of the outliers are a result of the poor averaging procedure over few or only one measured M1 transition. However, in this work we decided to use all measured data. For heavier nuclei with A > 100 the trend curves are in satisfactory agreement.

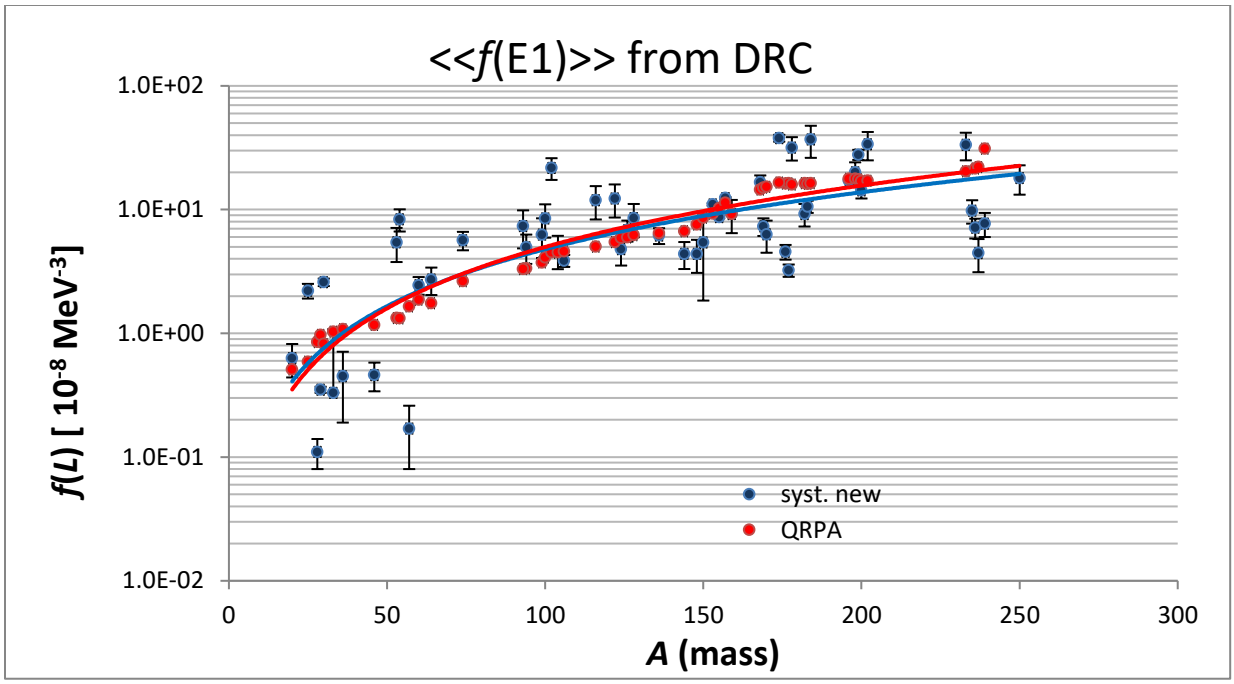

FIG. 4.1 Comparison between the E1 experimental DRC PSF binned in the 6.5±0.5MeV range and D1M+QRPA predictions in the same energy window.

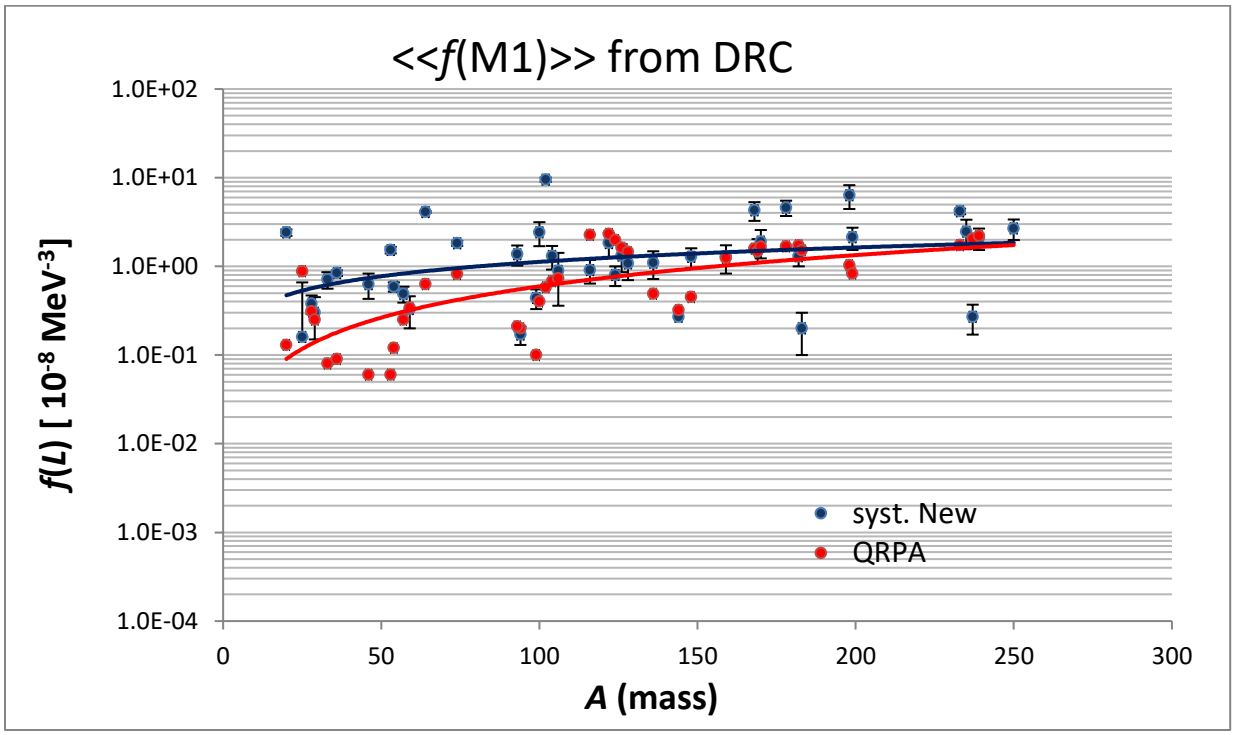

FIG. 4.2 Comparison between the M1 experimental DRC PSF binned in the 6.5±0.5MeV range and D1M+QRPA predictions in the same energy window

4.2. Comparison of binned ARC-2019 data

Similarly to the DRC data, the ARC-2019 data binned within the 6.5±0.5MeV range are compared with the D1M+QRPA predictions within the same energy window in Fig. 4.3 for the E1 PSF and in Fig. 4.4 for the M1 PSF. The E1 strengths are seen to be in rather good agreement, with a slight overestimate of the D1M+QRPA+0lim calculation for the rare earth nuclei in the $160 < A < 200$ range. The M1 PSF is also rather well predicted by the D1M+QRPA+0lim model, globally within a factor of 2. The M1 strength in ^{96,98}Mo as well as ^{135,136}Ba isotopes are however significantly underestimated. These nuclei are predicted to be spherical by the HFB calculation leading to a rather small PSF around 6.5MeV in contrast to the deformed nuclei for which a significant spreading of the scissors mode around 3MeV and the spin-flip mode around 9MeV give rise to a larger strength around 6.5MeV (see Sect. 4.4).

The E1/M1 ratios are compared in Fig. 4.5. The overall model overprediction is due to the underestimation of the M1 strength and slight overestimation of the E1 strength, as shown in Figs. 4.3 and 4.4.

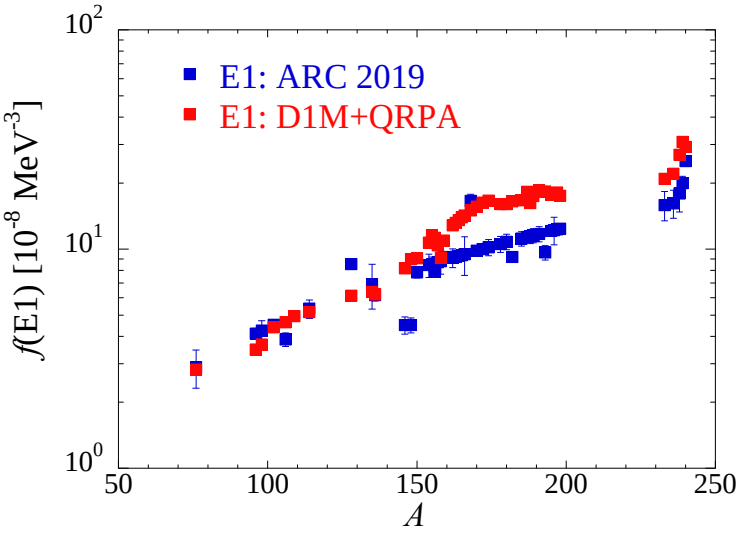

FIG. 4.3 Comparison between the E1 experimental ARC PSF binned in the 6.5±0.5MeV range and D1M+QRPA+0lim predictions in the same energy window

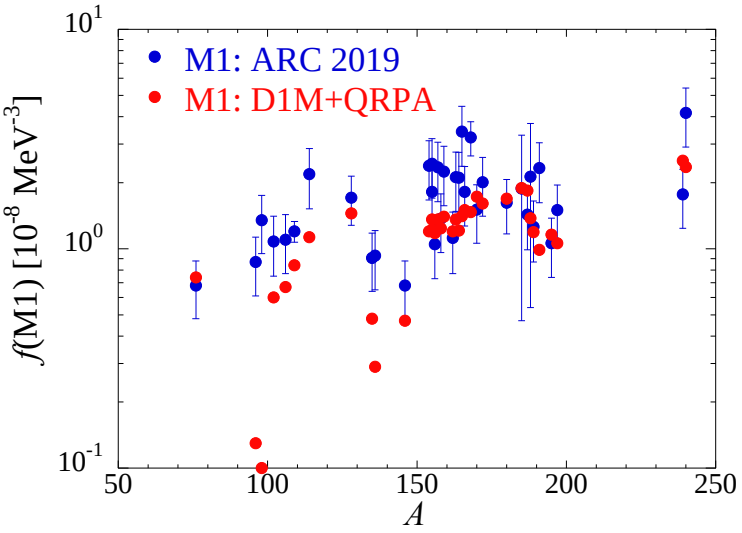

FIG. 4.4 Comparison between the M1 experimental ARC PSF binned in the 6.5±0.5MeV range and D1M+QRPA+0lim predictions in the same energy window

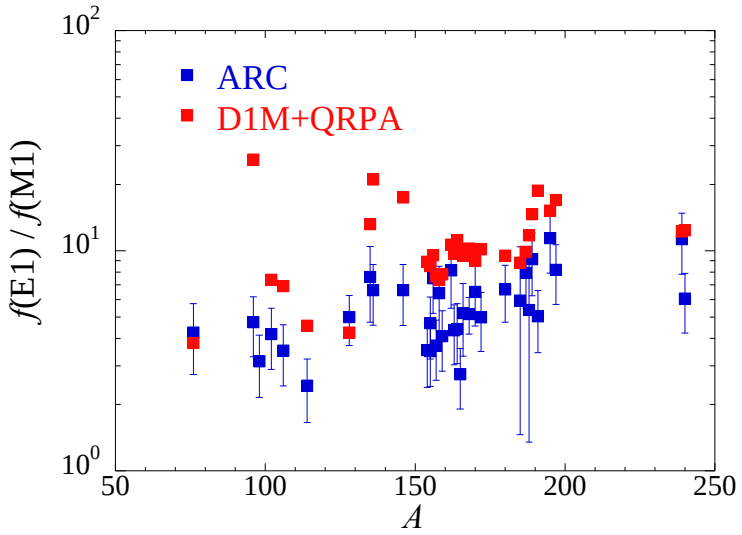

FIG. 4.5 Comparison between the E1/M1 ARC PSF data binned in the 6.5±0.5MeV range and D1M+QRPA+0lim predictions in the same energy window

4.3. Comparison of DRC and ARC data (TOTAL-2019) with QRPA predictions

All results for E1 and M1 strength taken from the final version of TOTAL 2019 against the model predictions are shown in Fig. 4.6-4.7 for DRC data and in Fig. 4.8-4.9 for ARC data.

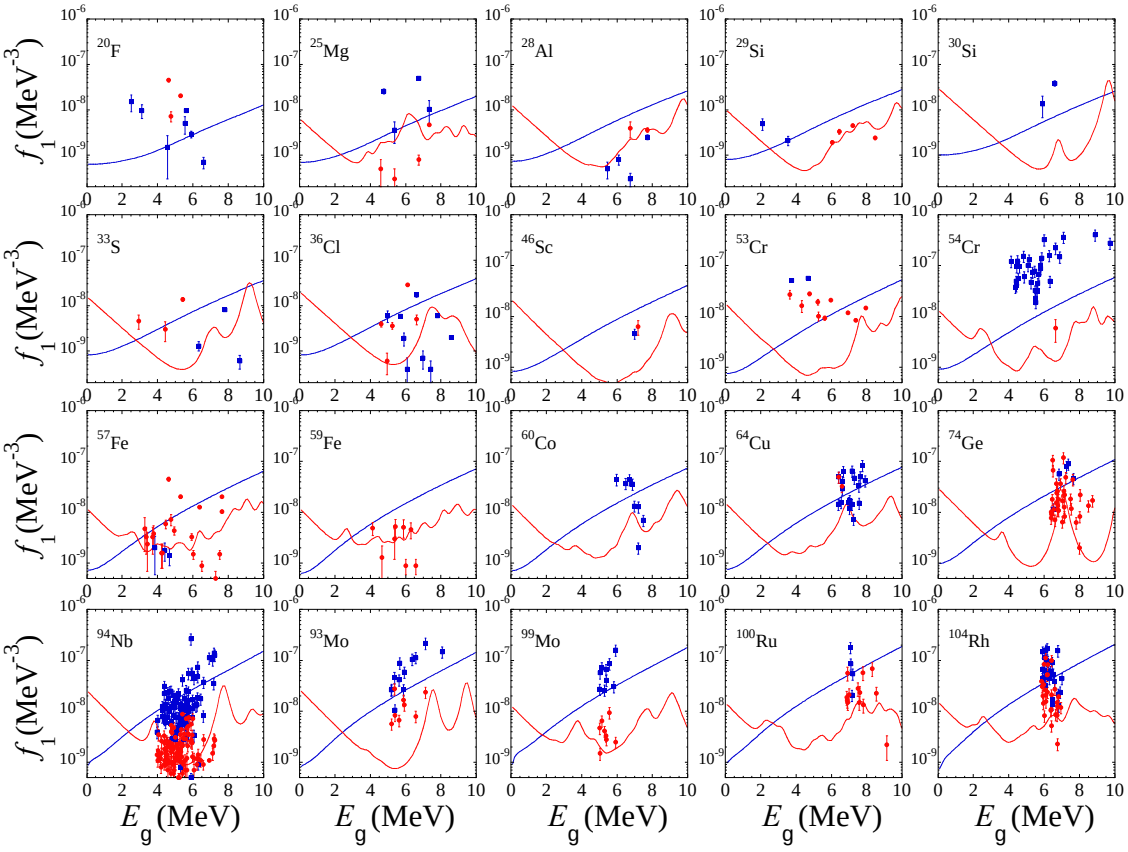

FIG. 4.6 Comparison between the E1 and M1 DRC PSF and D1M+QRPA+0lim predictions

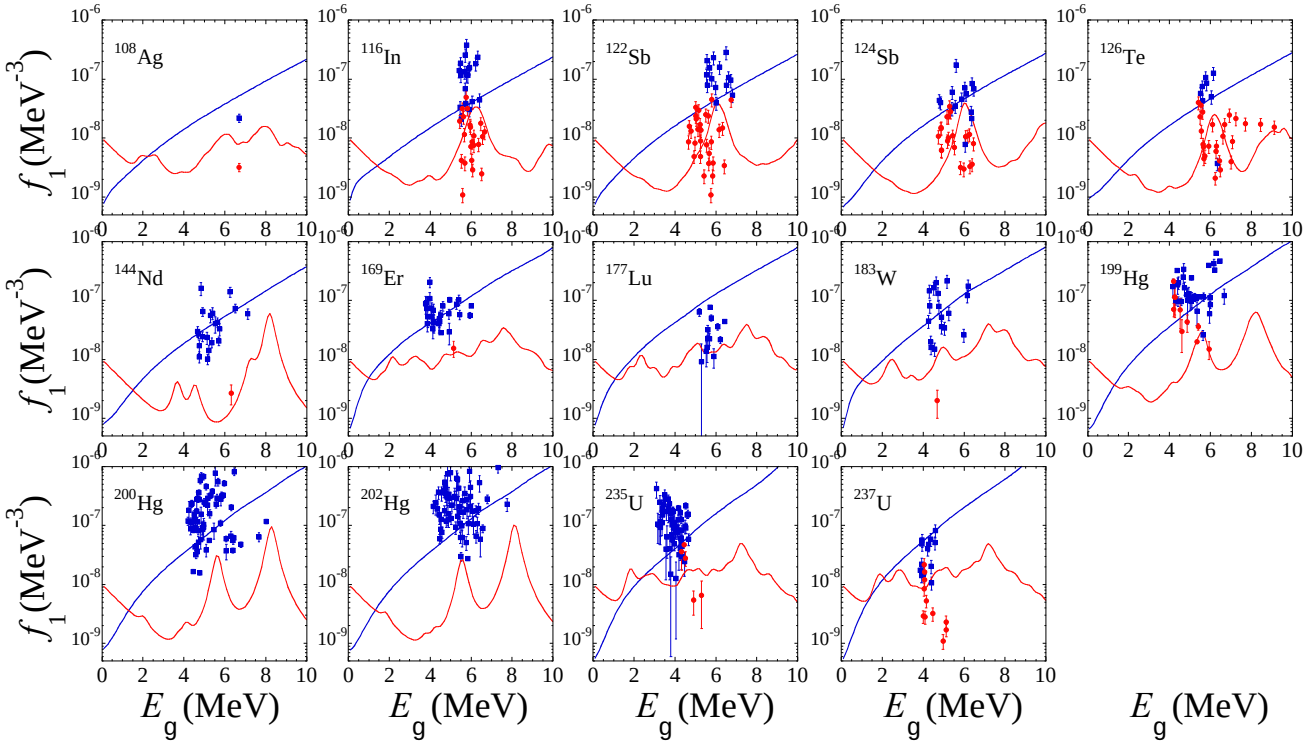

FIG. 4.7 Comparison between the E1 and M1 DRC PSF and D1M+QRPA+0lim predictions

The agreement for DRC data is in general rather satisfactory, in view of the limited averaging power, with some outliers observed for light nuclei. In these latter cases, one needs to consider that many DRC data originate from capture to a single or very few resonances and some are often *p*-waves, with a dominant non-statistical component. Another strong outlier is ^{54}Cr, where E1 data are from the capture in 8 *s*-wave resonances ($J = 1^-$ and 2^-) and 15 *p*-wave resonances ($J = 1^+2^+3^+$). The E1 strength overestimates strongly the QRPA calculation by factor of 10. We have at this moment no explanation for this effect. Some of the other discrepancies may be due to uncertainties in the absolute calibration of DRC TOF measurements.

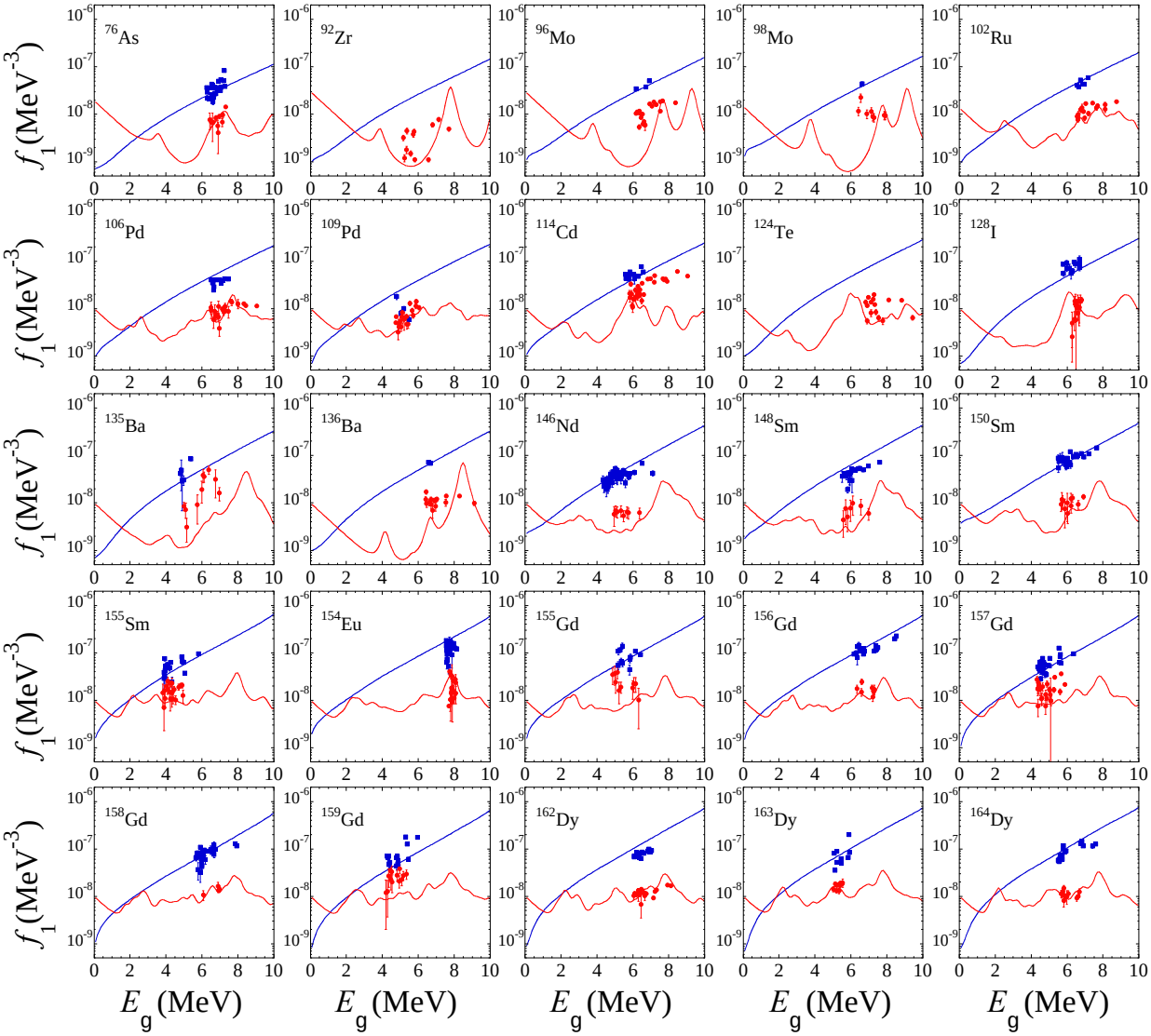

FIG. 4.8 Comparison between the E1 and M1 ARC PSF and D1M+QRPA+0lim predictions

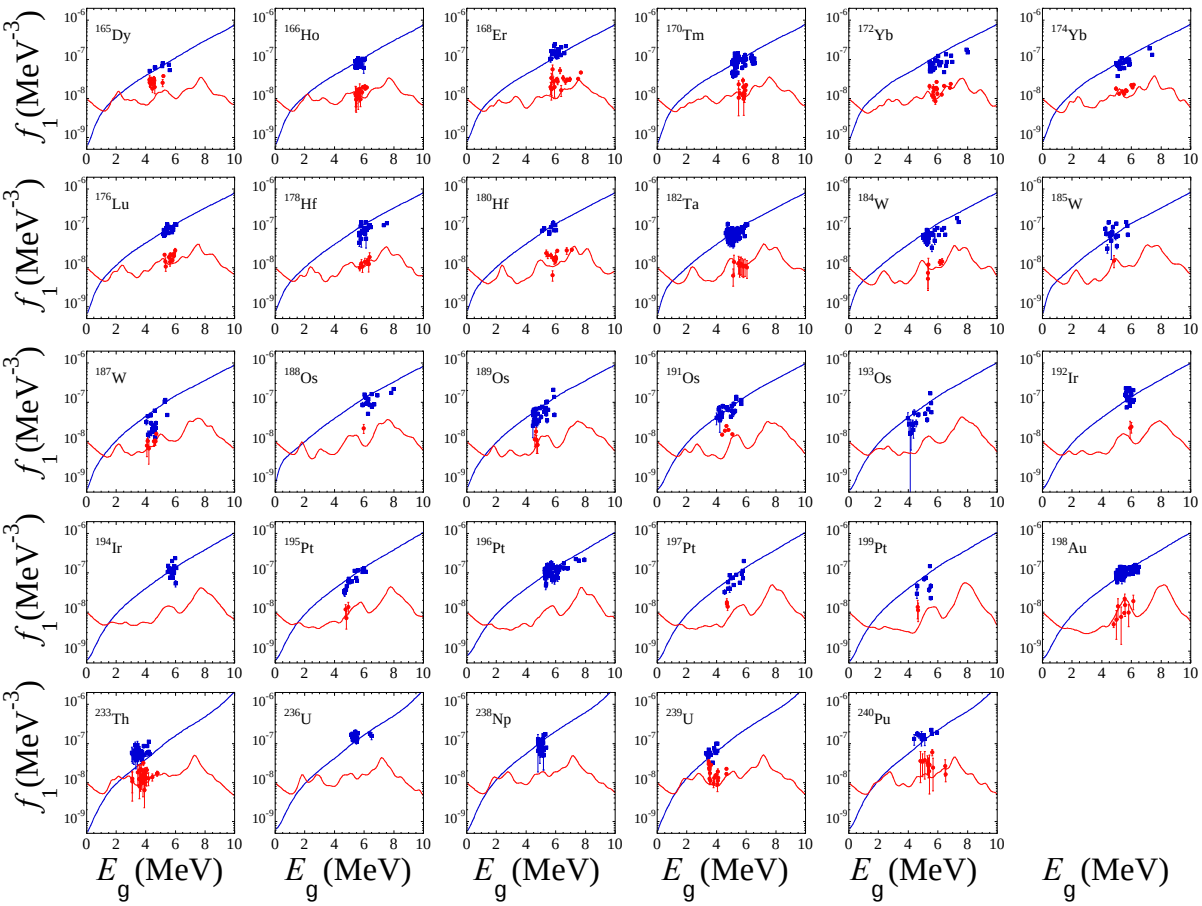

FIG. 4.9 Comparison between the E1 and M1 ARC PSF and D1M+QRPA+0lim predictions

The agreement between QRPA calculations and ARC data is overall very good. Some of minor disagreements may be due to the uncertainty in converting from I_γ/E_γ^3 into PSF format, which may be affected by uncertainties in the DRC evaluations. This is manifested by the fact that both E1 and M1 strengths are underestimated. Among the E1 transitions, there are minor discrepancies for the following nuclides, ^{128}I, ^{148}Sm, ^{162}Dy, ^{172}Yb and ^{184}W. Interpreting the comparison of M1 data with the QRPA predictions is more difficult. As discussed above and in the Section 3, the predicted QRPA M1 strength is composed of a combination of several M1 excitations with a rather complex shape as a function of E_γ. The absolute M1 strength of ARC data is also influenced by the *p*-wave E1 corrections, which also influences the M1 strength. There are no strong outliers for M1 data, however, the following nuclides exhibit minor discrepancies: ^{114}Cd, ^{135}Ba and $^{155, 157, 159}$Gd. For Gd nuclides, the systematic equation was used for the normalization and since this is the mass region for which DRC measurements and deduced systematics are in conflict, the calibrated ARC data may be affected. The ^{157}Gd DRC measurement seems to exceed the neighboring data very strongly.

4.4. Conclusion

The DRC and ARC data, used in the *TOTAL-2019* database, show that the recent QRPA calculations based on the D1M Gogny force give rather satisfactory predictions for E1 and M1 both in binned and differential PSF format. This fact can be used as validation tool for the processing of both DRC and ARC experimental data and the conversion in to the PSF format. This fact also justifies the use of both data sets, experimental as well theoretical, between them as a validation tool.

References to Section 4

[4.1] M. Martini et al. Phys.Rev.C94 0143 04(2016)

[4.2] S. Goriely et al., Phys.Rev. C94 044306 (2016)

[4.3] J. Kopecky et al., Phys.Rev. C95 054317 (2017)

[4.4] S. Goriely et al., "Reference Database for Photon Strength Functions", Eur. Phys. J. A (2019) to be published

5. Summary

This report covers the recent activity to analyze the neutron resonance capture experiments with the aim to create a comprehensive collection of gamma-ray photon strength functions (PSF). The earlier work, from the period up to nineteen nineties, was re-visited and formed the basis for the re-analysis with the aim of a major extension in the direction of the completeness of all available data sources. Another aim of this work was to process the data in a consistent manner, with one set of tools. The extracted data sources were limited to the resonance capture experiments, either from the capture in discrete resonances (DRC data) or from the filtered beam (B, Sc and Fe) experiments with data averaged over resonances present in specific neutron beams used, the so-called averaged resonance capture (ARC) data. The thermal capture data were not considered because they lack the resonance averaging and a different processing is required to address the Porter Thomas fluctuations.

During the period of this work, a number of IAEA NDS reports were issued covering the following periods. Firstly, the status of the earlier status of the PSF was reviewed in 2016 [5.1]. The next step was a revision and extension of ARC measurements and corresponding PSF data and this was described in 2017 in Ref. [5.2]. In order to update also the DRC data, a complete re-processing of DRC experiments was carried out and a new database of binned DRC PSF values was created and described in Ref. [5.3]. And finally, all these actions were combined in the present work, which merges all previous DRC and ARC results in one comprehensive database of PSF values in binned and differential format.

The main deliverables of this project are:

The differential DRC and ARC PSF data stored in the TOTAL_ DRC+ARC file (can be accessed from the IAEA NDS WEB data base). The data are graphically displayed in Fig.4.2 in Section 4.

The recommended binned DRC values. The DRC binned data are given in Table 5.1, extracted from Table 2.4 in Section 2, and are plotted in Fig. 5.1 together with the E1/M1 ratio.

Table 5.1 Recommended experimental quasi-mono energetic strength function $f(L)$ from DRC data binned at $\langle E_\gamma \rangle \sim 6.5 \pm 0.5$ MeV. Data values marked with * were not available in the differential format and are here adopted from Ref. [5.4] and private communications. For E1 transitions with an average energy $\langle E_\gamma \rangle$ differing from 6.5 MeV, the $(6.5/\langle E_\gamma \rangle)^2$ correction factor was applied and the estimated value is given in the lower row.

$\langle f(L) \rangle (d\langle f(L) \rangle)$ - the average PSF value with the uncertainty
$\langle E_\gamma \rangle / \Delta$- mean energy $E_\gamma \pm \Delta$ of the 2Δ window

Nuclide	$\langle f$(E1) ($d\langle f$(E1)$\rangle$)	$\langle E_\gamma \rangle / \Delta$	$\langle f$(M1) ($d\langle f$(M1)$\rangle$)	$\langle E_\gamma \rangle / \Delta$
	$*10^{-8}$ MeV^{-3}	MeV	$*10^{-8}$ MeV^{-3}	MeV
F-20	0.63(20) 1.26(40)	4.6/2.0 6.5	2.41(23)	5.0/0.3
Mg-25	2.21(30)	6.1/1.3	0.16(3)	6.1/1.3
Al-28	0.11(3)	6.6/1.1	0.38(9)	7.2/0.5
Si-29	0.35(10) 1.89(54)	2.8/0.7 6.5	0.30(3)	7.4/1.3
Si-30	2.59(56)	6.3/0.4		
S-33	0.33(3)	7.5/1.2	0.71(13)	4.2/1.2
Cl-36	0.45(7)	6.8/1.8	0.83(6)	5.6/1.0
Sc-46	0.46(10)	7	0.63(20)	7.2
Cr-53	5.44 (167)	4.2/0.5	1.53(13)	6.3/1.6
Cr-54	8.35(160)	6.9/2.8	0.59(7)	6.7/2.3
Fe-57	0.17(9) 0.39(18)	4.3/0.4 6.5	0.48(10)	5.5/2.2
Fe-59			0.33(13)	5.4/1.2
Co-60	2.45(60)	6.9/0.8		
Cu-64	2.72(68)	6.8/0.4	4.08(102)	6.3/0.1
Ge-74	5.65(140)	7.1/0.6	2.17(55)	7.6/1.1
Nb-94	4.96(124)	6.6/0.6	0.15(3)	6.6/0.6
Mo-93	7.36 (220)	6.9/1.2	1.38(35)	6.4/0.7
Mo-99	6.28(159)	5.5/0.5	0.44(11)	5.5/0.5

Nuclide	$<f(\mathrm{E1})$ ($d<f(\mathrm{E1})>$)	$<E_\gamma>/\Delta$	$<f(\mathrm{M1})$ ($d<f(\mathrm{M1})>$)	$<E_\gamma>/\Delta$
	$*10^{-8}$ MeV^{-3}	MeV	$*10^{-8}$ MeV^{-3}	MeV
Ru-100	8.48(212)	7.1/0.1	2.42(0.73)	7.2/0.4
Ru-102	21.7(54)	6.9/0.3	10.5(26)	7.1/0.5
Rh-104	4.72(118)	6.7/0.3	1.31(39)	6.8/0.2
Pd-106	3.87 (39)	7.0/0.4	0.91(28)	8.1/0.9
Ag-108	2.19(35)	7.3/0.6	0.32(15)	7.3/0.6
In-116	11.9(30)	6.1/0.3	0.91(23)	6.1/0.2
Sb-122	12.3(31)	6.3/0.5	1.64(46)	6.3/0.5
Sb-124	4.79(126)	6.2/0.2	0.8(2)	6.3/0.2
Te-126	6.83(167)	5.9/0.4	1.32(46)	5.9/0.5
I-128	8.54(256)	6.6/0.2	1.08(38)	6.6/0.3
Ba-136	6.17(123)	6.6	1.10(38)	7.0/0.3
Nd-144	6.17(117)	6.4/0.7	0.27(10)	6.3
Nd-146	4.50(18)*	6.7		
Sm-148	4.39(117)	6.3/0.7	1.39(35)	5.3/0.3
Sm-150	5.42 (136)	6.5/0.7		
Gd-153	11.0(3)*	na		
Gd-155	8.70(18)*	5.9		
Gd-157	12.4(223)*	6		
Gd-159	9.21(230)	5.2/0.7	1.22(32)	5.1/0.3
Er-168	16.6(325)	6.4/0.3	4.23(102)	6.4/0.3
Er-169	7.31(119)	5.3/0.7	1.56(47)	5.4
Tm-170	6.31(126)	6.1/0.5	1.42(43)	6.0/0.2
Lu-176	4.57(62)	5.8/0.2		
Lu-177	3.23(59)	5.8/0.6		
Y-174	37.8(67)	5.7/0.2		
Hf-178	31.7(676)	6.0/0.3	4.62(88)	6.0/0.3
Ta-182	9.2(19)	5.6/0.4	1.3(3)	5.6/0.4
W-183	10.6(26)	5.6/0.6	0.2(1)	4.9

Nuclide	$\langle f(\mathrm{E1}) \rangle$ ($d\langle f(\mathrm{E1})\rangle$)	$\langle E_\gamma \rangle / \Delta$	$\langle f(\mathrm{M1}) \rangle$ ($d\langle f(\mathrm{M1})\rangle$)	$\langle E_\gamma \rangle / \Delta$
	$*10^{-8}$ MeV^{-3}	MeV	$*10^{-8}$ MeV^{-3}	MeV
W-184	36.9(99)	6.5/0.9		
Pt-196	17.2(22)	7		
Au-198	20.0(41)	6.2/0.3	6.34(19)	5.4
Hg-199	27.8(30)	6.3/0.3	1.3(6)	5.6/0.3
Hg-200	14.3(209)	7.0/1.0		
Hg-202	33.7(80)	7.0/0.7		
Th-233	33.4(836) 88.5(222)	4.0/0.3 6.5	9.67(242)	4.2/0.3
U-235	9.8(19) 21.9(42)	4.4/0.3 6.5	2.46(11)	4.4/0.3
U-236	7.14(131)	5.8/0.6		
U-237	4.45(112) 9.66(243)	4.4/0.2 6.5	0.23(6)	4.6/0.5
U-239	7.70(173) 22.7(5.1)	3.8/0.3 6.5	2.10(57)	4.2/0.6
Pu-240	18.0(48)	5.8/0.7	2.68(67)	6.1/0.4

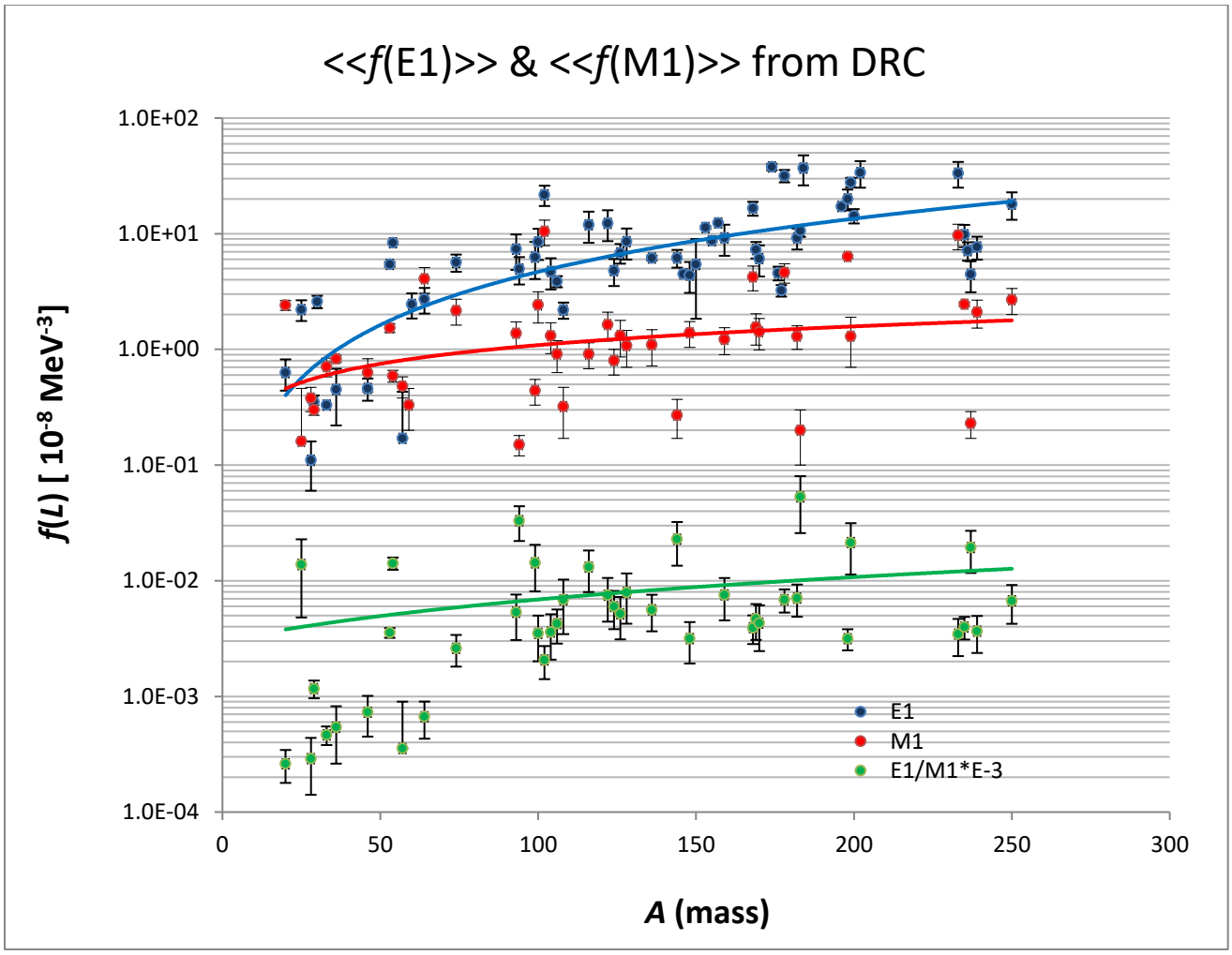

FIG. 5.1 *Plots of average quasi-monoenergetic E1 and M1 strength functions at $<E_\gamma> \simeq 6.5$ MeV derived from DRC-2018 data. Green data points show the E1/M1 ratio values using a 10^{-3} scale.*

The ratio of the E1 to M1 strength functions is found to remain within the range between 3 and 10 but not to follow any clear systematics, as expected from microscopic predictions of different excitation modes (spherical and deformed nuclides) for M1 radiation (see Fig. 4.1 in Section 4). The small E1/M1 values (<1) for nuclides with A < 60 are influenced by the often present nonstatistical reaction mode in this mass region of the 3p-neutron strength giant resonance. More discussion on some of the outlying values is given in Section 1.

Acknowledgments

Both authors acknowledge the long and important support of IAEA (P. Dimitriou and A. Koning), which also helped JK participate in this project.

References to Section 5

[5.1] J. Kopecky, "Present status of experimental gamma-ray strength functions derived from neutron capture" INDC(NED)-013 (2016)

[5.2] J. Kopecky, "Atlas of average resonance capture data (Starter file)" INDC(NDS)-0738

(2017)
[5.3] J. Kopecky, “Revision and Update of Experimental Gamma-ray Strength Functions Derived from the Discrete Neutron Resonance Capture”, INDC(NDS)-0772 (2018)

A. References to DRC Data Sources

(Table 2.1 in Sec. 2.1)

[1] M.J. Kenny et al., Austr.J.Phys. 27 (1974) 759 *F-20 Al-28 S-33*

[2] I. Bergqist et al., Phys.Rev. 158 (1967) 1049 *Mg-25Al-28*

[3] C.M. McCullagh, PhD thesis, Stony Brook, (1979) and C.M. McCullagh, M. Stelts and R.E. Chrien, Phys. Rev. C23, 1394 (1981) *Al-28 Cl-36 Pd-106 Te-126 I-128 Ba-136 Nd-144 Lu-176 Ta-182W-184 Pt-196 U-237*

[4] M.J. Kenny et al., Nucl.Phys. A170 (1976) 164 *Si-28,30*

[5] R.E. Chrien and J. Kopecky, Phys.Rev.Lett. 39 (1977) 911 *Cl-36*

[6] H.I. Liou and R.E. Chrien, *Proceedings of the 3rd International Symposium on Neutron Capture γ-ray Spectroscopy and Related Topics,* (Plenum, New York, 1979) p.67 *Sc-46*

[7] J. Kopecky et al., Nucl.Phys. A334 (1980) 35 *Cr-52*

[8] C. Coveva, Il Nuovo Cimento A 101 (1994) 85 *Cr-54*

[9] R.E. Chrien et al., Phys.Rev. C1 (1970) 973 *Fe-57*

[10] J.C. Wells Jr. Et al., Phys.Rev. C18 (1978) 707 *Fe-59*

[11] O. Wasson et al., Phys.Rev. 176 (1968) 1314 *Co-60*

[12] W. Stein et al., Phys.Rev. C1 (1969) 1468 *Cu-64*

[13] R.E. Chrien et al., Phys.Rev. C9 (1974) 1839 *Ge-74*

[14] R.E. Chrien et al., Phys.Rev. C3 (1971) 2054 *Nb-94*

[15] O.A. Wasson and G.C. Slaughter, Phys.Rev. C8 (1973) 297*Mo-93*

[16] R.E. Chrien et al., Phys.Rev. C13 (1976) 578 *Mo-99*

[17] K. Rimavi et al., Phys.Rev. C9 (1974) 1978 *Ru-100, 102*

[18] C. Coceva et al., Nucl.Phys. A385 (1982) 301 *Ru-100, 102*

[19] K. Rimavi et al., Phys.Rev. C2 (1970) 1793 *Rh-104*

[20] C. Coceva et al., Nucl. Phys. A170 (1971) 153 *Pd-106*

[21] F. Corvi and M. Stefanon, Nucl.Phys. A233 (1974) 185 *In-116*

[22] A. Lottin and D. Paya, J.Phys. (Paris) 32 (1971) 849 *Sb-122 Sb-124*

[23] S. Raman, private communication *Nd-146*

[24] F. Becvar et al., J. of Nucl.Phys. (Russian) 46 (1987) 3 *Sm-148*

[25] F. Becvar et al., Nucl.Phys. A236 (1974) 198 *Sm-150*

[26] F. Becvar et al., *Capture Gamma-Ray Spectroscopy,* (Inst. Of Physics Conference Series 88, Bristol 1988) p. 649 and private communication *Sm-150 Gd-153 Gd-157,159 Lu-177*

[27] F. Becvar et al., *Proc. Of the Int. Conference on Neutron Physics,* Kiev (1988) p.8 *Gd-155*

[28] C. Granja et al., Nucl.Phys. A729 (2003) 679 *Gd-159*

[30] S. Kahane et al., Phys.Rev. C30 (1984) 807 *Er-168*

[31] J.B. Garg et al., Phys.Rev. 174 (1968) 1139 *Er-169*

[32] M.A. Lone et al., Phys.Rev. 174 (1968) 1512 *Tm-170*

[33] O. Wasson and R.E. Chrien, Phys.Rev. C2 (1970) 675 *Lu-176*

[34] F. Becvar et al., Yad.Fiz. 46 (1987) 392 *Lu-176,177 Yb-174*

[35] M. Stefanon and F. Corvi, Nucl.Phys. A281 (1977) 240 *Hf-178*

[36] M.L. Stelts et al., Phys. Rev C16 (1977) 574 *Ta-182*
[37] S. Samour et al., Nucl.Phys. A121 (1968) 65 *Pt-196*
[38] O.A. Wasson et al., Phys.Rev. 173 (1968) 1170 *Au-198*
[39] M.A. Lone et al., Nucl.Phys. A243 (1975) 413 *Hg-198,199,202*
[40] B.K.S. Koene and R.E Chrien, Phys.Rev C16 (1977) 588 *Th-233 U-235*
[41] R.G. Graves et al., Phys.Rev. C8 (1973) 781 *U-236*
[42] T. von Egidy et al., Phys.Rev. C6 (1972) 266 *U-237*
[43] O.A. Wasson et al., Phys.Rev. C4 (1971) 900 *U-239*
[44] R.E. Chrien et al., Nucl.Phys. A436 (1985) 205 *Pu-240*

B. Neutron resonance parameters of present DRC measurements

The neutron spacing from two latest independent compilations is shown, in order to indicate possible additional uncertainty due to conflicting spacing. Such cases are printed in bold. J_t and J_i(#) are spins of target nuclide and of resonances with neutron l_n from the surveyed experiments. Two columns with J_i(#) symbol give the number of resonances with the spin Ji of used resonances. This is important information for the use of the proper spacing in the averaging process.

Product nuclide	**#res**	l_n	J_t	J_i^-(#)	J_i^+(#)	***D*** **[eV] RIPL-3**	***D*** **[eV] BNL-2018**
F-20	2	1	½+	1- (1)	2- (1)	60000	60 000
Mg-25	2	1	0+	3/2-(1)		16000	158 000
		2			3/2+ (1)		110000
Al-28	2	0	5/2+	2+ (1)		55000	53700
		1		2- (1)		27500	28400
Si-29	1	1	0+	½- (1)		**75000**	**109000**
Si-30	1	1	½+	2- (1)		**85400**	**52400**
S-33	1	1	0+	½- (1)		46300	46300
Cl-36	1	1	3/2+	2- (1)		**6600**	**22300**
Sc-46	2	0	7/2-	3+ (1)	4+ (1)	1030	1030
Cr-53	1	1	0+	3/2- (1)		**1030**	**10500**
Cr-54	8	0	3/2-	1- (3)	2- (5)	6700	5960
	15	1		1+(3)2+(2)	3+ (10)	3060	3060
Fe-57	1	1	0+	½- (1)		7700	8210
Fe-59	2	1	0+	½- (na)	3/2- (na)	5030	5030
Co-60	1	0	7/2-	4- (1)		1450	1390
Cu-64	3	0	3/2-	1- (1)	2- (2)	700	722
Ge-74	6	0	9/2+	4+ (5)	5+ (1)	62	60.1
Nb-94	3	0	9/2+	4+ (3)		94	84.8
	4	1		4- (2)	5- (2)	50	42.4
Mo-93	7	0	0+	½+ (7)		2700	2800
	16	1		1/2- (4)	3/2-(12)	900	780
Mo-99	5	0	0+	½+ (5)		1000	970
	11	1		1/2- (3)	3/2- (8)	290	286
Ru-100	4	0	5/2+	2+ (1)	3+ (3)	25	21.7
Ru-102	6	0	5/2+	2+ (3)	3+ (3)	18	18.5
Rh-104	7	0	½-	0- (1)	1- (6)	32	24.2
Pd-106	9	0	5/2+	2+ (3)	3+ (6)	10.3	10.9
In-116	22	0	9/2+	4+ (11)	5+ (11)	9.5	9

Sb-122	12	0	5/2+	2+ (5)	3+ (7)	13	10
Sb-124	4	0	7/2+	3+ (2)	4+ (2)	24	24
Te-126	12	0	½+	0+ (4)	1+ (8)	43	42.7
I-128	8	0	5/2+	2+ (4)	3+ (4)	15	9.7
Ba-136	6	0	3/2+	1+ (4)	2+ (2)	40	40
Nd-144	9	0	7/2-	3- (5)	4- (4)	38	37.6
Nd-146	10	0	7/2-	3- na	4- na	17	17.8
Sm-148	23	0	7/2-	3- (12)	4- (11)	5.7	5.7
Sm-150	3	0	7/2-		4- (3)	2.4	2.2
Gd-153	na	0	0+	½+ na		14	13.5
Gd-155	15	0	0+	½+ (15)		14.5	13.8
Gd-157	na	0	0+	½+ na		30	30.5
Gd-159	12	0	0+	½+ (12)		82	87
Er-168	45	0	7/2+	3+ na	4+ na	4.2	4
Er-169	7	0	0+	½+ (7)		100	94
Tm-170	10	0	½+	0+ (2)	1+ (8)	8.5	7.28
Lu-176	12	0	7/2+	3+ (7)	4+ (5)	3.45	3.45
Lu-177	6	0	7-	15/2- (6)		1.61	1.61
Yb-174	23	0	5/2-	2- (9)	3- (14)	7.5	8.06
Hf-178	20	0	7/2-	3- (9)	4- (11)	2.4	2.4
Ta-182	19	0	7/2+	3+ (9)	4+ (10)	4.2	4.17
W-183	7	0	0+	½ +(7)		60	63.4
W-184	7	0	½+	0+ (2)	1+ (5)	12	12
Pt-196	22	0	½-	0- na	1- na	18	17
Au-198	4	0	3/2+	1+ (1)	2+ (3)	15.5	15.7
Hg-199	2	0	0+	½+ (2)		105	250
Hg-200	3	0	½-	0- (1)	1- (2)	80	100
Hg-202	3	0	3/2-	1- (2)	2- (1)	90	90
Th-233	5	0	0+	½+ (5)		16.5	15.82
U-235	3	0	0+	½+ (3)		11.2	10.92
U-236	20	0	7/2-	3- (8)	4- (12)	11.2	0.49
U-237	7	0	0+	½+ (7)		14	14.7
U-239	23	0	0+	½+ (23)		20.3	16.4
Pu-240	7	0	½+	1+ (8)		2.2	2.07

C. List of ARC measurements with neutron filtered beams (B, Sc or Fe) selected for the final PSF data base

Selected ARC data for the PSF data base are denoted in red fonts. References are given in Appendix D.

Product nuclide	**B**	**Sc**	**Fe**	**Final *ATLAS f(L)***	**Excluded measurements**
Ti-49		x	x	[1]	Poor averaging
Co-60			x	[2]	24 keV only
Cu-64		x		[3]	Poor averaging
Cu-66		x		[4]	Poor averaging
As-76		x		[5]	
Zr-92		x		[6]	
Mo-96		x		[7] [8]	
Mo-98		x		[7]	
Ru-102		x		[8]	
Pd-106	x	x		[9]	[8][10][11][12]
Ag-108		x		[13]	No Iγ data
Cd-114		x		[8][14]	
Te-124		x		[15]	
I-128		x		[12]	
Ba-135		x		[16]	
Ba-136		x		[17]	
Ce-136		x	x	[18]	No Iγ data
Nd-146	x	x		[19]	[20]
Sm-155		x		[8] [21]	
Eu-154		x		[22]	
Gd-155		x		[23]	[24][25]
Gd-156	x	x		[9]	[8][26][27]
Gd-157		x		[24] [8]	[25]
Gd-158	x	x		[9]	[28]
Gd-159		x		[38]	[29]
Gd-161		x		[25]	
Dy-162		x		[30] [8]	
Dy-163		x		[31]	
Dy-164		x		[30] [8]	
Dy-165		x		[32]	
Ho-166	x			[9]	

Er-168	x	x		[9] [8]	[33]
Tm-170		x		[34]	
Yb-172		x		[35] [8]	
Yb-174		x		[36]	[46]
Lu-176		x		[38] [8]	
Hf-178		x		[39]	
Ta-182		x		[49]	
W-184	x	x		[41]	[42]
W-185		x		[43]	
W-187		x		[43]	
Os-188		x		[44]	
Os-189		x		[45]	
Os-191		x		[46]	
Os-193		x		[47]	
Ir-192		x		[48]	
Ir-194		x		[49]	
Pt-195		x		[50] [8]	
Pt-196		x		[51]	
Pt-197		x		[52]	
Pt-199		x		[52]	
Au-198		x		[53]	
Th-233		x		[54] [8]	
U-236		x		[55]	
U-239	x	x		[56] [8]	[57]
Pu-240		x		[58]	

D. References to filtered beams ARC data

[1] A.F. Gamalii et al., Sov.J.Nucl.Phys. 15(1972) 1 *Ti-49, Mo-96,98*

[2] J. Kopecky et al., Nucl. Phys.A427 (1984) 413 *Co-60*

[3] M.G. Delfini et al., Nucl. Phys. A404 (1983) 225 *Cu-64*

[4] M.G. Delfini et al., Nucl.Phys. A404 (1983) 250 *Cu-66*

[5] F. Hoyler at al., Nucl.Phys. A512 (1990) 189 *As-76*

[6] M.J. Kenny at al., *Proceedings of Neutron Gamma Ray Capture Spectroscopy and related topics, BNL*,(Upton 1978) 676 and BNL- 24698 *Zr-92,93,95*

[7] K. Rimavi and R.E. Chrien, Phys.Rev. C15 (1977) 1271 *Mo-93,95,97,99*

[8] BNL/ECN database (unpublished BNL data) *Mo-96,Ru-102, Pd-106*

[9] L.M. Bollinger and G.E. Thomas, Phys.Rev. C2 (1970) 1951 *Pd-106, Gd-156,158, Ho-166, Er-168*

[10] J. Kopecky and R.E. Chrien, Nucl.Phys. A468 (1987) 285 *Pd-106*

[11] B. Fogelberg et al., Nucl.Phys. A475 (1987) 301 *Pd-106*

[12] C. McCullagh, Univ. Stony Brook Thesis, (1978) *Pd-106, I-128*

[13] T.D. MacMahon et al., J.Phys. G11 (1985) 1231 *Ag-108, Gd-158*

[14] A. Meemeed et al., NP A412 (1984) 113 *Cd-114*

[15] R.F. Casten et al., Phys.Rev. C44 (1991) 523 *Te-124*

[16] R.E. Chrien et al., Phys.Rev. C48 (1973) 109 *Ba-135*

[17] K. Schreckenbach et al., *Capture Gamma-Ray Conf. Proc*., 1981) 200 *Ba-136*

[18] B.K. Koene et al., priv. com. 1981 *Ce-136*

[19] D.L. Bushnell et al., Phys.Rev. C14 (1975) 75 *Nd-146*

[20] S. Raman et al., J.Phys. G9 (1983) L137 *Nd-146*

[21] K. Schreckenbach et al. Nucl.Phys. A376 (1982) 149 *Sm-155*

[22] M.A. Balodis et al., Nucl.Phys. A572 (1987) 445 *Eu-154*

[23] H.H. Schmidt et al., J.Phys. (London) G12 (1986) 411*Gd-155*

[24] R.C. Greenwood et al., *Proceedings of Neutron Gamma Ray Capture Spectroscopy and related topics*, RCN Petten (September 1974) *Gd-155,157*

[25] R.G. Greenwood and R.E. Chrien, Bull. Am. Phys. Soc. 22 No.8 ED9 (1977) 1032 *Gd-155,157,159,161*

[26] A. Backlin et al., Nucl.Phys.A380(1982) 189 *Gd-156*

[27] J. Kopecky et al., Phys.Rev. C47(1993) 312 *Gd-156*

[28] R.C. Greenwood et al., Nucl.Phys. A304 (1978) 327 *Gd-158*

[29] C. Granja et al., Nucl.Phys. A279 (2003) 679 *Gd-159*

[30] D.D. Warner et al., Phys.Rev. C27(1983) 2292 *Dy-162,164*

[31] H.H. Schmidt, et al., Nucl. Phys. A504 (1989) 1 *Dy-163*

[32] E. Kaerts et al., Nucl.Phys. A514 (1990) 173 *Dy-165*

[33] W. Davidson et al., J.Phys. G7 (1981) 843 *Er-168*

[34] R.W. Hoff et al., Phys. Rev. C (1996) 78 *Tm-170*

[35] R. C. Greenwood et al., Nucl.Phys. A252(1975) 260 *Yb-172*

[36] C. Granja et al., Nucl.Phys. A757(2005) 287 *Yb-174*
[37] R.C. Greenwood et al., Phys.Rev. C23(1981) 153 *Yb-174*
[38] R.W. Hoff et al., Nucl.Phys. A437 (1985) 285 *Lu-176*
[39] A. Hague et al., Nucl.Phys. A455 (1986) 231*Hf-178*
[40] R.G. Helmers et al., Nucl.Phys, A168 (1971) 449 *Ta-182*
[41] R.C. Greenwood et al., Nucl.Phys. A223 (1974) 66 *W-184*
[42] D.L. Buschnell et al., Phys. Rev. C11 (1975) 1401 *W-184*
[43] A.M. Bruce et al., Nucl. Phys. A465 (1987) 221 *W-185,187*
[44] Proc. 40th *Ann. Conf. Nucl. Structure At. Nuclei*, (Leningrad 1990) *86 Os-188*
[45] A.M. Bruce et al., Nucl. Phys. A452 (1992) 1 *Os-189*
[46] R.F. Casten et al., Nucl. Phys. A285 (1977) 235 *Os-191*
[47] D. D. Warner et al., Nucl.Phys. A316 (1979) 13 *Os-193*
[48 J. Kern et al., Nucl. Phys. A534 (1991) 77 *Ir-192*
[49] M. Balodis et al., Nucl. Phys. A641 (1998) 133 *Ir-194*
[50] D.D. Warner et al., Phys.Rev. C26 (1982) 1921 *Pt-195*
[51] J. Cizewski et al., Nucl. Phys. A323 (1979) 349 *Pt-196*
[52] R.F. Casten et al., Phys. Rev. C 27(1983) 1310 *Pt-197, 199*
[53] U. Mayerhofer et al., Nucl.Phys. A492(1989) 1 *Au-198*
[54] P. Jeuch et al., Nucl.Phys. A317 (1979) 363 *Th-233*
[55] H. Ottmar et al., *Proc, Int. Symposium on Neutron Capture Gamma-rays Spectroscopy and related Topics*, Petten (NH) (1974) 658 *U-236*
[56] L.M. Bollinger and G.E. Thomas, Phys.Rev. C6(1972) 1322 *U-239*
[57] R.E. Chrien and J. Kopecky, Nucl. Phys. A414 (1984) 281 *U-239*
[58] R.E. Chrien et al., Nucl.Phys. A436 (1985) 205 *Pu-240*

APPENDIX

Nuclear Data Section
International Atomic Energy Agency
Vienna International Centre, P.O. Box 100
A-1400 Vienna, Austria

E-mail: nds.contact-point@iaea.org
Fax: (43-1) 26007
Telephone: (43-1) 2600 21725
Web: https://nds.iaea.org